

Applications of Deep Neural Networks to Protein Structure Prediction

---

A Dissertation

presented to

the Faculty of the Graduate School

at the University of Missouri-Columbia

---

In Partial Fulfillment

of the Requirements for the Degree

Doctor of Philosophy

---

by

CHAO FANG

Professor Yi Shang, Dissertation Advisor

Professor Dong Xu, Dissertation Co-advisor

July 2018

## **COPYRIGHTS**

Chapter 3 © Wiley Periodicals, Inc.

Chapter 4 © IEEE

Chapter 5 © IEEE

All other materials © Chao Fang

The undersigned, appointed by the Dean of the Graduate School, have examined the dissertation entitled

Applications of Deep Neural Networks to Protein Structure Prediction

presented by Chao Fang,

a candidate for the degree of Doctor of Philosophy

and hereby certify that, in their opinion, it is worthy of acceptance.

---

Dr. Yi Shang

---

Dr. Dong Xu

---

Dr. Jianlin Cheng

---

Dr. Tim Trull

## DEDICATIONS

*To my father Weimin Fang and my mother Li Li.*

## **ACKNOWLEDGEMENT**

I would like to take the opportunity to thank the following people who have supported me through my PhD experience. Without the support of them, this dissertation would not have been possible.

First, I would like to thank my advisor, Professor Yi Shang, for his eight years of patient teaching and guidance. I have been learning knowledge and perform research with him since I first came to Mizzou as a junior student in the “2+2” cooperative Computer Science undergraduate program. Working with him has become a great unforgettable experience in my life. He gradually teaches me hands-on experience on how to perform research, carry out experiments, teach, write scientific articles and give technical presentations step by step. He not only teaches me the knowledge of Artificial Intelligence and machine learning, but he also teaches me the scientific attitude of being a researcher, one should always be humble to take opinions from other researchers and always chasing the excellence in research. I thank his never-ending patient guidance and trust, warm-heart help, which are essential for the success of my PhD research. Professor Shang not only gives me suggestions on my research study, but also on my life and career path. His critical scientific research spirit will always inspire me.

I wish to thank my co-advisor, Professor Dong Xu, for his tireless help with answering my questions on Bioinformatics. He leads me walking into the fascinating research world of Bioinformatics to explore the beauty of life sciences. I once got lost in the bioinformatics research, it is Professor Xu led me step out of the maze. It is his confidence, optimism and

his insightful research suggestions inspire me to solve hard problems when facing the research difficulties.

I wish to thank my committee member, Professor Jianlin Cheng, for giving me constructive suggestions to my dissertation work. I took many of his interesting courses in the past few semesters, such as supervised learning, data mining, machine learning for Bioinformatics and computational optimization methods. Many of his class materials and projects are helpful to my PhD research. I also wish to thank my committee member, Professor Tim Trull, who gives me constructive advice for this dissertation.

Many thanks to my coworkers Zhaoyu Li, Peng Sun, Guang Chen, Duolin Wang, Junlin Wang, Wenbo Wang, Yang Liu, and Sean Lander for helping me learning protein structure prediction, helpful discussion, useful ideas and friendship. It is a memorable experience that we went to attend the ICTAI-2017 conference together in Boston to present our research work.

Last but not least, I wish to thank my father Weimin Fang and my mother Li Li. Without their support and foresight, I would not be able to study abroad in America. Without their encouragement and love, I would not have been this far. I wish to dedicate this dissertation to my parents.

This work was partially supported by the National Institutes of Health grant R01-GM100701. The high-performance computing infrastructure was partially supported by the National Science Foundation under grant number CNS-1429294.

# TABLE OF CONTENTS

<b>ACKNOWLEDGEMENT .....</b>	<b>ii</b>
<b>LIST OF TABLES.....</b>	<b>viii</b>
<b>LIST OF FIGURES.....</b>	<b>x</b>
<b>ABSTRACT .....</b>	<b>xiv</b>
<b>Chapter 1 INTRODUCTION .....</b>	<b>1</b>
<b>1.1 Protein Sequence, Structure and Function.....</b>	<b>1</b>
<b>1.2 Protein Secondary Structure Prediction.....</b>	<b>2</b>
<b>1.3 Protein Backbone Torsion Angle Prediction.....</b>	<b>4</b>
<b>1.4 Protein Beta Turn Prediction .....</b>	<b>6</b>
<b>1.5 Protein Gamma Turn Prediction .....</b>	<b>7</b>
<b>1.6 Contributions.....</b>	<b>8</b>
<b>1.7 Outline of the Dissertation .....</b>	<b>9</b>
<b>Chapter 2 RELATED WORK AND BACKGROUND.....</b>	<b>11</b>
<b>2.1 Protein Secondary Structure Prediction.....</b>	<b>11</b>
<b>2.2 Protein Backbone Torsion Angle Prediction.....</b>	<b>14</b>
<b>2.3 Protein Beta-turn Prediction.....</b>	<b>17</b>
<b>2.4 Protein Gamma-turn Prediction.....</b>	<b>19</b>
<b>2.5 Deep Neural Network .....</b>	<b>20</b>
<b>2.6 Convolutional Neural Network .....</b>	<b>21</b>
<b>2.7 Residual Neural Network (ResNet) .....</b>	<b>22</b>

2.8	ReLU, Batch Normalization and Fully Connected Layer.....	23
2.9	Dense Network .....	25
2.10	Capsule Network.....	25
<b>Chapter 3 NEW DEEP INCEPTION-INSIDE-INCEPTION NETWORKS FOR PROTEIN</b>		
<b>SECONDARY STRUCTURE PREDICTION.....</b>		
3.1	Problem Formulation.....	27
3.2	New deep inception networks for protein secondary structure prediction .....	29
3.3	New deep inception-inside-inception networks for protein secondary structure prediction (Deep3I) .....	31
3.4	Experimental Results .....	33
3.4.1	PSI-BLAST vs. DELTA-BLAST.....	35
3.4.2	Deep3I vs. the Best Existing Methods .....	36
3.4.3	Effects of Hyper-Parameters of Deep3I.....	38
3.4.4	Results Using Most Recently Released PDB Files.....	39
<b>Chapter 4 A NEW DEEP NEIGHBOR RESIDUAL NETWORK FOR PROTEIN SECONDARY</b>		
<b>STRUCTURE PREDICTION .....</b>		
4.1	DeepNRN – Deep Neighbor-Residual Network .....	41
4.1.1	DeepNRN Architecture .....	41
4.1.2	Batch Normalization and Dropout .....	44
4.1.3	Input Features .....	44
4.1.4	Struct2Struct Network and Iterative Fine-tuning .....	45
4.2	Experimental Results .....	47



4.2.1	Performance Comparison of DeepNRN with Other State-of-the-art Tools Based on the CB513 Data set .....	48
4.2.2	Performance Comparison of DeepNRN with Other State-of-the-art Tools Based on Four Widely Used Data sets .....	49
4.2.3	Effect of Convolution Window Size in Struct2Struct Network and Iterative Refinement.....	50
4.2.4	Exploration of other Network Configurations of DeepNRN .....	53
<b>Chapter 5 PROTEIN BACKBONE TORSION ANGLES PREDICTION USING DEEP RESIDUAL INCEPTION NETWORKS.....</b>		<b>55</b>
5.1	<b>Problem formulation .....</b>	<b>55</b>
5.2	<b>New Deep Residual Inception Networks (DeepRIN) for Torsion Angle Prediction ...</b>	<b>58</b>
5.3	<b>Experimental Results .....</b>	<b>62</b>
<b>Chapter 6 PROTEIN BETA TURN PREDICTION USING DEEP DENSE INCETPION NETWORKS .....</b>		<b>72</b>
6.1	<b>Methods and Materials.....</b>	<b>72</b>
6.1.1	Preliminaries and Problem Formulation.....	72
6.1.2	New Deep Dense Inception Networks for Protein Beta-turn Prediction (DeepDIN)	75
6.1.3	Apply Transfer Learning and Balanced Learning to DeepDIN to Handle Imbalanced Dataset	78
6.1.4	Benchmark datasets .....	80
6.2	<b>Results and Discussion .....</b>	<b>81</b>
6.2.1	How Feature Affects the DeepDIN Performance .....	81

6.2.2	Residue-Level and Turn-Level Two-Class Prediction on BT426 .....	83
6.2.3	Turn-level Nine-Class Prediction on BT6376.....	84
<b>Chapter 7 PROTEIN GAMMA TURN PREDICTION USING DEEP DENSE INCETPION</b>		
<b>NETWORKS .....</b>		<b>86</b>
<b>7.1</b>	<b>Materials and Methods.....</b>	<b>86</b>
7.1.1	Problem formulation .....	86
7.1.2	Model Design .....	88
7.1.3	Model Training.....	92
7.1.4	Experiment Dataset.....	92
<b>7.2</b>	<b>Experimental Results .....</b>	<b>94</b>
<b>7.3</b>	<b>Conclusion and Discussion .....</b>	<b>105</b>
<b>Chapter 8 SUMMARY.....</b>		<b>107</b>
<b>REFERENCE.....</b>		<b>114</b>
<b>VITA .....</b>		<b>132</b>

## LIST OF TABLES

TABLE 1.1 NINE TYPES OF BETA-TURNS AND THEIR DIHEDRAL ANGLES OF CENTRAL RESIDUES IN DEGREES (THE LOCATIONS OF $\text{PHI}_1$ , $\text{PSI}_1$ , $\text{PHI}_2$ AND $\text{PSI}_2$ ARE ALSO ILLUSTRATED IN FIGURE 1).....	6
TABLE 3.1 COMPARISON OF THE PROFILE GENERATION EXECUTION TIME AND DEEP3I Q3 ACCURACY USING PSI-BLAST AND DELTA-BLAST .....	36
TABLE 3.2 Q8 ACCURACY (%) COMPARISON BETWEEN MUFOLD-SS AND EXISTING STATE-OF-THE-ART METHODS USING THE SAME SEQUENCE AND PROFILE OF BENCHMARK CB513. ....	37
TABLE 3.3 Q3 ACCURACY (%) COMPARISON BETWEEN MUFOLD-SS AND OTHER STATE-OF-THE-ART METHODS ON CASP DATASETS. ....	37
TABLE 3.4 Q8 ACCURACY (%) COMPARISON BETWEEN DEEP3I AND OTHER STATE-OF-THE-ART METHODS ON CASP DATASETS. ....	37
TABLE 3.5 Q3 ACCURACY (%) COMPARISON BETWEEN MUFOLD-SS WITH DIFFERENT NUMBER OF BLOCKS AND DEEP INCEPTION NETWORKS WITH DIFFERENT NUMBER OF MODULES.....	38
TABLE 3.6 Q8 ACCURACY (%) COMPARISON BETWEEN DEEP3I WITH DIFFERENT NUMBER OF BLOCKS AND DEEP INCEPTION NETWORKS WITH DIFFERENT NUMBER OF MODULES. ....	39
TABLE 3.7 Q3 (%) AND Q8 (%) COMPARED WITH MUFOLD-SS AND OTHER STATE-OF-THE-ART TOOLS USING RECENTLY PDB. ....	40
TABLE 4.1 PERFORMANCE COMPARISON OF DEEPNRN, SPRO, AND PSIPRED ON Q3 AND Q8 ACCURACY ON THE CB513 DATA SET. ....	48
TABLE 4.2 Q3 (%) ACCURACY RESULTS OF VARIOUS PREDICTION METHODS ON FOUR DATA SETS. ....	49
TABLE 4.3 Q8 (%) ACCURACY RESULTS OF VARIOUS PREDICTION METHODS ON FOUR DATA SETS. ....	50
TABLE 4.4 OTHER NETWORK CONFIGURATION OF DEEPNRN AND PERFORMANCE .....	53
TABLE 5.1 COMPARISON OF MEAN ABSOLUTE ERRORS (MAE) OF PSI-PHI ANGLE PREDICTION BETWEEN DEEPRIN AND BEST EXISTING PREDICTORS USING THE TEST SETS FROM (LI ET AL., 2017).....	65

TABLE 5.2 COMPARISON OF MEAN ABSOLUTE ERRORS (MAE) AND PEARSON CORRELATION COEFFICIENT (PCC) OF PSI-PHI ANGLE PREDICTION BETWEEN DEEPRIN, SPIDER2 AND SPIDER3 USING THE CASP10, 11 AND 12 DATASETS. THE PCC IS WRITTEN IN PARENTHESES. BOLD-FONT NUMBERS IN EACH COLUMN REPRESENT THE BEST RESULT ON A PARTICULAR DATASET. ....	65
TABLE 5.3 COMPARISON OF MEAN ABSOLUTE ERRORS (MAE) AND PEARSON CORRELATION COEFFICIENT (PCC) OF PSI-PHI ANGLE PREDICTION BETWEEN DEEPRIN AND SPIDER2 AND SPIDER3 USING THE RECENTLY RELEASED PDB DATASET. THE PCC IS SHOWN IN PARENTHESES. ....	67
TABLE 5.4 COMPARISON OF MEAN ABSOLUTE ERRORS (MAE) OF PSI-PHI ANGLE PREDICTION BETWEEN DEEPRIN AND SPIDER3 USING THE SAME TRAINING DATASET (SPIDER’S TRAINING SET) AND THE SAME TEST DATASET. ....	71
TABLE 6.1 DIFFERENT FEATURE COMBINATIONS WILL AFFECT PREDICTION PERFORMANCE.....	82
TABLE 6.2 RESIDUE-LEVEL PREDICTION ON BT426.....	83
TABLE 6.3 TURN-LEVEL PREDICTION ON BT426 .....	83
TABLE 7.1 EFFECT OF WINDOW SIZE ON MCC PERFORMANCE.....	95
TABLE 7.2 EFFECT OF DROPOUT ON MCC PERFORMANCE .....	95
TABLE 7.3 EFFECT OF TRAINING SIZE ON TRAINING TIME AND MCC PERFORMANCE .....	95
TABLE 7.4 EFFECT OF DYNAMIC ROUTING ON MCC PERFORMANCE .....	95
TABLE 7.5 PERFORMANCE COMPARISON WITH PREVIOUS PREDICTORS USING GT320 BENCHMARK. ....	98
TABLE 7.6 NON-TURN, INVERSE AND CLASSIC TURN PREDICTION RESULTS.....	100
TABLE 7.7 ABLATION TEST.....	105

## LIST OF FIGURES

FIGURE 1-1 AN ILLUSTRATION OF WHAT PSI-PHI ANGLES ARE .....	5
FIGURE 1-2 AN ILLUSTRATION OF WHAT A BETA-TURN IS. C, O, N, AND H, REPRESENT CARBON, OXYGEN, NITROGEN AND HYDROGEN ATOMS, RESPECTIVELY. R REPRESENTS SIDE CHAIN. THE DASHED LINE REPRESENTS THE HYDROGEN BOND. ....	7
FIGURE-1-3 AN ILLUSTRATION OF GAMMA-TURNS. RED CIRCLES REPRESENT OXYGEN; GREY CIRCLES REPRESENT CARBON; AND BLUE CIRCLES REPRESENT NITROGEN. ....	8
FIGURE 2-1 A RELU ACTIVATION FUNCTION PLOT. ....	23
FIGURE 2-2 A FULLY CONNECTED NETWORK. ....	24
FIGURE 3-1 AN INCEPTION MODULE. THE RED SQUARE “CONV(1)” STANDS FOR CONVOLUTION OPERATION USING WINDOW SIZE 1 AND THE NUMBER OF FILTERS IS 100. THE GREEN SQUARE “CONV(3)” STANDS FOR CONVOLUTION OPERATION USING WINDOW SIZE 3 AND THE NUMBER OF FILTERS IS 100. THE YELLOW SQUARE “CONCATENATE” STANDS FOR FEATURE CONCATENATION..	30
FIGURE 3-2 A DEEP INCEPTION NETWORK CONSISTING OF THREE INCEPTION MODULES, FOLLOWED BY ONE CONVOLUTION AND TWO FULLY-CONNECTED DENSE LAYERS. ....	31
FIGURE 3-3 A DEEP INCEPTION-INSIDE-INCEPTION (DEEP3I) NETWORK THAT CONSISTS OF TWO DEEP3I BLOCKS. EACH DEEP3I BLOCK IS A NESTED INCEPTION NETWORK SELF. THIS NETWORK WAS USED TO GENERATE THE EXPERIMENTAL RESULTS REPORTED IN THIS PAPER.....	32
FIGURE 4-1 THE BASIC BUILDING BLOCK OF DEEPNRN, I.E., NEIGHBOUR-RESIDUAL UNIT. THE SQUARE “CONV3” STANDS FOR CONVOLUTION OPERATION USING A WINDOW SIZE 3, WHILE THE SQUARE “CONCATENATE” STANDS FOR FEATURE CONCATENATION.....	42
FIGURE 4-2 NEIGHBOUR-RESIDUAL BLOCK HAS STACKS OF NEIGHBOR-RESIDUAL UNITS. ....	43
FIGURE 4-3 DEEP NEIGHBOR-RESIDUAL NETWORK (DEEPNRN) ARCHITECTURE. ....	43

FIGURE 4-4 (A) EFFECT ON Q8 OF ITERATIVE REFINEMENT BY APPLYING THE STRUCT2STRUCT NETWORK REPEATEDLY. (B) LEFT TABLE SHOWS THE CONFUSION MATRIX OF THE PREDICTION RESULT OF DEEPRN, AND THE RIGHT TABLE SHOWS THE PREDICTION RESULT OF ADDING ONE STRUT2STRUCT NETWORK LAYER OF WINDOW-SIZE 21. .... 52

FIGURE 4-5 (A) EFFECT ON Q3 OF ITERATIVE REFINEMENT BY REPEATEDLY APPLYING STRUCT2STRUCT NETWORK. (B) LEFT TABLE SHOWS THE CONFUSION MATRIX OF THE PREDICTION RESULT OF DEEPRN, AND THE RIGHT TABLE SHOWS THE PREDICTION RESULT OF ADDING ONE STRUCT2STRUCT NETWORK LAYER OF WINDOW-SIZE 21. .... 53

FIGURE 5-1 AN EXAMPLE OF THE PHYSICO-CHEMICAL FEATURE VECTOR OF A PROTEIN SEQUENCE. EACH AMINO ACID IN THE PROTEIN SEQUENCE IS REPRESENTED AS A VECTOR OF 8 REAL NUMBERS RANGING FROM -1 TO 1. THE FEATURE VECTORS OF THE FIRST 5 AMINO ACIDS ARE SHOWN. .... 56

FIGURE 5-2 AN EXAMPLE OF THE PSI-BLAST PROFILE OF A PROTEIN SEQUENCE. EACH AMINO ACID IN THE PROTEIN SEQUENCE IS REPRESENTED AS A VECTOR OF 21 REAL NUMBERS RANGING FROM 0 TO 1. THE FEATURE VECTORS OF THE FIRST 5 AMINO ACIDS ARE SHOWN. THE THIRD THROUGH THE 19<sup>TH</sup> COLUMNS ARE OMITTED. .... 57

FIGURE 5-3 AN EXAMPLE OF THE HHBLITS PROFILE OF A PROTEIN SEQUENCE. EACH AMINO ACID IN THE PROTEIN SEQUENCE IS REPRESENTED BY A VECTOR OF 31 REAL VALUES RANGING FROM 0 TO 1. THE FEATURE VECTORS OF THE FIRST 5 AMINO ACIDS ARE SHOWN. .... 57

FIGURE 5-4 A RESIDUAL-INCEPTION MODULE OF DEEPRIN. THE GREEN RHOMBUS “CONV(1)” DENOTES A CONVOLUTION OPERATION USING WINDOW SIZE 1 AND THE NUMBER OF FILTERS IS 100. THE ORANGE SQUARE “CONV(3)” DENOTES A CONVOLUTION OPERATION USING WINDOW SIZE 3 AND THE NUMBER OF FILERS IS 100. THE BLUE OVAL “CONCATENATE” DENOTES FEATURE CONCATENATION. .... 59

FIGURE 5-5 ARCHITECTURE OF THE PROPOSED DEEP RESIDUAL INCEPTION NETWORK ARCHITECTURE (DEEPRIN)..... 60

FIGURE 5-6 AVERAGE PSI-PHI ANGLES PREDICTION ERROR (MAES) FOR EACH OF THE EIGHT TYPES OF SECONDARY STRUCTURE ON THE CASP12 DATASET BY DEEPRIN..... 68

FIGURE 5-7 PSI-PHI ANGLE PREDICTION RESULTS OF TWO PROTEINS IN CASP12, T0860 (TOP) AND T0861 (BOTTOM). PREDICTED ANGLE VALUE, TRUE ANGLE VALUE, AND ABSOLUTE ERROR ARE PLOTTED FOR EACH AMINO ACID POSITION, WHICH IS LABELLED BY ITS TRUE SECONDARY STRUCTURE TYPE. THE LOW BLUE BARS, WHICH DENOTE THE ERROR BETWEEN PREDICTED ANGLES AND TRUTH ANGELS..... 70

FIGURE 6-1 (A) SHOWS THE OVERALL PROPOSED MODEL FOR BETA-TURN PREDICTION. (B) SHOWS THE DETAILS OF A DENSE INCEPTION MODULE THAT CONSISTS OF FOUR INCEPTION MODULES, EACH OF WHICH IS FULLY CONNECTED IN A FEED FORWARD FASHION..... 78

FIGURE 7-1 (A) A DEEP INCEPTION CAPSULE NETWORK DESIGN. THE INPUT FEATURES ARE HHBLITS PROFILE (17-BY-30 2D ARRAY) AND PREDICTED SHAPE STRING USING FRAG1D (17-BY-15 2D ARRAY). EACH FEATURE IS CONVOLVED BY A CONVOLUTIONAL LAYER. BOTH CONVOLVED FEATURES THEN GET CONCATENATED. AN INCEPTION BLOCK IS FOLLOWED TO EXTRACT LOW TO MEDIUM FEATURES. A PRIMARY CAPSULE LAYER THEN EXTRACTS HIGHER LEVEL FEATURES. THE FINAL TURN CAPSULE LAYER MAKES PREDICTIONS. (B) AN INCEPTION BLOCK. INSIDE THIS INCEPTION BLOCK: RED SQUARE CONV(1) STANDS FOR CONVOLUTION OPERATION WITH KERNEL SIZE 1. GREEN SQUARE CONV(3) STANDS FOR CONVOLUTION OPERATION WITH KERNEL SIZE 3. YELLOW SQUARE STANDS FOR FEATURE MAP CONCATENATION. (C) ZOOM-IN BETWEEN PRIMARY CAPSULES AND TURN CAPSULES. THE PRIMARY CAPSULE LAYER CONTAINS 32 CHANNELS OF CONVOLUTIONAL 8D CAPSULES. THE FINAL LAYER TURN CAPSULE HAS TWO 16D CAPSULES TO REPRESENT TWO STATES OF THE PREDICTED LABEL: GAMMA-TURN OR NON-GAMMA-TURN. THE COMPUTATION BETWEEN THOSE TWO LAYERS IS DYNAMIC ROUTING. .... 90

FIGURE 7-2 THE FITTING CURVE OF PRECISION (PERCENTAGE OF TRUE POSITIVE IN THE BIN) VERSUS THE CAPSULE LENGTH. THE GREEN LINE IS THE FITTING CURVE AND THE BLUE LINE ( $Y=X^2$ ) IS FOR REFERENCE..... 97

FIGURE 7-3 TRAINING LOSS AND VALIDATION LOSS CURVE OF DEEP INCEPTION CAPSULE NETWORK FOR CLASSIC AND INVERSE GAMMA-TURN. .... 99

FIGURE 7-4 T-SNE PLOTS OF CAPSULE NETWORK FEATURES. **(A)** AND **(B)** ARE PLOTS OF THE INPUT FEATURES AND THE CAPSULE FEATURES, RESPECTIVELY FOR TRAINING DATASET (3000 PROTEINS WITH 1516 TURN SAMPLES). **(C)** AND **(D)** ARE PLOTS OF THE INPUT FEATURES AND THE CAPSULE FEATURES, RESPECTIVELY FOR THE TEST DATASET (500 PROTEINS WITH 312 TURN SAMPLES). RED DOTS REPRESENT NON-TURNS, GREEN DOTS REPRESENT INVERSE TURNS AND BLUE DOTS REPRESENT CLASSIC TURNS. .... 103

FIGURE 7-5 (A) CLASSIC TURN WEBLOGO; (B) INVERSE TURN WEBLOGO; AND (C) NON-TURN WEBLOGO ..... 104



## ABSTRACT

Protein secondary structure, backbone torsion angle and other secondary structure features can provide useful information for protein 3D structure prediction and protein functions. Deep learning offers a new opportunity to significantly improve prediction accuracy. In this dissertation, several new deep neural network architectures are proposed for protein secondary structure prediction: deep inception-inside-inception (Deep3I) networks and deep neighbor residual (DeepNRN) networks for secondary structure prediction; deep residual inception networks (DeepRIN) for backbone torsion angle prediction; deep dense inception networks (DeepDIN) for beta turn prediction; deep inception capsule networks (DeepICN) for gamma turn prediction. Every tool was then implemented as a standalone tool integrated into MUFold package and freely available to research community. A webservice called MUFold-SS-Angle is also developed for protein property prediction.

The input feature to those deep neural networks is a carefully designed feature matrix corresponding to the primary amino acid sequence of a protein, which consists of a rich set of information derived from individual amino acid, as well as the context of the protein sequence. Specifically, the feature matrix is a composition of physio-chemical properties of amino acids, PSI-BLAST profile, HHblits profile and/or predicted shape string. The deep architecture enables effective processing of local and global interactions between amino acids in making accurate prediction. In extensive experiments on multiple datasets, the proposed deep neural architectures outperformed the best existing methods and other deep neural networks significantly: The proposed DeepNRN achieved highest Q8 75.33,

72.9, 70.8 on CASP 10, 11, 12 higher than previous state-of-the-art DeepCNF-SS with 71.8, 72.3, and 69.76. The proposed MUFold-SS (Deep3I) achieved highest Q8 76.47, 74.51, 72.1 on CASP 10, 11, 12. Compared to the recently released state-of-the-art tool, SPIDER3, DeepRIN reduced the Psi angle prediction error by more than 5 degrees and the Phi angle prediction error by more than 2 degrees on average. DeepDIN outperformed significantly BetaTPred3 in both two-class and nine-class beta turn prediction on benchmark BT426 and BT6376. DeepICN is the first application of using capsule network to biological sequence analysis and outperformed all previous gamma-turn predictors on benchmark GT320.

# CHAPTER 1 INTRODUCTION

## 1.1 Protein Sequence, Structure and Function

Protein sequence, or called primary structure of protein, is a sequence of amino acid residues, pair of which is connected by peptide bonds (Sanger and Thompson, 1953). Each amino acid can be one of the twenty different amino acid residues.

Protein secondary structures can be alpha helix, beta sheet, and coil (Pauling and Corey, 1951). The secondary structure of a protein can provide constraints to the protein sequence. Due to hydrophobic forces and side chain interactions between amino acids, protein sequence will fold into stable tertiary structure (Dill, 1990). Two or more tertiary structures will bind together to form the protein quaternary structure.

Previous research work has found that protein structures can determine the protein function (Kendrew *et al.*, 1960; Bjorkman and Parham, 1990). Proteins functions can be enzymatic catalysis, transport and storage, coordinated motion, mechanical support, immune protection, generation and transmission of nerve impulses, and control of growth and differentiation (Laskowski *et al.*, 2003). To understand better what protein functions are, it is important to discovery the protein tertiary structure.

Currently, scientists applied physical methods to determine the protein tertiary structure by using X-ray Crystallography (Bragg, 1975) and Nuclear Magnet Resonance (NMR) spectroscopy (Wuthrich, 1986). So far, the number of discovered protein structure are around 125,000 by the year of 2017 according to the statistics in the Protein Data Bank (PDB) (Berman *et al.*, 1999). However, there are still millions of protein sequences, whose

structure remains unknown and it is time-consuming and labor-intensive to use the abovementioned physical methods to discover the protein tertiary structure.

Early researchers found that the protein sequence can dictate a tertiary structure (Sanger and Thompson, 1953; Anfinsen, 1973), which has founded a heated research area: predicting a protein tertiary structure from its sequence in computational or structural biology. On one hand, predicting protein tertiary structure from its sequence can save time and labor; on the other hand, it provides imperative and useful information to medical sciences such as drug design (Jacobson and Sali, 2004).

## **1.2 Protein Secondary Structure Prediction**

The way in which protein secondary structure elements are permuted and packed (Murzin *et al.*, 1995; Dai and Zhou, 2011) has a large effect on how the protein folds. If the protein secondary structure can be predicted accurately, it can provide useful constraints for 3D protein structure prediction. The protein secondary structure can also help identify protein function domains and may guide the rational design of site-specific mutation experiments (Drozdetskiy *et al.*, 2015). Thus, accurate protein secondary structure prediction would have a major impact on the protein 3D structure prediction (Zhou and Troyanskaya, 2014; Fischer and Eisenberg, 1996; Skolnick *et al.*, 2004; Rohl *et al.*, 2004; Wu *et al.*, 2007), solvent accessibility prediction (Fauchere *et al.*, 1988; Ahmad *et al.*, 2003; Adamczak *et al.*, 2004), and protein disorder prediction (Heffernan *et al.*, 2015; Schlessinger and Rost, 2005). The protein secondary structure is also useful in protein sequence alignment (Radivojac *et al.*, 2007; Zhou and Zhou, 2005) and protein function prediction (Deng and Cheng, 2011; Godzik *et al.*, 2007). The prediction of a

protein secondary structure is often evaluated by the accuracy of the three-class classification, i.e., helix (H), strand (E) and coil (C), which is called Q3 accuracy. In the 1980s, the Q3 accuracy of prediction software was below 60% due to a lack of input features. In the 1990s, the Q3 accuracy increased to over 70% by using the protein evolutionary information in the form of position-specific score matrices. Recently, significant improvement was achieved in Q3 accuracy by applying deep neural networks. Overall, the reported Q3 accuracy went from 69.7% by PHD server (Rost and Sander, 1993), (as well as 76.5% by PSIPRED (Jones, 1999) and 80% by structural property prediction with integrated neural network (SPINE) (Taherzadeh *et al.*, 2016)) to 82% by structural property prediction with the integrated deep neural network (SPIDER2) (Dor and Zhou, 2007). The Q8 accuracy is another evaluation metric to evaluate the accuracy of eight-class classification:  $3_{10}$ -helix (G),  $\alpha$ -helix (H),  $\pi$ -helix (I),  $\beta$ -strand (E),  $\beta$ -bridge (B),  $\beta$ -turn (T), bend (S) and loop or irregular (L) (Murzin *et al.*, 1995; Wang *et al.*, 2016). Q8 accuracy has always been lower than Q3 accuracy. Again, in recent years, significant improvement was achieved on Q8 accuracy by deep neural networks. For example, Wang *et al.* (2016) applied a deep convolutional neural network (CNN) with a conditional random field for secondary structure prediction. They achieved 68.3% Q8 accuracy and 82.3% Q3 accuracy per amino acid on the benchmark CB513 data set. Li and Yu (2016) used a multi-scale convolutional layer followed by three-stacked bidirectional recurrent layers to achieve 69.7% Q8 accuracy on the same test data set. Busia and Jaitly (2017) used CNN and next-step conditioning to achieve 71.4% Q8 accuracy on the same test data set. Heffernan *et al.* (2017) applied long short-term memory bidirectional recurrent neural

networks (LSTM-brNN) and achieved 84% Q3 accuracy on the data set used in their previous studies (Heffernan *et al.*, 2015).

There are some limitations in the earlier methods; for example, they cannot effectively account for non-local interactions between residues that are close in 3D structural space but far from each other in their sequence position (Heffernan *et al.*, 2017). Many existing techniques rely on sliding windows of sizes 10–20 amino acids to capture some “short to intermediate” non-local interactions (Rost and Sander, 1993; Jones, 1999). The recent deep-learning methods for protein secondary structure prediction have some significant advantages over previous methods. For example, the most recent work in (Heffernan *et al.*, 2017) uses the LSTM-brNN network and iterative training. The RNN can capture the long-range interactions without using a window, as traditional machine learning methods do (Rost and Sander, 1993; Jones, 1999). Busia and Jaitly (2017), and Li and Yu (2016) used a multi-scale convolutional layer and a residue network to capture interactions in different ranges. The current deep-learning methods/tools introduced different deep architectural innovations, including Residual network (He *et al.*, 2016; He *et al.*, 2016; Zhang *et al.*, 2017), DenseNet (Huang *et al.*, 2016), Inception network (Szegedy *et al.*, 2016; Szegedy *et al.*, 2016), Batch Normalization (Ioffe and Szegedy, 2015), dropout and weight constraining (Srivastava *et al.*, 2014), etc.

### **1.3 Protein Backbone Torsion Angle Prediction**

Predicting a protein structure accurately from its amino acid sequence information alone has remained difficult for half a century (Gibson and Scheraga, 1967; Dill and Caccallum, 2012; Zhou *et al.*, 2010). One approach of helping predict a protein structure is to predict

its backbone torsion angles (Psi and Phi). The backbone structure of a protein can be determined by its torsion angles (see Figure 1.1 for illustration of what Psi Phi angles are). Given an amino acid sequence, a number of machine-learning methods have been applied to predict the real-value torsion angles for each residue. The prediction accuracies have improved gradually over the years (Dor and Zhou, 2007, Xue *et al.*, 2008, Faraggi *et al.*, 2009) and are approaching the ones estimated from NMR chemical shifts (Faraggi *et al.*, 2009). It has been demonstrated that the predicted torsion angles are useful to improve *ab initio* structure prediction (Faraggi *et al.*, 2009, Simons *et al.*, 1999), sequence alignment (Huang and Bystroff., 2005), secondary structure prediction (Mooney *et al.*, 2006; Wood and Hirst, 2005), and template-based tertiary structure prediction and fold recognition (Yang *et al.*, 2011; Karchin *et al.*, 2003, Zhang *et al.*, 2008).

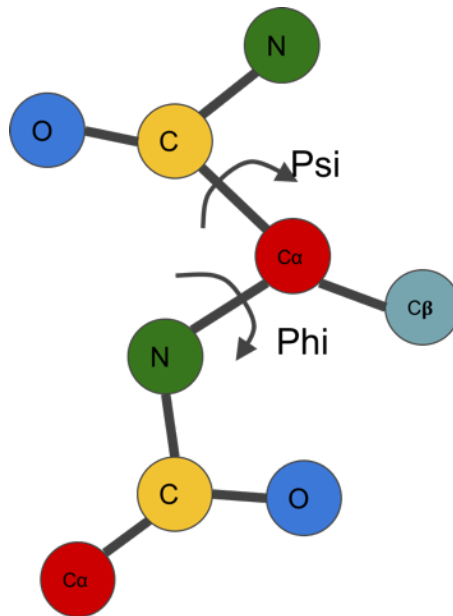


Figure 1-1 an illustration of what Psi-Phi angles are

Existing torsion angle prediction methods formulate the problem slightly differently. Some convert torsion angles to discrete classes (Kuang *et al.*, 2004; Kang *et al.*, 1993),

while others treat them as continuous values (Dor and Zhou, 2007; Xue *et al.*, 2008; Wood and Hirst, 2005; Lyons *et al.*, 2014). Various machine-learning methods, especially deep neural networks in recent years, have been applied to this prediction problem. In (Li *et al.*, 2017), a deep recurrent restricted Boltzmann machine (DreRBM) was developed to achieve comparable results to SPIDER2 (Yang *et al.*, 2016), a well-known software tool. SPIDER3 (Heffernan *et al.*, 2017), a recently released tool that improved over SPIDER2, applied long-short term memory (Hochreiter and Schmidhuber, 1997) bidirectional recurrent neural networks (LSTM-biRNN) (Mikolov and Zweig, 2012) to achieve 5% to 10% reduction in the mean absolute error for Psi and Phi angle predictions, respectively, over SPIDER2.

#### 1.4 Protein Beta Turn Prediction

By definition, a beta-turn contains four consecutive residues (denoted by  $i$ ,  $i+1$ ,  $i+2$ ,  $i+3$ ) if the distance between the  $C\alpha$  atom of residue  $i$  and the  $C\alpha$  atom of residue  $i+3$  is less than 7 Å and if the central two residues are not helical (Lewis *et al.*, 1973) (see Figure 1-2, an illustration of what a beta-turn is). There are nine types of beta-turns, which are classified based on the dihedral angles of central residues in a turn as shown in Table 1.1, can be assigned by using the PROMOTIF software (Hutchinson and Thornton, 1994). Beta-turns play an important role in mediating interaction between peptide ligands and their receptors (Li *et al.*, 1999). In protein design, loop segments and hairpins can be formed by introducing beta-turns in proteins and peptides (Ramirez-Alvarado *et al.*, 1997). Hence, it is important to predict beta-turns from a protein sequence (Kaur *et al.*, 2002).

*Table 1.1 Nine types of beta-turns and their dihedral angles of central residues in degrees (The locations of  $\Phi_i$ ,  $\Psi_i$ ,  $\Phi_2$  and  $\Psi_2$  are also illustrated in Figure 1)*



Turn Type	Phi <sub>1</sub>	Psi <sub>1</sub>	Phi <sub>2</sub>	Psi <sub>2</sub>
I	-60	-30	-90	0
I'	60	30	90	0
II	-60	120	80	0
II'	60	-120	-80	0
IV	-61	10	-53	17
VIII	-60	-30	-120	120
VIb	-135	135	-75	160
VIa1	-60	120	-90	0
VIa2	-120	120	-60	0

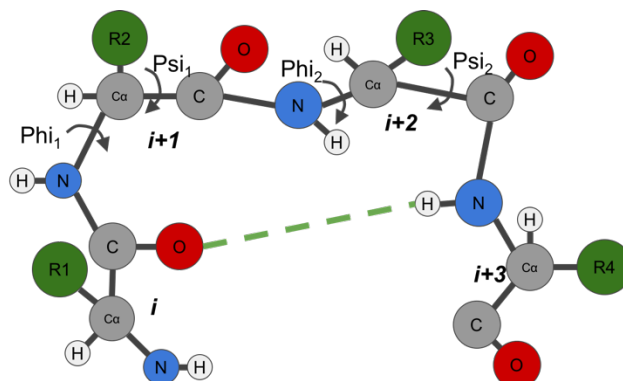


Figure 1-2 An illustration of what a beta-turn is. C, O, N, and H, represent carbon, oxygen, nitrogen and hydrogen atoms, respectively. R represents side chain. The dashed line represents the hydrogen bond.

## 1.5 Protein Gamma Turn Prediction

Gamma-turns are the second most commonly found turns (the first is beta-turns) in proteins. By definition, a gamma-turn contains three consecutive residues (denoted by  $i$ ,  $i+1$ ,  $i+2$ ) and a hydrogen bond between the backbone  $CO_i$  and the backbone  $NH_{i+2}$  (see Figure 1-3). There are two types of gamma-turns: classic and inverse (Bystrov *et al.*, 1969). According to (Guruprasad and Rajkumar, 2000), gamma-turns account for 3.4% of total amino acids in proteins. Gamma-turns can be assigned based on protein 3D structures by using Promotif software (Hutchinson and Thornton, 1994). There are two types of gamma-turn prediction problems: (1) gamma-turn/non-gamma-turn prediction (Guruprasad *et al.*, 2003; Kaur and Raghava, 2002; Pham *et al.*, 2005), and (2) gamma-turn type prediction (Chou, 1997; Chou and Blinn 1999; Jahandideh *et al.*, 2007).

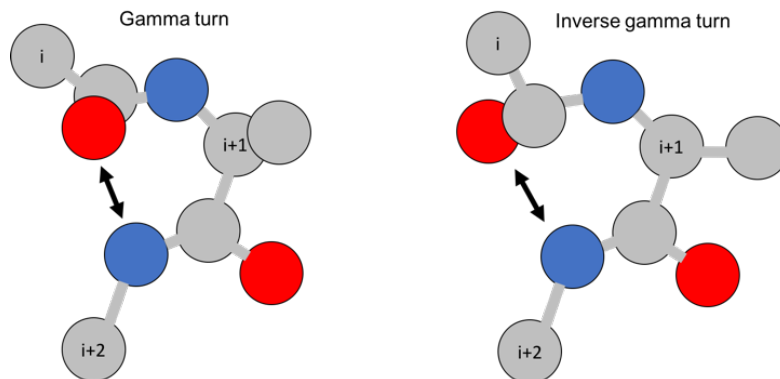


Figure-1-3 An illustration of gamma-turns. Red circles represent oxygen; grey circles represent carbon; and blue circles represent nitrogen.

## 1.6 Contributions

- (1) A new very deep learning network architecture, Deep3I, was proposed to effectively process both local and global interactions between amino acids in making accurate secondary structure prediction and Psi-Phi angle prediction. Extensive experimental results show that the new method outperforms the best existing methods and other deep neural networks significantly. An open-source tool Deep3I-SS was implemented based on the new method. This tool can predict the protein secondary structure and the Psi-Phi angles fast and accurately.
- (2) DeepNRN, a new deep-learning network with new architecture, is proposed for protein secondary structure prediction; and experimental results on the CB513, CASP10, CASP11, CASP12 benchmark data sets show that DeepNRN outperforms existing methods and obtains the best results on multiple data sets.
- (3) A new deep neural network architecture, DeepRIN, is proposed to effectively capture and process both local and global interactions between amino acids in a protein sequence. Extensive experiments using popular benchmark datasets were conducted to demonstrate that DeepRIN outperformed the best existing tools

significantly. A software tool based on DeepRIN is made available to the research community for download.

(4) A new deep dense inception network (DeepDIN) is proposed for beta-turn prediction, which takes advantages of the state-of-the-art deep neural network design of DenseNet and Inception network. A test on a recent BT6376 benchmark shows that the DeepDIN outperformed the previous best BetaTPred3 significantly in both the overall prediction accuracy and the nine-type beta-turn classification. A tool, called MUFold-BetaTurn, was developed, which is the first beta-turn prediction tool utilizing deep neural networks.

(5) A deep inception capsule network for gamma-turn prediction. Its performance on the gamma-turn benchmark GT320 achieved an MCC of 0.45, which significantly outperformed the previous best method with an MCC of 0.38. This is the first gamma-turn prediction method utilizing deep neural networks. Also, to our knowledge, it is the first published bioinformatics application utilizing capsule network, which will provide a useful example for the community.

## **1.7 Outline of the Dissertation**

The dissertation is arranged as followed:

Chapter 1 describes the introduction

Chapter 2 describes the background and related work of protein secondary structure prediction and backbone torsion angle prediction.

Chapter 3 describes the deep inception-inside-inception network (Deep3I) to predict the protein secondary structure. The Deep3I is consists of hierarchical layers of Inception

networks (Szegedy *et al.*, 2017). The stacked inception blocks effectively capture the long-range residue interactions. The proposed Deep3I network outperforms previous best predictors such as DeepCNF-SS in three-state and eight-state. A secondary structure prediction tool was made using this network and is freely available for research community to use.

Chapter 4 describes the deep near neighbor residual network (DeepNRN) to predict the protein secondary structure. It modifies the residual network (He *et al.*, 2016), which was originally used for image classification, and then applies to protein structure prediction problem. The modified residual network can also alleviate the gradient vanishing problem and but also propagate the features into deep layers of network.

Chapter 5 describes the deep inception residual network (DeepIRN) and applies it to protein Psi-Phi angle prediction. This method significantly outperforms current state-of-art tool SPIDER3 in public benchmarks and recently released PDB data sets. DeepIRN combines inception and residual network and take advantages of both networks.

Chapter 6 describes the deep dense inception network (DeepDIN) and applies it to protein beta-turn prediction. This method significantly outperforms current state-of-art tool BetaTPred3 in public benchmarks BT426 and BT6376. DeepDIN combines inception and dense network and take advantages of both networks.

Chapter 7 describes the deep inception capsule network (DeepICN) and applies it to protein gamma-turn prediction. This method significantly outperforms previous predictors on public benchmarks GT320. DeepICN combines inception and capsule network and take advantages of both networks. Some other capsule features were explored and tested.

Chapter 8 summarizes the achievements and major contributions.

## CHAPTER 2 RELATED WORK AND BACKGROUND

### 2.1 Protein Secondary Structure Prediction

Protein secondary structure prediction has been a very active research area in the past 30 years. A small improvement of its accuracy can have a significant impact on many related research problems and software tools.

Various machine learning methods, including different neural networks, have been used by previous protein secondary structure predictors. Over the years, the reported Q3 accuracy on benchmark datasets went from 69.7% by the PHD server (Rost and Sander, 1993) in 1993, to 76.5% by PSIPRED (Jones 1999), to 80% by structural property prediction with integrated neural networks (SPINE) (Dor and Zhou, 2007), to 79-80% by SSPro using bidirectional recurrent neural networks (Cheng *et al.*, 2005), and to 82% by structural property prediction with integrated deep neural network (SPIDER2) (Heffernan *et al.*, 2015). The previous predictors can be classified into two categories: template based, which is using the template information and template free., which is using only profile information. In terms of method, they can be classified into two categories: machine learning or deep learning.

Some well-known secondary structure predictors are PHD server (Rost and Snader, 1993), PSIPRED (Jones, 1999), SSPro (Cheng *et al.*, 2005) to name a few, which utilizing two-layer traditional neural network and sliding window to preprocess the input. Until recently the DeepCNF-SS (Wang *et al.*, 2016) server is the first method using deep convolutional neural fields for secondary structure prediction. Some popular predictors are reviewed in detail as followed:

PSIPRED (Jones, 1999), one of the most cited and/or used secondary structure predictor in the Bioinformatics community, represents the traditional machine learning template-free category of secondary structure prediction. It consists of three states: 1) sequence profile generation 2) prediction of initial secondary structure and 3) fine-tune/filter of the predicted structure using Struct2Struct, network. For the profile, it is often generated by PSI-BLAST (Altschul *et al.*, 1997). The profile then is used to extract the position-specific scoring matrix (PSSM) and the matrix is used as input for the neural network. PSIPRED applied a sliding window of size 15 on the sequence length dimension of PSSM to get chunks of input data to train the network. The output from the first network is then fed into a second network (Struct2Struct) to make a final 3-state prediction. The application of Struct2Struct is to fine-tune the prediction from first network. There could be some prediction violate the consecutive patterns of a protein secondary structure sequence. (For example, an alpha helix should consist of at least three consecutive amino acids). The overall performance of PSIPRED achieved average Q3 score 78%.

Porter (Mirabello and Pollastri, 2013) server applied two cascaded bidirectional recurrent neural networks: one for prediction and the other act as Struct2Struct network. The Porter was trained using five-fold cross validation on 7522 non-redundant protein sequences with less than 25 percent sequence identity and a high-resolution of 2218 proteins. The Q3 accuracy achieved 82%.

Template-based C8-SeCOndaRy Structure PredictION (SCORPION) (Yaseen and Li, 2014) server falls into the template-based method for secondary structure prediction. It applied three separate neural networks: first for prediction, second for structure filter, and third for refinement using PSSM and modified SS scores. Their innovation is to use

statistical context-based scores as well as the structural information as encoded features to train neural networks to achieve the improvement on secondary structure up to Q3 82.7%.

SPIDER2 (Heffernan *et al.*, 2015) falls into the template-free, deep learning category. It applied deep neural networks and used an iterative training to improve the secondary structure. SPIDER2's input features contain the predicted backbone torsion angle, predicted secondary structure and predicted solvent accessibility. The predicted features are reused to train the deep neural network for three times, iteratively. SPIDER2 achieved Q3 81.2% on the independent test set containing 1199 high-resolution proteins.

The current state-of-the-art DeepCNF-SS (Wang *et al.*, 2016) is the first method using deep convolutional neural fields for secondary structure prediction. The DeepCNF model contains two modules: 1) the Conditional Random Fields (CRF) module consisting of the top layer and the label layer; 2) the deep convolutional neural network (DCNN) module covering the input to the top layer. Experimental results show that the DeepCNF can obtain about 84% Q3 accuracy.

In recent years, significant improvement has also been achieved on Q8 accuracy by deep neural networks. In (Wang *et al.*, 2016), deep convolutional neural networks integrated with a conditional random field was proposed and achieved 68.3% Q8 accuracy and 82.3% Q3 accuracy on the benchmark CB513 dataset. In (Li and Yu, 2016), a deep neural network with multi-scale convolutional layers followed by three stacked bidirectional recurrent layers was proposed and reached 69.7% Q8 accuracy on the same test dataset. In (Busia and Jaitly, 2017), deep convolutional neural networks with next-step conditioning technique were proposed and obtained 71.4% Q8 accuracy. In (Heffernan *et al.*, 2017), long short-term memory bidirectional recurrent neural networks (LSTM-bRNN) were

applied to this problem and a tool named SPIDER3 was developed, achieving 84% Q3 accuracy and a reduction of 5% and 10% in the mean absolute error for Psi-Phi angle prediction on the dataset used in their previous studies (Heffernan *et al.*, 2015). These successes encouraged us to explore more advanced deep-learning architectures. The current work improves upon the previous methods through the development and application of new neural network architectures, including Residual networks (He *et al.*, 2016), Inception networks (Szegedy *et al.*, 2017), and Batch Normalization (Ioffe and Szegedy, 2015). Other than the prediction accuracy, secondary structure prediction provides an ideal testbed for exploring and testing these state-of-the-art deep learning methods.

In the earlier predictors, they rely on sliding window and neural network to predict secondary structure. This way of processing the input has some limitations because it does not take into consider the far range residue interactions. Also, the sliding window can only cover a fix number of amino acids. In this dissertation, the whole protein sequence is taken into consider and feed into the deep neural network. The design of our network uses of the state-of-the-art deep neural networks, i.e. Inception Network (Szegedy *et al.*, 2017) and ResNet (He *et al.*, 2016), which has shown successful results in image classification applications. The ability of those deep neural networks can effectively extract high level features from protein sequences.

## **2.2 Protein Backbone Torsion Angle Prediction**

Traditional neural networks have been applied to torsion angle prediction for a long time. They typically used windows of neighboring amino acid residues to capture



relationship between residues within a short range (Yang *et al.*, 2016; Wu and Zhang, 2008). The ability of capturing the interactions between residues is limited by a small, fixed window size. Long-range, non-local residue relationships are not captured and used in these prediction methods. With the development of deep learning, deep neural networks are capable of capturing and using long-range information in prediction. For example, SPIDER3 used LSTM-biRNN to capture both short and long-range residue information effectively. In addition to deep recurrent networks, deep convolutional neural networks (DCNN) has been applied in a large number of challenging machine learning tasks, such as image recognition (Krizhevsky *et al.*, 2017; Pfister *et al.*, 2015; Lawrence *et al.*, 1997), automatic machine translation (Collobert and Weston, 2008), text generation (Vinyals *et al.*, 2015), and achieved great success.

Several predictors can be classified into two categories: machine learning and deep learning for protein backbone torsion angle prediction:

ANGLOR (Wu and Zhang, 2008) server falls into machine learning categories. It applied neural network and support vector machines (SVM) for Psi-Phi angle prediction. The profiles of the input protein sequence are generated by PSI-BLAST. A sliding window of size 21 is applied to preprocess the input. In ANGLOR server, the Psi and Phi angles are predicted separately, Phi is predicted using neural network and Psi is predicted using SVM. The ANGLOR achieved mean absolute errors (MAE) of Psi-Phi angles: 46 and 28 degrees.

SPIDER2 (Heffernan *et al.*, 2015) falls into deep learning categories of backbone torsion angle prediction. It applied deep neural networks and used an iterative training to improve the secondary structure. SPIDER2's input features contain the predicted backbone

torsion angle, predicted secondary structure and predicted solvent accessibility. The predicted features are reused to train the deep neural network for three times, iteratively. SPIDER2 achieved MAE of 30 and 19 degrees on Psi-Phi angles.

SPIDER3 (Heffernan *et al.*, 2017) applied bidirectional recurrent neural networks (biRNN) for improving prediction of protein backbone angles. SPIDER3's input features contain the predicted backbone torsion angle, predicted secondary structure and predicted solvent accessibility. The predicted features are reused to train the biRNN for four times, iteratively. SPIDER3 achieved MAE of 10 and 5 degrees reduction on Psi-Phi angles compared to SPIDER2.

In the earlier predictors, they rely on sliding window and neural network to predict backbone torsion angle. This way of processing the input has some limitations because it does not take into consider the far range residue interactions. Also, the sliding window can only cover a fix number of amino acids. Also, early predictors rely on PSIPRED to get the predicted three state secondary structure for the input feature of torsion angle prediction. In our proposed method, our network can effectively predict eight state secondary structure by itself, which can be again used as input feature for torsion angle prediction. The early method like ANGLOR server predict Psi and Phi separately using two different system, which have some drawback because Psi and Phi angle comes in pairs and may have interactions with each other. The prediction may be improved if both angles can be predicted in pairs together.

Recently, many advanced deep-learning architectures, such as VGG (Pfister *et al.*, 2015), Inception (Szegedy *et al.*, 2017), Xception (Chollet, 2016), ResNet (He *et al.*, 2016), DenseNet (Huang *et al.*, 2016), have emerged in recent years with improved performance

over previous methods in various applications. Inspired by these cutting-edge architectures, in this dissertation, a new deep residual inception network architecture, called DeepRIN, is proposed for the prediction of torsion angles. The input to DeepRIN is a carefully designed feature matrix representing the primary sequence of a protein, which consists of a rich set of information for individual amino acid and the context of the protein sequence. DeepRIN is designed based on the ideas of inception networks and residual networks and predicts sine and cosine values of Psi and Phi angles to remove periodicity, which can then be converted back to angle values. Our design is utilizing the state-of-the-art deep neural networks i.e. Inception Network (Szegedy *et al.*, 2017) and ResNet (He *et al.*, 2016), which has shown successful results in image classification applications. The ability of those deep neural networks can effectively extract high level features from protein sequences. Also compared with early predictors, the proposed DeepRIN takes whole protein sequence as input and used to train the neural network for angle prediction. In this way, the long range of amino acid interaction will be considered, and the high-level features will be able to be extracted.

### **2.3 Protein Beta-turn Prediction**

The early predictors (Hutchinson and Thornton, 1994; Chou and Fasman 1974; Chou and Fasman, 1979) used statistical information derived from protein tertiary structures to predict beta-turns. The statistical methods were based on the positional frequencies of amino acid residues. Zhang and Chou (1997) further observed the pairing of first and the fourth residues, and of the second and the third residues, which plays an important role in beta-turn formation. They proposed the 1-4 and 2-3 correlation model to predict beta-turns

(Zhang and Chou, 1997). Later, Chou's team applied a sequence coupled approach based on the first-order Markov chain to further improve their prediction model (Chou, 1997). Kaur and Raghava (2002) developed a web server, called BetaTPred, which implemented this model and achieved a maximum (Matthew Correlation Coefficient) MCC of 0.26 in beta-turn prediction.

McGregor *et al.* (1989) used neural networks to predict beta-turns, which is the first machine learning approach for beta-turn prediction, and they achieved an MCC of 0.20. Shepherd *et al.* (1999) developed BTPred using secondary structure information as input and achieved MCC of 0.34. Kim (2004) applied a K-nearest neighbor method for beta-turn prediction and improved MCC to 0.40. Fuchs and Alix (2005) further improved the MCC to 0.42 by incorporating multiple features such as propensities, secondary structure and position specific scoring matrix (PSSM). Kaur and Raghava (2004) developed the BetaTPred2 server, which used a two-layer neural network with an MCC of up to 0.43. Kirschner and Frishman (2008) developed MOLEBRNN using a novel bidirectional recurrent neural network, with an MCC of up to 0.45. Hu and Li (2008) used support vector machine (SVM) and incorporated features such as increment of diversity, position conservation scoring function and secondary structure to raise the MCC up to 0.47. Zheng and Kurgan (2008) used the predicted secondary structure from PSIPRED (Jones 1999), JNET (Cole *et al.*, 2008), TRANSEEC (Montgomerie *et al.*, 2006), and PROTEUS2 (Montgomerie *et al.*, 2008) to improve the performance. Kountouris and Hirst (2010) used predicted dihedral angles along with PSSM and predicted secondary structures to achieve MCC of 0.49. Petersen *et al.* (2010) developed the NetTurnP server with an MCC of 0.50 by using independent four models for predicting four positions in a beta-turn. Singh *et al.*

(2015) developed the BetaTPred3 server to achieve MCC of 0.51 using a random forest method.

The above-mentioned machine-learning methods achieved some successful results in beta-turn prediction. However, there is large room for improvement, particularly in predicting nine types of beta-turns. Most of these previous methods relied on a sliding window of 4-10 amino acid residues to capture short interactions. Also, previous neural networks with one or two layers (shallow neural networks) could not extract high-level features from input datasets. So far, no deep neural networks have been applied to beta-turn prediction. Deep neural networks can learn representations of data with multiple levels of abstraction (LeCun et al., 2015), which provides a new opportunity to this old research problem.

## **2.4 Protein Gamma-turn Prediction**

The previous methods can be roughly classified into two categories: statistical methods and machine-learning methods. Early predictors (Alkorta *et al.*, 1994; Kaur and Raghava, 2002; Guruprasad *et al.*, 2003) built statistical model and machine-learning method to predict gamma-turns. For example, Garnier *et al.* (1978), Gibrat *et al.* (1987), and Chou (1997) applied statistical models while Pham *et al.* (2005) employed support vector machine (SVM). The gamma-turn prediction has improved gradually, and the improvement comes from both methods and features used. Chou and Blinn (1997) applied a residue-coupled model and achieved prediction MCC 0.08. Kaur and Raghava (2003) used multiple sequence alignments as the feature input and achieved MCC 0.17. Hu and Li (2008) applied SVM and achieved MCC 0.18. Zhu *et al.* (2012) used shape string and position specific scoring matrix (PSSM) from PSIBLAST as inputs and achieved MCC

0.38, which had the best performance prior to this study. The machine-learning methods outperformed statistical methods greatly. However, the gamma-turns prediction performance is still quite low due to several reasons: (1) the dataset is very imbalanced, with about 30:1 of non-gamma-turns and gamma-turns; (2) gamma-turns are relatively rare in proteins, yielding a small training sample size; (3) previous machine-learning methods have not fully exploited the relevant features of gamma-turns. The deep-learning framework may provide a more powerful approach for protein sequence analysis and prediction problems. (Fang *et al.*, 2017; Fang *et al.*, 2018; Fang *et al.*, 2018; Wang *et al.*, 2017) than previous machine-learning techniques.

## **2.5 Deep Neural Network**

Compared with traditional neural networks, deep neural networks usually have many layers. In deep neural networks, each layer of nodes can extract a distinct set of features from its previous layer's activation output. The deeper of the network, the more complex and higher level feature the nodes will recognize. The deeper layer can aggregate and recombine features from shallow previous layers. The deeper layer can learn/extract higher level features from shallow layer. This hierarchy of increasing complexity and feature abstraction makes deep neural network can handle very large dataset.

Deep neural networks usually have stacked neural networks, which means the networks can have several layers. Each layer has many nodes and a node is the place where multiply the inputs with weights and added by biases.

## 2.6 Convolutional Neural Network

Convolutional Neural Networks (CNNs) are within category of Neural Networks. CNNs are effectively used and have shown successful results in image recognition and classification (Razavian *et al.*, 2014; Ciregan *et al.*, 2012; Krizhevsky *et al.*, 2012). CNNs have also been used in recognizing faces (Parkhi *et al.*, 2015), objects (Ren *et al.*, 2015) and traffic signs (Stallkamp *et al.*, 2011). CNNs are very important for many machine learning applications today.

Several new deep CNNs have been proposed recently which are all improvement based on the LeNet (LeCun *et al.*, 1998).

In CNNs, several important terminologies are used and defined as followed:

- **Channel:** is used to describe a certain component of an image. Usually, an image taken from a standard digital camera consists of red, green, and blue channels. Each channel contains pixel values ranging from 0 to 255.
- **Grayscale:** is used to describe a one channel image. The value of each pixel of a grayscale image is ranging from 0 to 255, where 0 is black and 255 is white.
- **Depth:** is the number of filters used to perform the convolution operation. For example Conv(3) means using three distinct filters to perform convolution on the input image.
- **Stride:** is the number of pixels that filter matrix is slid over the input image. For example, when the stride is 2, two pixels will be skipped at a time when the convolution filter is slid around.

- **Padding:** Usually zeros are padded to the input matrix around the board so that the convolution filter can be applied to the border of the input matrix so that the output has the same length as the original input. This is often used in full convolution.

The Convolution operation from CNNs can effectively extract features from input images. It can extract/learn the spatial relationship between pixels using small convolution kernels. The convolution between two function  $f$  and  $g$  can be defined as followed:

$$(f * g)(t) = \int_{-\infty}^{+\infty} f(\tau)g(t - \tau)d\tau$$

## 2.7 Residual Neural Network (ResNet)

Residual neural network (ResNet) was first proposed by He *et al* (2016). Their networks won the first place in ImageNet (Deng *et al.*, 2009) competition. The powerfulness and robustness of ResNets has been applied to various image recognition tasks (He *et al.*, 2016), speech recognition (Xiong *et al.*, 2017).

The ResNet was proposed to tackle the degradation problem that many deep neural networks suffer from.

**Degradation problem:** when the network depth is increasing, the accuracy gets saturated and then degrades rapidly. Such kind of degradation is not caused by overfitting, so simply adding more layers to a deep model will not solve the problem but on the contrary causing higher training error.

He *et al* (2016) proposed residual block to tackle the degradation problem. The shortcut connection from the input to output can effectively solve the vanishing/ exploding gradients problem. Inspired by ResNet, other variations of ResNet has been proposed:



Wide Residual Network (Zagoruyko and Komodakis, 2016), ResNet in ResNet (Targ *et al.*, 2016), Weighted ResNet (Shen *et al.*, 2016).

## 2.8 ReLU, Batch Normalization and Fully Connected Layer

Rectified Linear Unit (ReLU) (Nair and Hinton, 2010) has been used after Convolution operation. The ReLU activation function is used to replace all negative values in the feature map by zero. The purpose of applying ReLU activation after the convolution operation is to introduce the non-linearity. In different applications, *tanh* or *sigmoid* activation functions are also used. The ReLU activation function is defined as followed:

$$f(x) = \max(0, x)$$

where  $x$  is the input to a neuron. Figure 2-1 shows a plot of ReLU function.

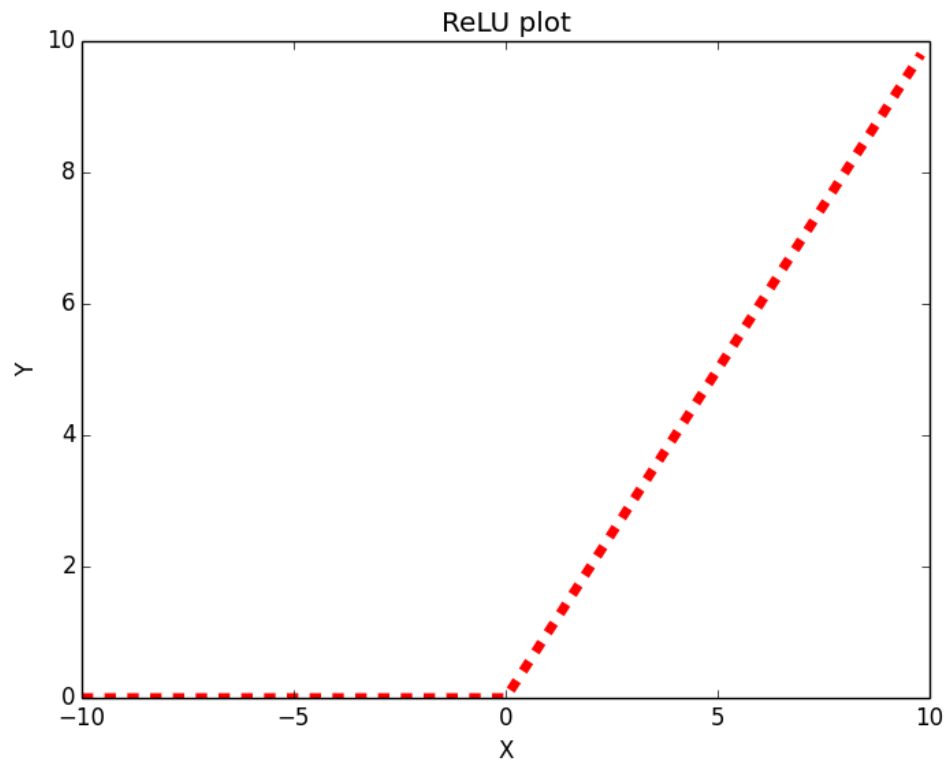


Figure 2-1 a ReLU activation function plot.

Fully connected layer is usually used in the output layer with Softmax as the activation function. A fully connect layer means every neuron in the previous layer is fully connected with every neuron in the next layer. The output of CNNs are high-level features extracted from input data. Those features can then be fed into fully connect layer for performing the classification task.

Since the Softmax is used as activation function, the output probabilities from the fully connected layer sums to 1. Softmax activation function is defined as followed:

$$\sigma(z)_j = e^{z_j} / \sum_{k=1}^K e^{z_k}, \text{ for } j = 1, \dots, K$$

Figure 2-2 shows a fully connected network:

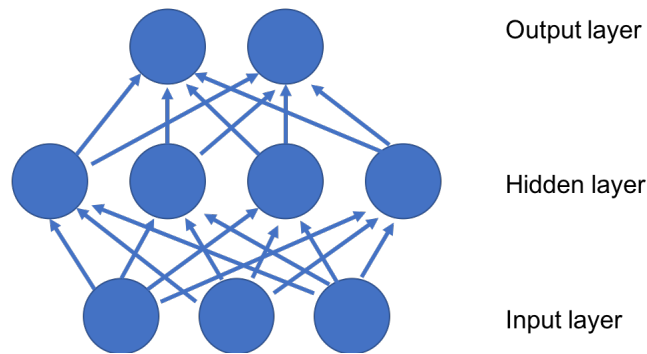


*Figure 2-2 a fully connected network.*

Batch Normalization is proposed by Ioffe and Szegedy (2015). It helps deep network to train fast and overall have higher accuracy. The potential training time is shortened. The mechanism behind normalization is that it shifts input to zero-mean and unit variance so that features have the same scale. When deep neural networks are trained, the weights and parameters are adjusted which may cause the data too large or small again. The batch normalization technique can normalize the data in each batch to solve the problem.

## 2.9 Dense Network

Residual networks (He *et al.*, 2016) add skip-connection so that the feature maps from earlier layer can be bypassed into deep layers. To further improve the information flow between layers, Huang *et al.*, (2016) proposed a different connectivity pattern: apply direct connections from any layer to all the subsequent layers in a fully connected fashion. Consequently, the  $l$ -th layer receives the feature-maps of all preceding layers,  $x_0, \dots, x_{l-1}$  as input:  $x_l = H_l([x_0, x_1, \dots, x_{l-1}])$  where  $[x_0, x_1, \dots, x_{l-1}]$  are the concatenation of the feature-maps produced in layers  $0, \dots, l-1$ .

## 2.10 Capsule Network

Capsule Network (Sabour *et al.*, 2017) is using capsule which is a group of neurons whose outputs represent different properties of the same entity. A capsule is a group of neurons that not only capsule the likelihood but also the parameters of the specific feature. Compared with a neuron, which outputs a value, a capsule  $v$  can output a vector. Each dimension of  $v$  represents the characteristics of patterns and the norm of  $v$  represents the existence.

In the capsule network, squashing activation function (Sabour *et al.*, 2017) was applied in the computation between the primary capsule layer and the turn capsule layer as follows:

$$v_j = \frac{\|s_j\|}{1 + \|s_j\|^2} \frac{s_j}{\|s_j\|}$$

where  $v_j$  is the vector output of capsule  $j$  and  $s_j$  is its total output.

The dynamic routing algorithm (Sabour *et al.*, 2017) is as follows:

---

Routing Algorithm:

---

Routing ( $\hat{u}_{j|i}, r, l$ )

For all capsule  $i$  in layer  $l$  and capsule  $j$  in layer  $(l+1)$ :  $b_{i,j} \leftarrow 0$

For  $r$  iteration do

For all capsule  $i$  in layer  $l$ :  $c_i \leftarrow \text{softmax}(b_i)$

For all capsule  $j$  in layer  $(l + 1)$ :  $\mathbf{s}_j \leftarrow \sum_i c_{ij} \hat{\mathbf{u}}_{j|i}$

For all capsule  $j$  in layer  $(l + 1)$ :  $\mathbf{v}_j \leftarrow \text{squash}(\mathbf{s}_j)$

For all capsule  $i$  in layer  $l$  and capsule  $j$  in layer  $(l + 1)$ :  $b_{i,j} \leftarrow b_{i,j} + \hat{u}_{j|i} \cdot \mathbf{v}_j$

---

# CHAPTER 3 NEW DEEP INCEPTION-INSIDE-INCEPTION NETWORKS FOR PROTEIN SECONDARY STRUCTURE PREDICTION

## 3.1 Problem Formulation

Protein secondary structure prediction is that given the amino acid sequence, also called primary sequence, of a protein, predict the secondary structure type of each amino acid. In three-class classification, the secondary structure type is one out of three, helix (H), strand (E) and coil (C). In eight-class classification, the secondary structure type is one out of eight: (G, H, I, E, B, T, S, L).

To make accurate prediction, it is important to provide useful input features to machine learning methods. In our method, we carefully design a feature matrix corresponding to the primary amino acid sequence of a protein, which consists of a rich set of information derived from individual amino acid, as well as the context of the protein sequence.

Specifically, the feature matrix is a composition of physio-chemical properties of amino acids, PSI-BLAST profile, and HHblits profile. Figure 3.1 shows an example of the physio-chemical feature vector. Each amino acid in the protein sequence is represented as a vector of 8 real numbers ranging from -1 to 1. The vector consists of the seven physio-chemical properties as in (Frauchere *et al.*, 1988) plus a number of value 0 or 1 representing the existence of an amino acid at this position as an input (called *NoSeq* label). The reason of adding the *NoSeq* label is because the proposed deep neural networks are designed to take a fixed size input, such as a sequence of length 700 in our experiment. Then, to run a protein sequence shorter than 700 through the network, the protein sequence will be padded

at the end with 0 values and the *NoSeq* label is set to 1. For example, if the length of a protein is 500, then the first 500 rows have *NoSeq* label set to 0, and the last 200 rows have 0 values in the first 7 columns and 1 in the last column.

The second set of useful features comes from the protein profiles generated using PSI-BLAST (Altschul *et al.*, 1997). In our experiments, the PSI-BLAST software parameters were set to (*evaluate*: 0.001; *num\_iterations*: 3; *db*: UniRef50) to generate PSSM, which was then transformed by the sigmoid function into the range (0, 1). Each amino acid in the protein sequence is represented as a vector of 21 real numbers ranging from 0 to 1, representing the 20 amino acids PSSM value plus a *NoSeq* label in the last column. The feature vectors of the first 5 amino acids are shown. The third through nineteenth columns are omitted.

The third set of useful features comes from the protein profiles generated using HHBlits (Remmert *et al.*, 2012). In our experiments, the HHBlits software used database uniprot20\_2013\_03, which can be downloaded from [http://wwwuser.gwdg.de/~compbiol/data/hhsuite/databases/hhsuite\\_dbs/](http://wwwuser.gwdg.de/~compbiol/data/hhsuite/databases/hhsuite_dbs/). Again, the profile values were transformed by the sigmoid function into the range (0, 1). Each amino acid in the protein sequence is represented as a vector of 31-real numbers, of which 30 from amino acids HHM Profile values and 1 *NoSeq* label in the last column.

The three sets of features can be combined into one feature vector of length 58 for each amino acid as input to our proposed deep neural networks. For the deep neural networks that take fixed size input, e.g., sequence of length 700, the input feature matrix would be of size 700 by 58. If a protein is shorter than 700, the input matrix would be padded with

*NoSeq* rows at the end to make it full size. If a protein is longer than 700, it would be split into segments  $<700$ .

For our new deep neural networks, the predicted secondary structure output of a protein sequence is represented as a fixed size matrix, such as a 700 by 9 matrix for 8-state labels plus 1 *NoSeq* label) matrix or a 700 by 4 matrix for 3-state labels plus 1 *NoSeq* label. One of the first 8 columns have a value 1 (one hot encoding of the target class), while the others are 0.

### **3.2 New deep inception networks for protein secondary structure prediction**

In this section, a new deep inception network architecture is proposed for protein secondary structure and Psi-Phi angle prediction. The architecture consists of a sequence of inception modules followed by a number of convolution and fully connected dense layers.

Figure 3.1 shows the basic Inception module (Szegedy et al., 2016). The inception model was used for image recognition and achieved the state-of-the-art performance. It consists of multiple convolution operations (usually with different convolutional window sizes) in parallel and concatenates the resulting feature maps before going into next layer. Usually, different convolutional window sizes can be 1x1, 3x3, 5x5, 7x7 along with a 3x3 max pooling (see Supporting Information). The 1x1 convolution is used to reduce the feature map dimensionality and the max pooling is used for extracting image region features. In our protein secondary structure prediction experiment, the max pooling is not suitable because the sequence length will change and hence it was not applied in our study.

The inception module consists of several parallel convolutional networks that can extract diverse features from input. In this work, an inception network is applied to extract both local and nonlocal interactions between amino acids and a hierarchical layer of convolutions with small spatial filters is used to be computationally efficient. By stacking convolution operations on top of one another, the network has more ability to extract nonlocal interaction of residues.

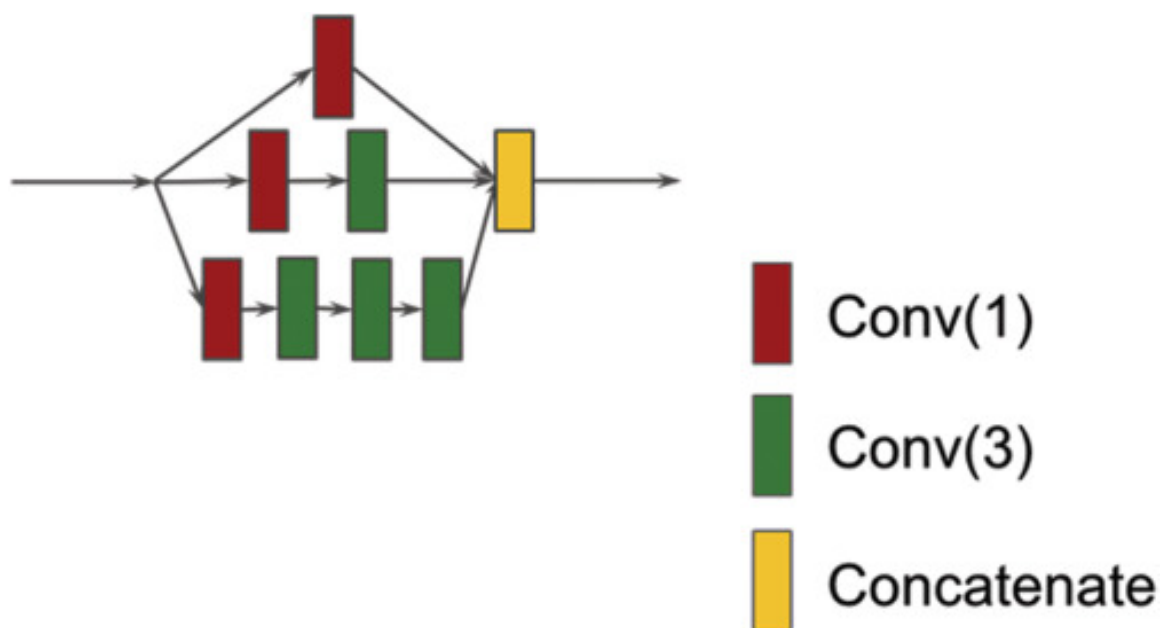


*Figure 3-1 An Inception module. The red square “Conv(1)” stands for convolution operation using window size 1 and the number of filters is 100. The green square “Conv(3)” stands for convolution operation using window size 3 and the number of filters is 100. The yellow square “Concatenate” stands for feature concatenation.*

A deep Inception network consists of a sequence of Inception modules. Figure 3.2 shows a network with three Inception modules followed by a convolutional layer and two dense layers. A dense layer is a fully connected neural network layer. The input of the network is the feature matrix for a protein sequence, such as a matrix of size 700 by 58, and the output is the target label matrix. Different numbers of Inception modules were tried



in our experiments to find appropriate values for our prediction tasks. The deep neural networks were implemented, trained, and experimented using TensorFlow (Abadi *et al.*, 2016) and Keras (Chollet, 2015; <https://github.com/fchollet/keras>).

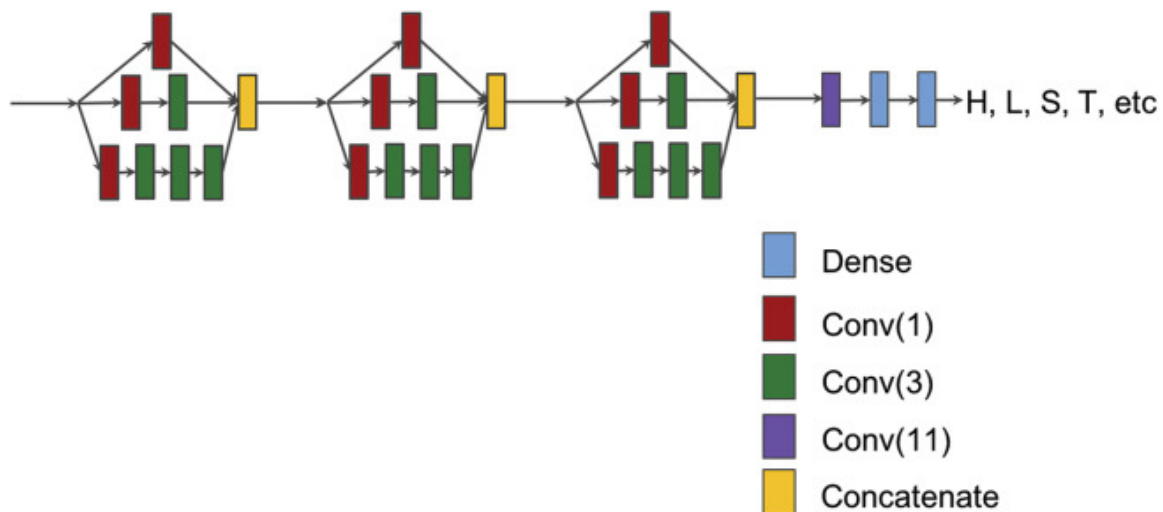


Figure 3-2 A deep Inception network consisting of three Inception modules, followed by one convolution and two fully-connected dense layers.

### 3.3 New deep inception-inside-inception networks for protein secondary structure prediction (Deep3I)

In this section, a new deep Inception-Inside-Inception network architecture (Deep3I) is presented. The architecture extends deep Inception networks through nested Inception modules.

Figure 3.3 shows a deep Inception-Inside-Inception network (Deep3I) consisting of two Deep3I blocks, followed by a convolutional layer and two dense layers. A Deep3I block is constituted by a recursive construction of an Inception model inside another Inception module. Stacked Inception modules could extract non-local interactions of residues over a

diverse range in a more effective way. Adding more Deep3I blocks is possible but requires more memory.

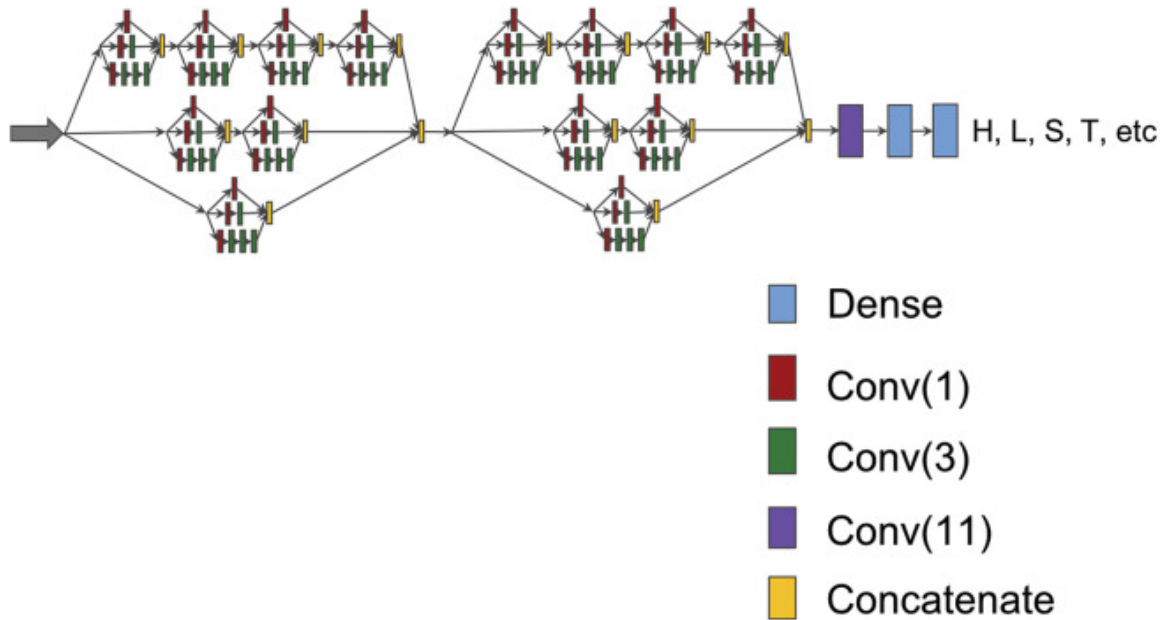


Figure 3-3 A deep Inception-Inside-Inception (Deep3I) network that consists of two Deep3I blocks. Each Deep3I block is a nested Inception network self. This network was used to generate the experimental results reported in this paper.

Each convolution layer, such as ‘Conv (3)’ in Figure 3.3, consists of four operations in sequential order: 1) A one- dimensional convolution operation using the kernel size of three; 2) The Batch normalization technique (Ioffe and Szegedy, 2015) for speeding up the training process and acting as a regularizer; 3) The activation operation, ReLU (Radford *et al.*, 2015); and 4) The Dropout operation (Srivastava *et al.*, 2014) to prevent the neural network from overfitting by randomly dropping neurons during the deep network training process so that the network can avoid co-adapting.

Deep3I networks were implemented, trained, and experimented using Tensorflow and Keras. In our experiments, a large number of network parameters and training parameters were tried. For the results reported, the dropout rate was set at 0.4. During training, the learning rate scheduler from Keras was used to control the learning rate. The initial learning

rate was 0.0005, and after every 40 epochs, the learning rate dropped as shown by the following formulas:  $lrate = 0.0005 * pow(0.8, floor(epoch + 1)/40)$ . An early stopping mechanism from Keras was used to stop the network training when the monitored validation quantity (such as validation loss and/or validation accuracy) stopped improving. The “patience” (number of epochs with no improvement after which training was stopped) was set as a number from 5 to 8. TensorBoard from Keras was used to visualize dynamic graphs of the training and validation metrics.

The new Deep3I networks are different from existing deep neural networks. The networks in (Li and Yu, 2016; Busia and Jaitly, 2017) consist of residual blocks and a multi-scale layer containing convolutional layers with convolution window sizes of 3, 7, and 9 to discover the protein local and global context. Although Deep3I uses convolution window size of 1 or 3, through stacked deep convolution blocks, the network can represent both local and global context well, while maintains efficient computation.

### 3.4 Experimental Results

In this section, extensive experimental results of the proposed deep neural networks on multiple commonly used datasets and performance comparison with existing methods are presented.

The following five publically available datasets were used in our experiments:

- 1) **CullPDB dataset.** CullPDB (Wang and Dunbrack, 2003) was downloaded on 15 June 2017 with 30% sequence identity cutoff, resolution cutoff 3.0Å and R-factor cutoff 0.25. The raw CullPDB dataset contains 10,423 protein sequences. All sequences with length shorter than 50 or longer than 700 were filtered out, which left the remaining 9972

protein sequences. CD-HIT (Fu *et al.*, 2012) was then used to remove similar sequences between CullPDB and CASP10, CASP11 and CSAP12 datasets. After that, there were 9589 proteins left. Among them, 8 protein sequences were ignored because they are too short to generate PSI-BLAST profile. For the final 9581 proteins, 9000 were randomly selected as the training set and the rest 581 as the validation set.

- 2) **JPRED** (Drozdetskiy *et al.*, 2015) dataset. All proteins from the JPRED dataset belong to different super-families, which gives the experimental result a more objective evaluation.
- 3) **CASP** datasets. CASP10, CASP11 and CASP12 datasets were downloaded from the official CASP website <http://predictioncenter.org>. The Critical Assessment of protein Structure Prediction, or CASP, is a bi-annual worldwide experiment for protein structure prediction since 1994. The CASP datasets have been widely used in the bioinformatics community. To get the secondary structure labels of the proteins, the DSSP program (Kabsch and Sander, 1983) was used. Some of the PDB files (including T0675, T0677 and T0754) could not generate the DSSP result; so, they were discarded. Some protein sequences (including T0709, T0711, T0816 and T0820) are too short and PSI-BLAST could not generate profiles; so, they were also removed. Finally, 98 out of 103 in CASP10, 83 out of 85 in CASP11 and 40 out of 40 in CASP12 were used as our CASP dataset.
- 4) **CB513 benchmark** (Zhou and Troyanskaya, 2014). This benchmark has been widely used for testing and comparing the performance of secondary structure predictors.
- 5) **Most recently PDB** (Protein Data Bank). Because training data used in different tools are not same, it is important to use PDB files that have not been seen by any previous

predictors (including ours) to objectively evaluate the performance. For this purpose, the most recently published protein PDB files dated from July 1, 2017 to August 15, 2017 were downloaded. This set contains 614 proteins, each of which share <30% sequence identity. Then, 385 proteins with a length between 50 and 700 were kept. To perform a more objective test, each of the 385 proteins was searched against CullPDB using BLAST and was classified into two categories: 1) easy cases where e-value is less than or equal to 0.5; and 2) hard cases which can have no hit or e-value higher than 0.5. After the classification, there are 270 easy cases and 115 hard cases.

In our experiments, the Deep3I configuration as shown in Fig. 3.3 was used to generate the results reported in this article. In most cases, the CullPDB dataset was used to train various deep neural networks, while the other datasets were only used in testing and performance comparison with other methods and existing results.

#### **3.4.1 PSI-BLAST vs. DELTA-BLAST**

When generating the sequence profiles, most researchers (Zhou and Troyanskaya, 2014; Wang et al., 2016; Li and Yu, 2016; Busia and Jaitly, 2017) chose PSI-BLAST (Altschul et al., 1997), which can reliably generate a good protein sequence profiles. Besides PSI-BLAST, other profile search tools are available, such as CS-BLAST (Biegert and Soding, 2009), DELTA\_BLAST (Boratyn et al., 2012), PHI-BLAST (Zhang et al., 1998), etc. In this work, the performance between two popular tools were compared: PSI-BLAST vs. DELTA-BLAST on the JPRED dataset to decide which tool to use to generate the input feature vectors for the new Deep3I network. For the PSI-BLAST experiment: both training and test data profiles were generated by setting the *e-value* at 0.001, *num\_iterations* at 3

and *db* is UniRef50. The JPRED dataset itself contains a training set of 1348 protein sequences and a test set of 149 protein sequences. The JPRED training dataset was used to train the Deep3I network and the JPRED test dataset was used to report the prediction Q3. The Deep3I network were trained five times from random initial weights, and the average Q3 accuracy and standard deviation are reported in Table 3.1. The same procedure was used for DELTA-BLAST with its default search database (2017/4/1, with a size of 8.7GB). The comparison of their results is shown in Table 3.1. Even though the average profile generation time of DELTA-BLAST is faster than PSI-BLAST, the Q3 accuracy of Deep3I using DELTA-BLAST is not as high as using PSI-BLAST. Hence, PSI-BLAST was chosen to generate profiles in the rest of our experiments.

*Table 3.1* Comparison of the profile generation execution time and Deep3I Q3 accuracy using PSI-BLAST and DELTA-BLAST

Tool	avg. profile generation time (minutes)	Q3 accuracy %
PSI-BLAST*	16.8(+/-10.14)	84.21(+/-0.49)
DELTA-BLAST	7.56(+/-3.96)	83.63(+/-0.31)

\*Database for PSI-BLAST search was UniRef50 download on 2017/4/12, 8.7GB.

### 3.4.2 Deep3I vs. the Best Existing Methods

Many previous researchers (Busia et al., 2017; Li and Yu, 2016; Wang et al., 2016) benchmarked their tools or methods using the dataset CB513 (Zhou and Troyaskaya, 2014). For a fair comparison, the same CullPDB dataset was used to train and test the MUFOLD-SS in the same way as for existing methods reported in previous publications.

Table 3.2 shows the performance comparison between Deep3I and four of the best existing methods (SSPro, DeepCNF-SS, DCRNN, and DCNN) in terms of the Q8

prediction accuracy on the CB513 dataset. All these methods were compared under the condition of the same input and features. In this case, only the protein sequence and PSI-BLAST profiles were provided. No additional technique like the next-step condition proposed in (Busia *et al.*, 2017) was involved. SSPro was run without using template information. The result shows Deep3I obtained the highest accuracy.

Table 3.2 Q8 accuracy (%) comparison between MUFOLD-SS and existing state-of-the-art methods using the same sequence and profile of benchmark CB513.

Tool	CB513
SSPro (Cheng <i>et al.</i> , 2005)	63.5*
DeepCNF-SS (Wang <i>et al.</i> , 2016)	68.3*
DCRNN (Li and Yu, 2016)	69.7*
DCNN (Busia <i>et al.</i> , 2017)	70.0**
MUFOLD-SS	<b>70.63</b>

\*Results reported by (Wang *et al.*, 2016)

\*\*Results reported by (Busia *et al.*, 2017)

Tables 3.3 and 3.4 show the performance comparison between MUFold-SS and the best existing methods (SSPro, PSIPRED, DeepCNF-SS) in terms of the Q3 prediction accuracy on the CASP datasets. PSIPRED could not predict 8-class classification, and thus do not have result on Q8 accuracy.

Table 3.3 Q3 accuracy (%) comparison between MUFOLD-SS and other state-of-the-art methods on CASP datasets.

	CASP10	P value	CASP11	P value	CASP12	P value
PSIPRED	0.8390( $\pm 0.0731$ )	6.829e-5	0.8262( $\pm 0.0648$ )	0.0298	0.8051( $\pm 0.0905$ )	0.446
SSpro	0.7882( $\pm 0.0744$ )	3.315e-20	0.7826( $\pm 0.0632$ )	1.195e-14	0.7577( $\pm 0.0913$ )	2.169e-8
DeepCNF-SS	0.8386( $\pm 0.0657$ )	8.293e-7	0.8286( $\pm 0.0604$ )	0.0774	0.8131( $\pm 0.0771$ )	0.213
MUFOLD-SS	0.8598( $\pm 0.0683$ )	-	0.8359( $\pm 0.0711$ )	-	0.8059( $\pm 0.0933$ )	-

P values indicates the significance of the difference between MUFOLD-SS and PSIPRED/SSpro/DeepCNF-SS

Table 3.4 Q8 accuracy (%) comparison between Deep3I and other state-of-the-art methods on CASP datasets.

	CASP10	P value	CASP11	P value	CASP12	P value
SSpro	0.6703( $\pm 0.0951$ )	1.347e-24	0.6651( $\pm 0.0820$ )	2.022e-21	0.6348( $\pm 0.1180$ )	1.584e-9
DeepCNF-SS	0.7403( $\pm 0.0933$ )	1.713e-8	0.7325( $\pm 0.0897$ )	0.133	0.7009( $\pm 0.1088$ )	0.334
MUFOLD-SS	0.7710( $\pm 0.0985$ )	-	0.7392( $\pm 0.1008$ )	-	0.7048( $\pm 0.1163$ )	-

P values indicates the significance of the difference between MUFOLD-SS and SSpro/DeepCNF-SS

For all methods, their prediction accuracies on the CASP10 and CASP11 datasets are generally higher than their accuracies on the CASP12 dataset. This is because CASP12 contains more hard cases and the profiles generated are not as good as for those in CASP10 and CSAP11 datasets. Furthermore, MUFOLD-SS outperformed SSPro with template in all cases, even though SSPro used the template information from similar proteins, whereas MUFOLD-SS did not.

### 3.4.3 Effects of Hyper-Parameters of Deep3I

Tables 3.5 and 3.6 show the Q3 and Q8 accuracy comparison between MUFOLD-SS with 1 or 2 blocks and the proposed Deep Inception Networks with 1 to 4 inception modules. The results of Deep Inception Networks with different number of modules are similar, whereas MUFOLD-SS with two blocks is slightly better than that with one block. Both Deep3I networks performed better than Deep inception networks. The reason may be that the ability of inception network in capturing nonlocal interaction between residues is not as good as MUFOLD-SS. MUFOLD-SS consists of integrated hierarchical inception modules, which gives more ability to extract high level features, that is, nonlocal interactions of residues.

*Table 3.5* Q3 accuracy (%) comparison between MUFOLD-SS with different number of blocks and Deep Inception Networks with different number of modules.

	# of modules	CASP10	CASP11	CASP12
Deep Inception	1	86.05	84.13	82.48
	2	86.12	84.31	82.80
	3	86.03	84.29	82.69
	4	86.02	84.44	82.67
Deep3I	1	86.51	84.56	82.94
	<b>2</b>	<b>86.49</b>	<b>85.20</b>	<b>83.36</b>



Table 3.6 Q8 accuracy (%) comparison between Deep3I with different number of blocks and Deep Inception Networks with different number of modules.

	# of modules	CASP10	CASP11	CASP12
Deep Inception	1	75.41	73.12	71.22
	2	75.70	73.26	71.55
	3	75.14	73.33	71.31
	4	75.23	73.37	71.42
Deep3I	1	76.03	73.74	71.54
	2	<b>76.47</b>	<b>74.51</b>	<b>72.1</b>

### 3.4.4 Results Using Most Recently Released PDB Files

The purpose of this test was to conduct a real-world testing, just like CASP, by using the most recently published PDB protein files dated from July 1, 2017 to August 15, 2017. These PDB files had not been viewed by any previous predictors. As mentioned before, the most recently released PDB proteins were classified into two categories: the 270 easy cases and 115 hard cases.

MUFOLD-SS is compared with the best available tools in this field, including PSIPRED, SSPro, and the newly developed SPIDER3 on this set of data. Some protein files in this dataset has special amino acid like ‘B’, which causes SPIDER3 prediction failure. To make a fair comparison, proteins containing those special cases were excluded (20 hard cases and 44 easy cases in total) and the remaining proteins were used as test cases to compare the four tools. Again, MUFOLD-SS was trained using the CullPDB dataset and tested on the new dataset.

Table 3.7 shows the performance comparison of the 4 tools. Again, Deep3I outperformed the other state-of-the-art tools in both easy and hard cases. Different from

traditional neural networks that use a sliding window of neighbor residues to scan over a protein sequence in making prediction, MUFOLD-SS takes the entire protein sequence (up to 700 amino acids) as the input and processes local and global interactions simultaneously. It is remarkable that MUFOLD-SS can outperform SPIDER3 in both easy and hard cases. Another advantage of MUFOLD-SS is that it can generate prediction for 3-class and 8-class classification at the same time, while some other tools like PSIPRED and SPIDER3 can predict only 3-class or 8-class classification. Last but not the least, MUFOLD-SS can even outperform SSPro with template in hard cases. (For hard cases, SSPro with template get 81.88% in Q3 and 71.8% in Q8.)

*Table 3.7* Q3 (%) and Q8 (%) compared with MUFOLD-SS and other state-of-the-art tools using recently PDB.

	Easy case		Hard case	
	Q3	Q8	Q3	Q8
PSIPRED	82.55	N/A	80.76	N/A
SSPro	78.76	66.53	76.01	63.14
SPIDER3	86.23	N/A	82.64	N/A
MUFOLD-SS	<b>88.20</b>	<b>78.65</b>	<b>83.37</b>	<b>72.84</b>

# CHAPTER 4 A NEW DEEP NEIGHBOR RESIDUAL NETWORK FOR PROTEIN SECONDARY STRUCTURE PREDICTION

## 4.1 DeepNRN – Deep Neighbor-Residual Network

In this section, the proposed DeepNRN method is presented. Subsection 4.1.1 presents its building block and network architecture. Subsection 4.1.2 describes some details in training the network. Subsection 4.1.3 describes the input features to the network model. Subsection 4.1.4 discusses the effect of applying different Struct2Struct networks and different numbers of iterative training to fine-tune the network result.

### 4.1.1 DeepNRN Architecture

Figure 4.1 shows the basic building block of DeepNRN, the neighbor residual unit, which consists of a sequence of convolutions and concatenations with two shortcuts, and the number of filters (feature planes) is 100. Since the convolutions with large spatial filters are computationally expensive, we use a hierarchical layer of convolutions with small spatial filters. A detailed explanation of factorization into smaller convolutions can be found in (Szegedy *et al.*, 2016) and (Szegedy *et al.*, 2016). Besides that, residual shortcut lines (He *et al.*, 2016; He *et al.*, 2016; Zhang *et al.*, 2017; Huang *et al.*, 2016) are used so that the flow of information from a predecessor can be passed to the successor layers. The reason behind this is discussed in (He *et al.*, 2016) and (He *et al.*, 2016) as deep network architecture may cause the vanishing-gradient problem. The neighbor-residual design is different from denseNet in (Huang *et al.*, 2016) in that the latter network with  $L$  layers can

have as many as  $L(L + 1)/2$  direct connections, which may lead to an explosion of feature-maps and consume large computational resources. Our network connection design is not as dense as denseNet but still preserves the long distance of four (far neighbor) and short distance of two (near neighbor) connections. This design can also alleviate the vanishing-gradient problem for deep neural networks and reduce the burden of propagating large feature-maps to the deeper layer comparing with the network flow of denseNet.

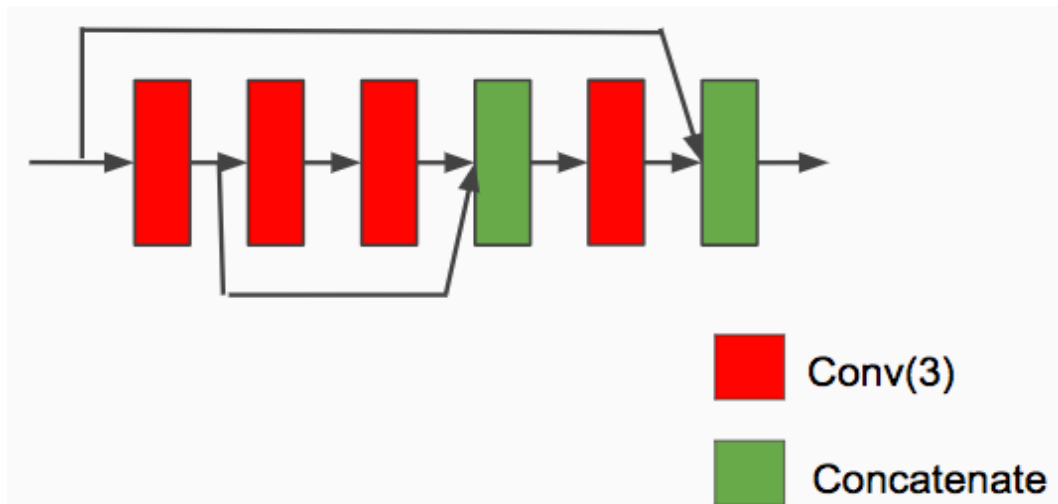


Figure 4-1 The basic building block of DeepNRN, i.e., neighbour-residual unit. The square “Conv3” stands for convolution operation using a window size 3, while the square “Concatenate” stands for feature concatenation.

Figure 4.2 shows a neighbor-residual block that consists of five neighbor-residual units strung together. The output of one neighbor-residual unit is the input to the next neighbor-residual unit.

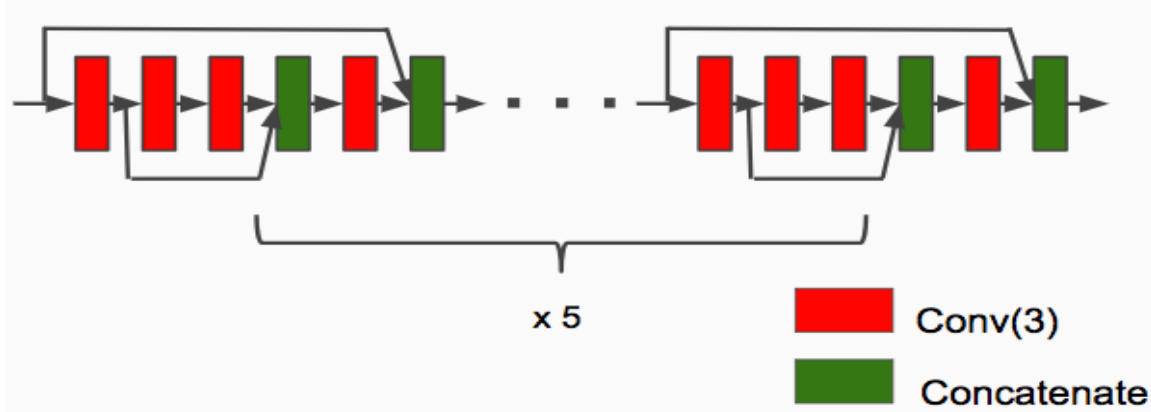


Figure 4-2 Neighbour-residual block has stacks of neighbor-residual units.

Figure 4.3 shows the overall DeepNRN architecture that consists of three neighbor-residual blocks with size-3 convolutions in between, followed by one size 11 convolution layer, and two dense fully-connected layers. Before each neighbor-residual block, the size-3 convolutional layer acts as a transition. The input of the network is the sequence and profiles. The output is the predicted secondary structure labels. We explored many other ways of placing residual shortcuts between neighbor-residual blocks, and different numbers of neighbor-residual blocks. Empirically, the architecture shown in Figure 4.3 works the best.

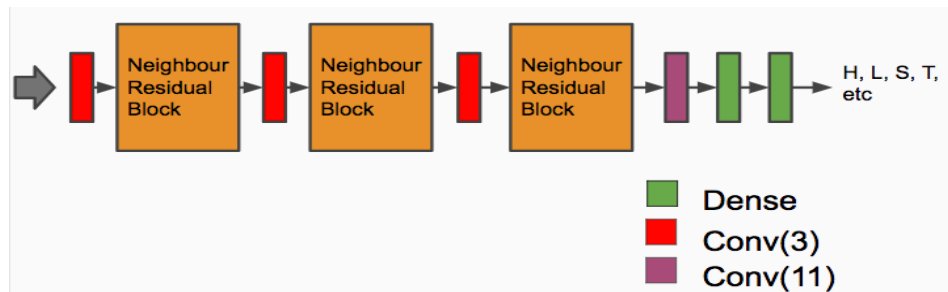


Figure 4-3 Deep neighbor-residual network (DeepNRN) architecture.

### 4.1.2 Batch Normalization and Dropout

The TensorFlow 1.0 version (Abadi *et al.*, 2016) and the Keras 2.0 version (Chollet, 2015) of machine learning environments were used for training the DeepNRN networks. To speed up the training, batch normalization (Ioffe and Szegedy, 2015) was applied after convolutions, which also acted as a regularizer. The rectified linear unit (ReLU) (Zeiler *et al.*, 2013), as the activation function, was used after batch normalization. To reduce network overfitting, dropout (Srivastava *et al.*, 2014) was added after the activation layer. Several dropout ratios, ranging from 0.3 to 0.8, were tested in our experiments and the value 0.4 was used in our final experiments. Adam optimization (Kingma and Ba, 2014) was used to train the networks. The learning rate scheduler from Keras was used to control the learning rate. The validation loss was monitored and used to early-stop the training process to avoid overfitting. The early-stopping “patience” (i.e., the number of epochs with no improvement after which training was stopped) was set between 8 to 12 in experiments, case by case. The experiments were performed on an Alienware Area desktop computer with a Titan-X GPU card equipped.

### 4.1.3 Input Features

The input features to DeepNRN consists of a protein sequence and its profiles generated by PSI-BLAST (Altschul *et al.*, 1997) and HHblits (Remmert *et al.*, 2012), respectively. One-hot vector encoding was used to represent protein sequences. To be consistent with the position specific scoring matrix (PSSM) results were generated by PSI-BLAST, which contains only 20 different kinds of amino acids, some special cases were handled as followed: Amino acid ‘*X*’ is treated like amino acid ‘*A*’; ‘*B*’ is like ‘*N*’; and ‘*Z*’ is like ‘*Q*’.

The input length of the amino acid sequence was fixed at 700. If a protein sequence is shorter than 700, a ‘NoSeq’ label is padded to the end of the sequence, which means no amino acid is there. If a protein sequence is longer than 700, it is broken into segments shorter than 700. In the implementation, a protein sequence is represented as a 700-by-21 (20 amino acids + NoSeq label) array. Next, protein profiles were generated using PSI-BLAST (Altschul *et al.*, 1997) and HHBlits (Remmert *et al.*, 2012), respectively, like the previous work in (Wang *et al.*, 2016; Heffernan *et al.*, 2017). The PSI-BLAST tool parameters were set to (*evaluate* 0.001, *num\_iterations* 3, and *db* UniRef50) to generate PSSM. PSSM values were then converted to the range (0, 1) through the Sigmoid function. The PSI-BLAST profile information is represented as a 700-by-21 array. The HHBlits tool parameters are set to (*d* uniprot20\_2013\_03, *maxres* 40 000, *Z* 0) to generate HHM profiles. The HHM files are represented as a 700-by-30 array and the information retrieved from HHM is processed the same as in (Heffernan *et al.*, 2017): Convert ‘\*’ to 0 and other non-‘\*’ value to  $f(x) = 2 \frac{-x}{1000}$ . By combining the three arrays together. The final input to DeepNRN is a 700-by-72 array.

#### 4.1.4 Struct2Struct Network and Iterative Fine-tuning

The Struct2Struct network proposed by (Rost and Sander., 1993) was added after the DeepNRN network to fine-tune the predicted results and take into consideration the consecutive patterns. For example:  $\alpha$ -helix should consist of at least 3 consecutive patterns. The predicted secondary structure from DeepNRN may violate such a pattern, i.e. not protein-like. The initial testing predicted that secondary structures are fine-tuned and more protein-like after passing through the Struct2Struct network.

Heffernan *et al.* (2017) employed an iterative learning process in their protein secondary structure prediction. We adopted a similar approach, but only on the fine-tuning part, i.e., we iteratively fine-tuned the Struct2Struct network. One of the inputs to the Struct2Struct network is the output from a previous DeepNRN prediction, i.e., the predicted probability of each class from the last Softmax layer, and another input to the Struct2Struct network is the physico-chemical properties (PP) of amino acids (Heffernan *et al.*, 2017). The output of the Struct2Struct network is again the secondary structure labels. This fine-tuning process can be iteratively repeated, which takes the predicted output from the Struct2Struct network and feeds it back into the network as its input.

The existing Struct2Struct network described in (Rost and Sander, 1993) used single-layer neural networks. In our work, different size convolution kernels were tested and, in the end, size 21 was chosen based on the fine-tuning performance. The Struct2Struct network may not improve the prediction accuracy much, but it can make the prediction more protein like and increase prediction accuracy of some small classes, such as B, G, S, T.

In summary, the proposed DeepNRN method is different from existing methods. The DeepNRN architecture differs from Busia's (Busia and Jaitly, 2017) and Li's (Li and Yu, 2016) architecture in that (Li and Yu, 2016) used residual blocks and multi-scale layer containing CNN layers with convolution window sizes of 3, 7, and 9 to discover protein local and global context. In contrast, DeepNRN consists of stacked CNN layers with a convolution window size 3 only. When deep convolution blocks are stacked, they can capture both short- and long-range sequence information. DeepNRN is also different from Heffernan's network (Heffernan *et al.*, 2017), where the latter applied long short-term



memory (LSTM) (Sak *et al.*, 2014) and a bidirectional neural network (BiNN) to perform the global context extraction. Furthermore, the key advantage of DeepNRN, the near and far neighbor residual connections, can reduce the vanishing-gradient problem in deep networks and strengthen the feature propagation. The Struct2Struct network was added after the DeepNRN network because fine-tuning makes the prediction results more protein-like.

## 4.2 Experimental Results

In our experiments, three public data sets were used: (1) the CullPDB (Wang and Dunbrack, 2003) preprocessed data set from (Li and Yu, 2016) and (Busia and Jaitly, 2017); (2) the CB513 benchmark in (Li and Yu, 2016) and (Busia and Jaitly, 2017); (3) CASP10, CASP11 and CASP12 data sets (<http://predictioncenter.org/>). The CullPDB data set was used to train the deep networks, while the other data sets were used for testing and comparison with other state-of-the-art tools. Please note that the CullPDB data set from (Zhou and Troyanskaya, 2014) was constructed before January 2014 and any two proteins in this set share less than 25% sequence identity with each other. Originally, this CullPDB had 6128 proteins. We used the filtered CullPDB data set, in which the sequence identity with the CB513 test data is less than 25%. The filtered CullPDB data set contains 5534 protein sequences, and 5278 of them were randomly selected to form the training set and the remaining 256 sequences form the validation set.

As in (Li and Yu, 2016) and (Busia and Jaitly, 2017), the Q3 and Q8 accuracies were used as the performance metrics in evaluation. The Q3 or Q8 accuracy measures the percentage of residues being correctly predicted among three-state or eight-state protein

secondary structure classes. In addition, the Matthew correlation coefficient (Matthews, 1975) was used, as it provides a more balanced measurement of classification quality.

#### **4.2.1 Performance Comparison of DeepNRN with Other State-of-the-art Tools Based on the CB513 Data set**

In our experiments, two widely used state-of-the-art tools, SCRATCH\_1D (SSPro *ab initio*) (Cheng *et al.*, 2005), (Magnan *et al.*, 2014) and Psipred (Jones, 1999) were used to compare their performance with that of DeepNRN on the data set CB513. For a fair comparison, the same PSI-BLAST data base (a smaller version of UniRef50 included in the SSPro package) was used by all three methods. SSPro contains the legacy Blast 2.2.26 for profile searches. Since Psipred does not contain PSI-BLAST, the legacy Blast 2.2.26 was installed for it. The new Blast+ package 2.6.0+ was used in our DeepNRN system.

Table 4.1 shows the Q3 and Q8 results of all three methods. The new DeepNRN method outperforms the other two methods by a large margin.

*Table 4.1 Performance comparison of DeepNRN, SSPro, and PSIPRED on Q3 and Q8 accuracy on the CB513 data set.*

	<b>Q3 (%)</b>	<b>Q8 (%)</b>
SSPro	78.6	66.5
Psipred	79.2	N/A
DeepNRN	<b>83.7</b>	<b>71.1</b>

## 4.2.2 Performance Comparison of DeepNRN with Other State-of-the-art Tools Based on Four Widely Used Data sets

In this set of experiments, the results of DeepNRN were compared with published results of other state-of-the-art methods in (Zhou and Troyanskaya, 2014) and (Wang *et al.*, 2016) on CB513, as well as three data sets from the world-wide contest of protein structure prediction, i.e., the Critical Assessment of Protein Structure Prediction (CASP). To prepare the data sets, we downloaded the PDB files from the official CASP website <http://prediction-center.org/>. Note that some of the PDB files provided do not have corresponding FASTA files. For example, T0644.fasta contains 166 amino acids; however, T0644.pdb contains only 141 amino acids. To be consistent, protein sequences were extracted from PDB; then, the DSSP program (Touw *et al.*, 2015; Kabsch and Sander, 1983) was used to retrieve the ground truth secondary structure for those extracted sequences. Some of the PDB files, including T0675, T0677 and T0754, could not generate the DSSP output; so, they were discarded. Some protein sequences, including T0709, T0711, T0816 and T0820, were too short to have any PSI-BLAST hit; so, they were removed as well. Overall, the proteins used in the experiments were CASP10 (98 out of 103), CASP11 (83 out of 85) and CASP 12 (40 out of 40).

Tables 4.2 and 4.3 show the Q3 and Q8 accuracy results, respectively, of various methods. Bold-face numbers in each column represent the best result on a particular data set, and ‘-’ denotes that no result was available. The results show that DeepNRN is significantly better than previous methods in all cases, except for Q3 on CASP11, where DeepCNF-SS is slightly better.

*Table 4.2 Q3 (%) accuracy results of various prediction methods on four data sets.*

	<i>CB513</i>	<i>CASP10</i>	<i>CASP11</i>	<i>CASP12</i>
SSPro*	78.5	78.5	78.6	76.0**
SPINE-X*	78.9	80.7	79.3	-
PSIPRED*	79.2	81.2	80.7	80.3**
JPRED*	81.7	81.6	80.4	-
RaptorX-SS8*	78.3	78.9	79.1	-
DeepCNF-SS*	82.3	84.4	<b>84.7</b>	-
DeepNRN**	<b>83.7</b>	<b>85.6</b>	83.6	<b>81.6</b>

\*Results reported in (Wang *et al.*, 2016).

\*\* Our experimental results.

Table 4.3 Q8 (%) accuracy results of various prediction methods on four data sets.

	<i>CB513</i>	<i>CASP10</i>	<i>CASP11</i>	<i>CASP12</i>
SSPro*	63.5	64.9	65.6	63.1**
RaptorX-SS8*	64.9	64.8	65.1	-
DeepCNF-SS*	68.3	71.8	72.3	-
DeepNRN**	<b>71.1</b>	<b>75.33</b>	<b>72.9</b>	<b>70.8</b>

\* Results reported in (Wang *et al.*, 2016).

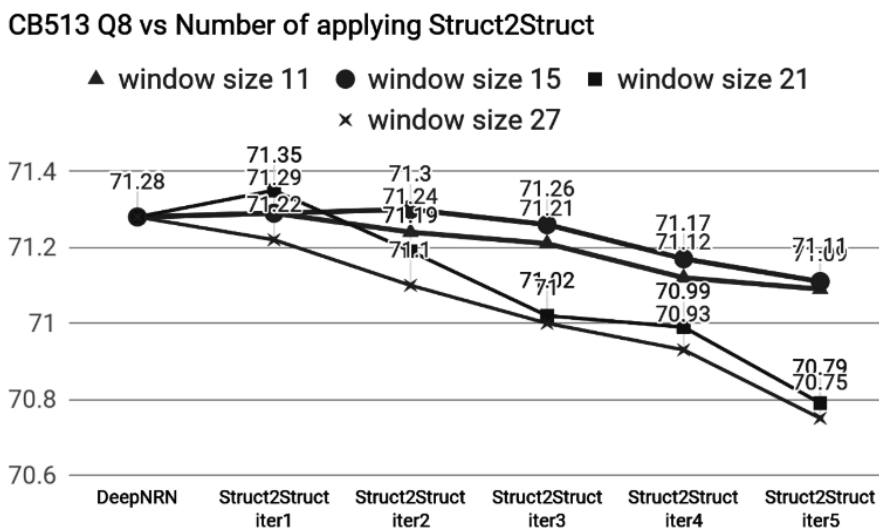
\*\* Our experimental results.

### 4.2.3 Effect of Convolution Window Size in Struct2Struct Network and Iterative Refinement

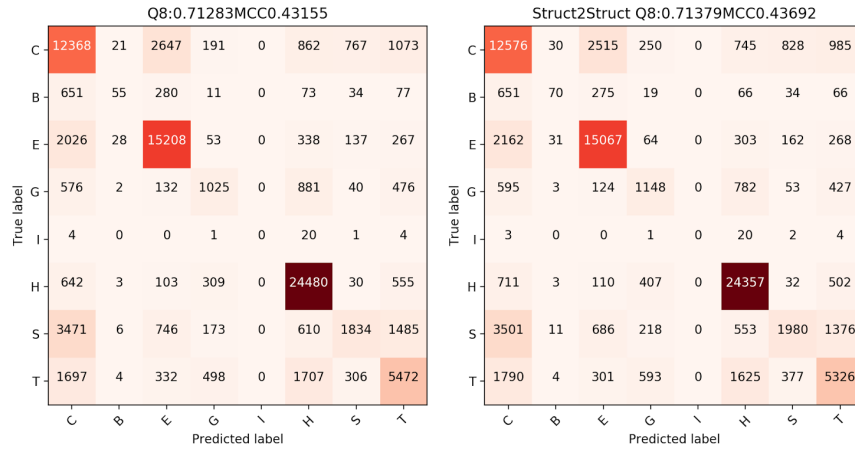
The Struct2Struct network was implemented as a convolutional layer, and different convolutional window sizes were tried to find out its effect on the results. Figures 4.4 and 4.5 show the effects of different convolutional window sizes and iterative refinement using repeated Struct2Struct networks on Q8 and Q3 accuracies, respectively. As shown in Fig.

4.4(a) and 4.5(a), the general trend is that the accuracies decrease slightly as the number of iterations increases, and a large window size leads to lower accuracy. Occasionally, the accuracy could increase slightly, as in the case of window size 21 after one iteration of fine-tuning on Q8. More iterations may not necessarily increase the fine-tuning results, but the accuracy will drop. The reason may lie in too much iterative training causing the network to become over-trained, and causing the performance to drop. The convolutional window size is a way of considering near-intermediate interactions of residues. From the experiment results, a window size was chosen between 15 and 21, which is reasonable, on a case by case basis, depending on the problem. If the window was too small, not enough neighboring residues could cover and the purpose of Struct2Struct was to take into consideration the consecutive neighboring residues.

Figures 4.4(b) and 4.5(b) compare the confusion matrices of the prediction results of DeepNRN alone vs. an additional Struct2Struct network layer of window-size 21. Although the added Struct2Struct network did not significantly change Q3 and Q8 accuracy, more instances of the smaller classes, including B, G, S and T, were correctly predicted for Q8.



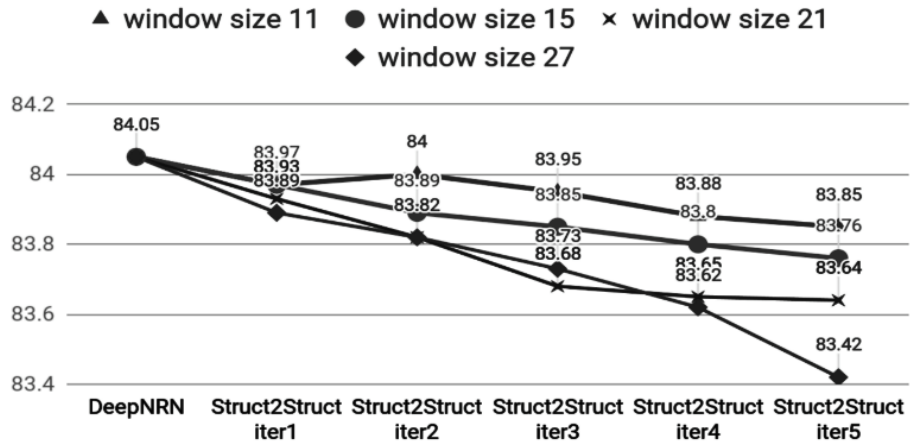
(A)



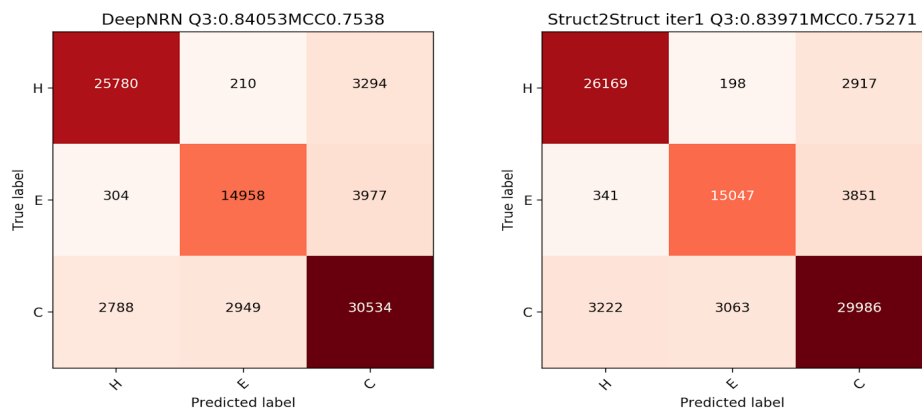
(B)

Figure 4-4 (a) Effect on Q8 of iterative refinement by applying the Struct2Struct network repeatedly. (b) Left table shows the confusion matrix of the prediction result of DeepNRN, and the right table shows the prediction result of adding one Struct2Struct network layer of window-size 21.

### CB513 Q3 vs Number of applying Struct2Struct



(A)



(B)

Figure 4-5 (a) Effect on Q3 of iterative refinement by repeatedly applying Struct2Struct network. (b) Left table shows the confusion matrix of the prediction result of DeepNRN, and the right table shows the prediction result of adding one Struct2Struct network layer of window-size 21.

#### 4.2.4 Exploration of other Network Configurations of DeepNRN

Other configurations of DeepNRN design were explored, and the performance was tested and compared in Table 4.4. As the experiment results show, the neighbor shortcuts played a very important role in propagating a large feature map to deep layers of networks because without them, the performance dropped. The far-neighbor shortcuts were also very important as shown in Table IV; without them, the performance dropped significantly. Also, adding more NRN blocks was possible but consumed more computational resources, e.g., GPU memory.

Table 4.4 Other Network Configuration of DeepNRN and Performance

	<i><b>CB513</b></i>
Without near neighbor shortcuts	70.8
Without far neighbor shortcuts	62.7
1 NRN Block	70.4
2 NRN Blocks	70.7
DeepNRN	<b>71.1</b>



# CHAPTER 5 PROTEIN BACKBONE TORSION ANGLES

## PREDICTION USING DEEP RESIDUAL INCEPTION

### NETWORKS

#### 5.1 Problem formulation

For a given amino acid sequence of a protein, the goal is to predict the backbone torsion angles (Psi and Phi) of each residue. Psi is the  $N(i)$ ,  $Ca(i)$ ,  $C(i)$ ,  $N(i+1)$  torsion angle for residue  $i$  and Phi is the  $C(i-1)$ ,  $N(i)$ ,  $Ca(i)$ ,  $C(i)$  torsion angle for residue  $i$  (see Figure 1.1). The ranges of Psi-Phi angle are between -180 to 180 degrees. It is important to feed the deep neural networks with useful inputs in order to make accurate prediction. In the proposed method, the input is designed to include as much useful information that can be obtained or generated based on the amino acid sequence. Specifically, the input features consist of physico-chemical properties of amino acids, PSI-BLAST profile, HHBlits profile, and predicted secondary structures. Figure 5.1 shows an example of the physico-chemical feature vector. Each amino acid in the protein sequence is represented as a vector of 8 real numbers ranging from -1 to 1. The vector consists of the seven physico-chemical properties as in (Fauchere *et al.*, 2009) plus a number 0 or 1 representing the existence of an amino acid at this position as an input (called *NoSeq* label). The reason of adding the *NoSeq* label is because the proposed deep neural networks are designed to take a fixed size input, such as a sequence of length 700 residues in our experiment. Then, to run a protein sequence shorter than 700 through the network, the protein sequence will be padded at the end with 0 values and the *NoSeq* label is set to 1. For example, if the length of a protein is 500, then the first 500 rows are similar to the example in Figure 5.1 with *NoSeq* label set

to 0 and the last 200 rows have 0 values in the first 7 columns and 1 in the last column. If the protein is longer than 700 residues, it can be split into multiple segments, each shorter than 700 residues.

<b>S</b>	<b>-0.337</b>	<b>-0.637</b>	<b>-0.544</b>	<b>-0.364</b>	<b>-0.265</b>	<b>-0.466</b>	<b>-0.212</b>	<b>0</b>
<b>R</b>	<b>0.105</b>	<b>0.373</b>	<b>0.466</b>	<b>-0.9</b>	<b>0.9</b>	<b>0.528</b>	<b>-0.371</b>	<b>0</b>
<b>M</b>	<b>0.11</b>	<b>0.066</b>	<b>0.087</b>	<b>0.337</b>	<b>-0.262</b>	<b>0.652</b>	<b>-0.001</b>	<b>0</b>
<b>P</b>	<b>0.247</b>	<b>-0.9</b>	<b>-0.294</b>	<b>0.055</b>	<b>-0.01</b>	<b>-0.9</b>	<b>0.106</b>	<b>0</b>
<b>S</b>	<b>-0.337</b>	<b>-0.637</b>	<b>-0.544</b>	<b>-0.364</b>	<b>-0.265</b>	<b>-0.466</b>	<b>-0.212</b>	<b>0</b>
				...				
				...				

*Figure 5-1 An example of the physico-chemical feature vector of a protein sequence. Each amino acid in the protein sequence is represented as a vector of 8 real numbers ranging from -1 to 1. The feature vectors of the first 5 amino acids are shown.*

The second set of features comes from the protein profiles generated using PSI-BLAST (Altschul *et al.*, 1999). In our experiments, the PSI-BLAST parameters were set to (evaluate: 0.001; num\_iterations: 3; db: UniRef50) to generate PSSM, which was then transformed by the sigmoid function  $S(x) = 1 / (1 + e^{-x})$  into the range (0, 1). Figure 5.2 shows an example of the PSI-BLAST profile. Each amino acid in the protein sequence is represented as a vector of 21 real values ranging from 0 to 1, representing the 20 amino acids PSSM values plus a *NoSeq* label in the last column.

The third set of features comes from the protein profiles generated using HHBlits (Remmert *et al.*, 2011). In our experiments, the HHBlits software used database uniprot20\_2013\_03, which can be downloaded from [http://wwwuser.gwdg.de/~compbiol/data/hhsuite/databases/hhsuite\\_dbs/](http://wwwuser.gwdg.de/~compbiol/data/hhsuite/databases/hhsuite_dbs/). Again, the profile values were transformed by the sigmoid function into the range (0, 1). Figure 5.3 shows an example of the HHBlits profile. Each amino acid in the protein sequence is

represented as a vector of 31 real numbers, of which 30 from amino acids HHM profile values and 1 *NoSeq* label in the last column.

The fourth set of features comes from the predicted eight-class secondary structures by DeepRIN itself. In our experiment, DeepRIN first takes the above-mentioned three sets of features as input to predict the eight-class secondary structure features. The prediction result is used as the fourth set of features for Psi-Phi angle prediction. The secondary structure prediction result is a vector of nine numbers, of which the first eight are the probabilities of the eight secondary structure classes and the last one is the *NoSeq* label.

<b>S</b>	<b>0.731</b>	<b>0.268</b>	...	<b>0.119</b>	<b>0</b>
<b>R</b>	<b>0.268</b>	<b>0.993</b>	...	<b>0.119</b>	<b>0</b>
<b>M</b>	<b>0.268</b>	<b>0.119</b>	...	<b>0.731</b>	<b>0</b>
<b>P</b>	<b>0.268</b>	<b>0.119</b>	...	<b>0.047</b>	<b>0</b>
<b>S</b>	<b>-0.731</b>	<b>-0.268</b>	...	<b>-0.119</b>	<b>0</b>
			...		
			...		

*Figure 5-2 An example of the PSI-BLAST profile of a protein sequence. Each amino acid in the protein sequence is represented as a vector of 21 real numbers ranging from 0 to 1. The feature vectors of the first 5 amino acids are shown. The third through the 19<sup>th</sup> columns are omitted.*

<b>S</b>	<b>0.016</b>	<b>0.018</b>	...	<b>1</b>	<b>0</b>
<b>R</b>	<b>0.004</b>	<b>0.011</b>	...	<b>1</b>	<b>0</b>
<b>M</b>	<b>0</b>	<b>0.006</b>	...	<b>0.5</b>	<b>0</b>
<b>P</b>	<b>0.130</b>	<b>0.003</b>	...	<b>0.483</b>	<b>0</b>
<b>S</b>	<b>0.081</b>	<b>0.022</b>	...	<b>1</b>	<b>0</b>
			...		
			...		

*Figure 5-3 An example of the HHblits profile of a protein sequence. Each amino acid in the protein sequence is represented by a vector of 31 real values ranging from 0 to 1. The feature vectors of the first 5 amino acids are shown.*

The four sets of features are combine into one feature vector of length 66 for each amino acid as the input to our proposed deep neural networks. For the deep neural networks that take the fixed-size input, the input feature matrix would be of size 700 by 66.

The new deep neural network will not predict Psi-Phi angle values directly. Instead, the outputs for each amino acid positon are  $\sin(\phi)$ ,  $\cos(\phi)$ ,  $\sin(\varphi)$ , and  $\cos(\varphi)$ , in order to remove the effect of angle's periodicity. The predicted angles can be calculated by using the *sine* and *cosine* predictions via equation  $\alpha = \tan^{-1}[\sin \alpha / \cos \alpha]$ .

## 5.2 New Deep Residual Inception Networks (DeepRIN) for Torsion

### Angle Prediction

In this section, a new deep inception residual network architecture is proposed for protein torsion angle prediction. The architecture consists of stringed inception modules and shortcut lines followed by some convolution and fully connected dense layers. Figure 5.4 shows the basic residual inception module of DeepRIN, which is designed based on InceptionNet (Szegedy *et al.*, 2017) and ResNet (He *et al.*, 2016). The residual inception module consists of two stacked inception modules to extract diverse features from the input. Convolutions with small windows are used to make the networks computationally efficient. The shortcut through Conv1 is designed to propagate feature maps into deeper layers of the network to address the vanishing-gradient problem.

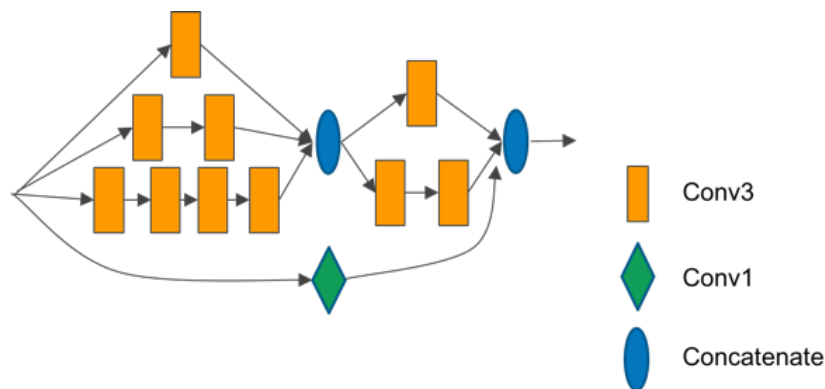


Figure 5-4 A residual-inception module of DeepRIN. The green rhombus “Conv(1)” denotes a convolution operation using window size 1 and the number of filters is 100. The orange square “Conv(3)” denotes a convolution operation using window size 3 and the number of filters is 100. The blue oval “Concatenate” denotes feature concatenation.

Figure 5.5 shows two DeepRIN networks with two residual inception modules followed by a convolutional layer and two dense layers. The first one predicts 8-class secondary structure and the second one predicts torsion angles. The input of the first network is a 700x58 feature matrix of the given protein sequence of length 700, whereas the input of the second network is a 700x66 feature matrix of the given protein sequence. Different numbers of residual inception modules were tried and compared in our experiments to find optimal values for our prediction tasks. The deep neural networks were implemented, trained, and experimented using TensorFlow (Abadi *et al.*, 2016) and Keras (Chollet, 2015).

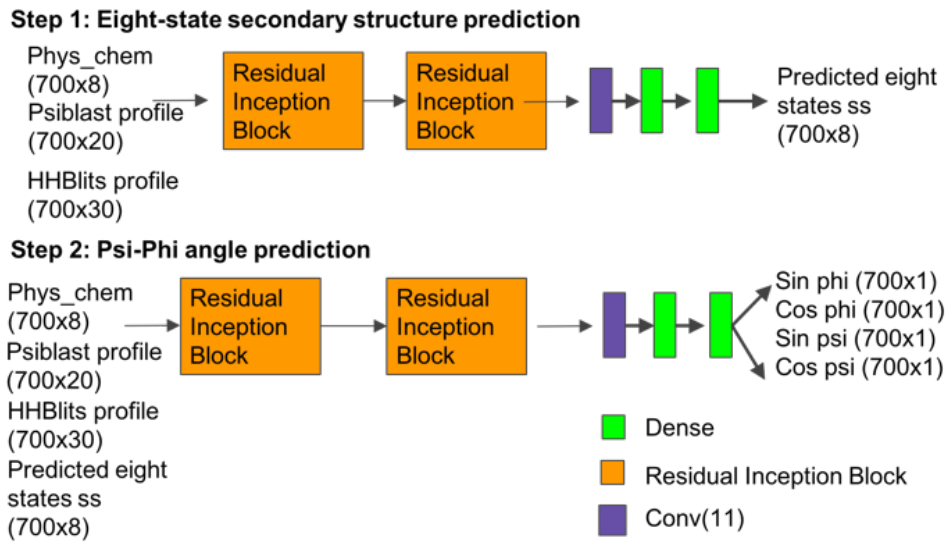


Figure 5-5 Architecture of the proposed deep residual inception network architecture (DeepRIN).

Each convolution layer, such as ‘Conv (3)’ in Figure 5.5, consists of four operations in the following sequential order: 1) A one-dimensional convolution operation using the kernel size of three; 2) the batch normalization technique (Ioffe and Szegedy, 2015) for speeding up the training process and acting as a regularizer; 3) the activation operation, ReLU (Radford *et al.*, 2015), for nonlinear transformation; and 4) the dropout operation (Srivastava *et al.*, 2014) to prevent the neural network from overfitting by randomly dropping connections during the deep network training process so that the network can avoid coadapting.

In our experiments, a large number of network parameters and training parameters were tried. For the experimental results reported in the next section, the dropout rate was set at 0.4. During training, the learning rate scheduler from Keras was used to control the learning rate. The initial learning rate was 0.0005, and after every 40 epochs, the learning rate dropped as shown by the following formulas:  $learning\ rate = 0.001 *$

$pow(0.8, floor(epoch + 1)/40)$ . An early stopping mechanism from Keras was used to stop training when the monitored validation performance (such as validation loss and/or validation accuracy) stopped improving. The “patience” (number of epochs with no improvement after which the training was stopped) was set between 5 and 8. The activation function used for the last layer is  $tanh$ , as the predicted  $sine$  and  $cosine$  value should be within the range  $[-1,1]$ .

The new DeepRIN networks are different from existing deep neural networks. The networks in (Heffernan *et al.*, 2017) consisted of stacked RNN and iterative training, while in DeepRIN, a stacked inception module and residual shortcuts were used to capture both local and global interactions between residues efficiently. Also, DeepRIN is different from DReRBM and DRNN in (Li *et al.*, 2017) because they used a sliding window to create input to deep neural networks, which is unable to capture long-range interactions between amino acids. In DeepRIN, the input is the entire protein sequence.

At a convolutional layer, the previous layer’s feature maps are convolved with learnable kernels and go through the activation function to generate the output feature map. The convolution operation can be expressed in the following formulas:

$$\mathbf{x}_j^l = f\left(\sum_{i \in M_j} \mathbf{x}_i^{l-1} * \mathbf{k}_{ij}^l + b_j^l\right)$$

where  $M_j$  represents a selection of input maps,  $b$  is bias,  $k$  is kernel, and  $x$  is feature maps.

The cross-entropy loss function used during the training is defined as following:

$$Loss(w) = \frac{1}{N} \sum_{n=1}^N H(p_n - q_n)$$

$$= -\frac{1}{N} \sum_{n=1}^N (y^n \log \hat{y}^n + (1 - y^n) \log (1 - \hat{y}^n))$$

where  $\hat{y}^n = 1/(1 + e^{-w \cdot x_n})$ ,  $N$  is the total number of samples,  $w$  is the vector of weights, the true probability  $p$  represents the percentage of the true labels, the given distribution  $q$  is the predicted value of the current model, and  $x$  is the input vector.

### 5.3 Experimental Results

This section presents experimental results of the proposed deep neural networks on multiple benchmarks in comparison with the best existing methods. The following four publically available datasets were used in our experiments:

- 1) **CullPDB dataset.** CullPDB (Wang and Dunbrack, 2006) was downloaded on 15 June 2017 with 30% sequence identity cutoff, resolution cutoff 3.0Å and R-factor cutoff 0.25. The raw CullPDB dataset contains 10,423 protein sequences. All sequences with length shorter than 50 or longer than 700 were filtered out, which left the remaining 9972 protein sequences. CD-HIT (Li and Godzik, 2006) was then used to remove similar sequences between CullPDB and CASP10, CASP11 and CASP12 datasets. After that, there were 9589 proteins left. Among them, 8 protein sequences were ignored because they are too short to generate PSI-BLAST profiles. For the final 9581 proteins, 9000 were randomly selected as the training set and the rest 581 as the validation set.
- 2) **CASP datasets.** CASP10, CASP11 and CASP12 datasets were downloaded from the official CASP website <http://predictioncenter.org>. The Critical Assessment of protein Structure Prediction, or CASP, is a bi-annual worldwide experiment for



protein structure prediction since 1994. The CASP datasets have been widely used in the bioinformatics community. To get the secondary structure labels of the proteins, the DSSP program (Kabsch and Sander, 1983) was used. Some of the PDB files (including T0675, T0677 and T0754) could not generate the DSSP results, and hence they were discarded. Some protein sequences (including T0709, T0711, T0816 and T0820) are too short and PSI-BLAST could not generate profiles so that they were also removed. Finally, 98 out of 103 in CASP10, 83 out of 85 in CASP11 and 40 out of 40 in CASP12 were used as our CASP dataset.

- 3) **Recently released PDB proteins.** Because different tools used different training data, it is important to use PDB (Protein Data Bank) files that have not been seen by any previous predictors (including ours) to objectively compare their performance. For this purpose, recently published protein PDB files dated from 2017-7-1 to 2017-8-15 were downloaded. This set contains 614 proteins, each of which share less than 30% sequence identity. Then, 385 proteins with a length between 50 and 700 were kept. To perform a more objective test, each of the 385 proteins was searched against CullPDB using BLAST and was classified into two categories: 1) easy cases where e-value is less than or equal to 0.5; and 2) hard cases which have no hit or e-value higher than 0.5. After the classification, there are 270 easy cases and 115 hard cases.
- 4) **SPIDER3's training and test datasets.** These datasets are available from <http://sparks-lab.org/server/SPIDER3/>. The training data was used to train our model, and the test set performance was reported and compared with SPIDER3. In this experiment, only the sequences with length less than 700 residues were

retained. In total 4532 out of 4590 training cases were used to train our DeepRIN model, and 1174 out of 1199 test cases were used to benchmark SPIDER3 and DeepRIN.

In our experiment, the DeepRIN configuration shown in Figure 6 was used to generate the results reported in this paper. The DeepRIN networks consisted of two inception blocks and short-cut connected by residual network. We tried some different hyper-parameters, such as different numbers of inception blocks (ranging from 1 to 5), in our experiments. The configuration in Figure 5.5 worked well in general and used in the final networks.

In most cases, the CullPDB dataset was used to train various deep neural networks, while the other datasets were only used in testing and performance comparison of different methods and with results in the literature.

The Psi-Phi angle prediction was evaluated by the mean absolute error (MAE) between the truth angle ( $A_i^{true}$ ) and the predicted angle ( $A_i^{pred}$ ) for each residue  $i$ . To remove the periodicity in angles, the error in prediction of residue  $i$  is defined as the smaller value of  $d_i$  and  $360-d_i$ , where  $d_i = |A_i^{pred} - A_i^{true}|$ . In addition, Pearson Correlation Coefficient was also used to evaluate the predicted Psi-Phi angles.

Table 5.1 compares the prediction results of DeepRIN and the best methods published in (Li *et al.*, 2017) using the same test dataset. In (Li *et al.*, 2017), Li *et al.* proposed DRerBM, which is a deep recurrent restricted Boltzmann machine (Nair and Hinton, 2010) and DRNN, which is a deep recurrent neural network (Mikolov *et al.*, 2010) to predict backbone torsion angle. SPIDER2 and SPIDER3 are two well-known tools representing the state-of-the-art. The testset contains 11 free modeling targets selected from CASP12 as described in (Li *et al.*, 2017). The results show that DeepRIN outperformed all

existing methods significantly, reducing the Psi MAE by over 2.6 degree over the second best, DReRBM, and the Phi MAE by nearly 1 degree over the second best, SPIDER3.

Table 5.1 Comparison of mean absolute errors (MAE) of Psi-Phi angle prediction between DeepRIN and best existing predictors using the test sets from (Li *et al.*, 2017)

	Psi MAE	Phi MAE
DReRBM (Li <i>et al.</i> , 2017) *	35.99	22.47
DRNN (Li <i>et al.</i> , 2017) *	37.54	22.38
SPIDER2*	37.67	22.61
SPIDER3	39.06	21.24
DeepRIN	<b>33.34</b>	<b>20.30</b>

\*Published results in (Li *et al.*, 2017)

Table 5.2 compares the results of DeepRIN, SPIDER2 and SPIDER3 on three datasets, CASP10, CASP11 and CASP12. Again, DeepRIN outperformed SPIDER2 and SPIDER3 in all cases. The improvements are significant, reducing Psi angle prediction error by more than 5 degrees and Phi angle prediction error by more than 1.5 degrees. The improvement on the CASP12 dataset is slightly less than those on CASP10 and CASP11 datasets, which may be because targets in CASP12 are harder targets and PSI-BLAST or HHblits did not generate good profiles for them.

Table 5.2 Comparison of mean absolute errors (MAE) and Pearson Correlation Coefficient (PCC) of Psi-Phi angle prediction between DeepRIN, SPIDER2 and SPIDER3 using the CASP10, 11 and 12 datasets. The PCC is written in parentheses. Bold-font numbers in each column represent the best result on a particular dataset.

	Angle	CASP10	CASP11	CASP12
SPIDER2	Psi	49.18 (0.693)	48.13 (0.699)	50.59 (0.688)
	Phi	25.83 (0.766)	26.06 (0.756)	26.85 (0.758)
SPIDER3	Psi	31.17 (0.824)	33.05 (0.805)	35.67 (0.783)
	Phi	20.41 (0.831)	21.38 (0.815)	21.12 (0.809)
DeepRIN	Psi	<b>25.79 (0.861)</b>	<b>27.96 (0.841)</b>	<b>31.39 (0.813)</b>
	Phi	<b>17.39 (0.874)</b>	<b>18.97 (0.853)</b>	<b>20.21 (0.838)</b>

Figure 5.6 shows the average Psi-Phi angle prediction errors (MAEs) of DeepRIN for protein targets in the CASP12 dataset across eight types of secondary structures, which are  $3_{10}$ -helix (G),  $\alpha$ -helix (H),  $\pi$ -helix (I),  $\beta$ -strand (E),  $\beta$ -bridge (B),  $\beta$ -turn (T), bend (S) and loop or irregular (L). The result shows that for H (Helix), Psi-Phi angle prediction errors

are the lowest, yet the errors for T (Turn), S (Bend) and C (Loop Region) are the highest. There is no “I” region in the targets.

Figure 5.7 shows the detailed Psi-Phi angle prediction results of two proteins in CASP12: T0860 and T0861. Predicted angle value, true angle value, and absolute error are plotted for each amino acid position, with its true secondary structure type labelled. T0860 is an example of hard cases with higher prediction errors, whereas T0861 is an example of accurate prediction. The H (helix) regions generally have lower prediction errors, whereas the C (coil) regions usually are harder to predict.

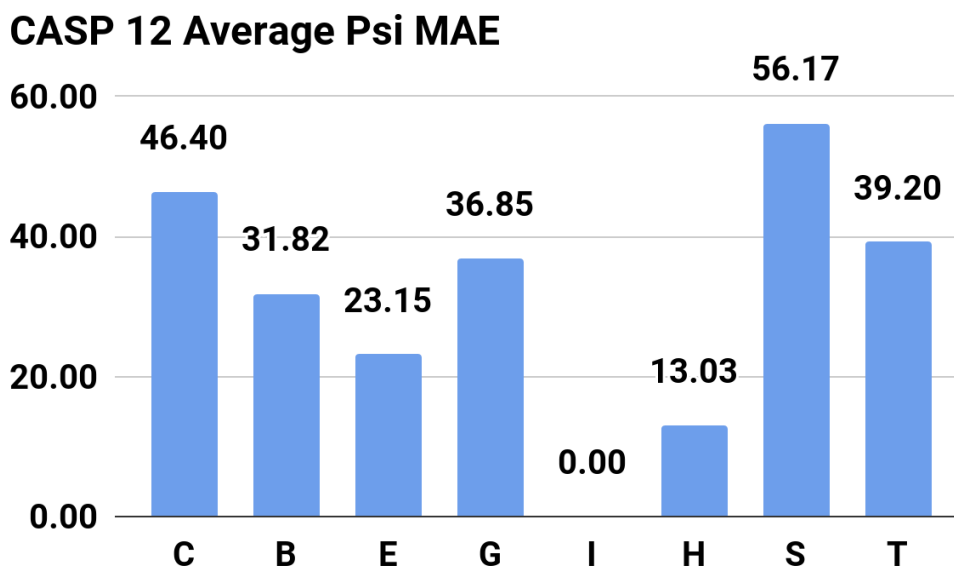
As shown in Figures 5.6 and 5.7, loop regions (T, S, C) generally have large prediction errors. The H (Helix) regions and strand (E) regions can be predicted accurately. Sometimes, Psi angles in beta sheets were predicted 180-degree reversely. For Phi angles, the predictions are relatively better in helix and beta sheet regions. T0861 was predicted quite well except for some turn and loop regions. An observation is that when the Psi-Phi angles were predicted relatively well, the variance of the predicted Psi-Phi angles were relatively large, as it captured the diversity of different angles. When the Psi-Phi angles were not predicted accurately, the predicted angles had smaller variations.

Table 5.3 compares the results of DeepRIN, SPIDER2 and SPIDER3 on the recently released PDB dataset. On both the easy target subset and the hard target subset, DeepRIN outperformed both SPIDER2 and SPIDER3 significantly. These results provide an objective assessment because no predictors used these recently released PDB proteins in their training or development.

Table 5.3 Comparison of mean absolute errors (MAE) and Pearson Correlation Coefficient (PCC) of Psi-Phi angle prediction between DeepRIN and SPIDER2 and SPIDER3 using the recently released PDB dataset. The PCC is shown in parentheses.

	Angle	Recent PDB easy cases (226)	Recent PDB hard cases (94)
SPIDER2	Psi	28.13 (0.849)	33.42 (0.808)
	Phi	18.46 (0.850)	20.24 (0.830)
SPIDER3	Psi	24.93 (0.867)	29.53 (0.827)
	Phi	17.49 (0.861)	19.35 (0.838)
DeepRIN	Psi	<b>22.67 (0.882)</b>	<b>28.94 (0.834)</b>
	Phi	<b>15.98 (0.881)</b>	<b>18.67 (0.850)</b>

Table 5.4 compares the performances of DeepRIN and SPIDER3 using SPIDER3's training data. DeepRIN was trained using SPIDER3's training data (sequences length less than 700) with 4532 out of 4590 proteins in total. DeepRIN used less training data than SPIDER3. This experiment was designed to compare the two different deep neural network methods. After training, both methods were run on six different test datasets (including SPIDER3's test sets (sequences length less than 700, 1174 out of 1199 test proteins in total) and the results are shown in Table 4.4. Across all test datasets, DeepRIN outperformed SPIDER3.



### CASP12 Average Phi MAE

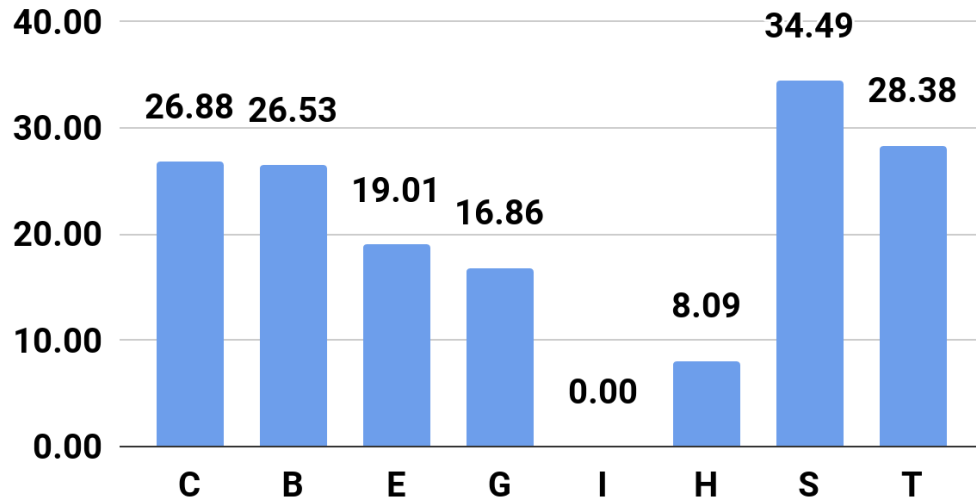


Figure 5-6 Average Psi-Phi angles prediction error (MAEs) for each of the eight types of secondary structure on the CASP12 dataset by DeepRIN.



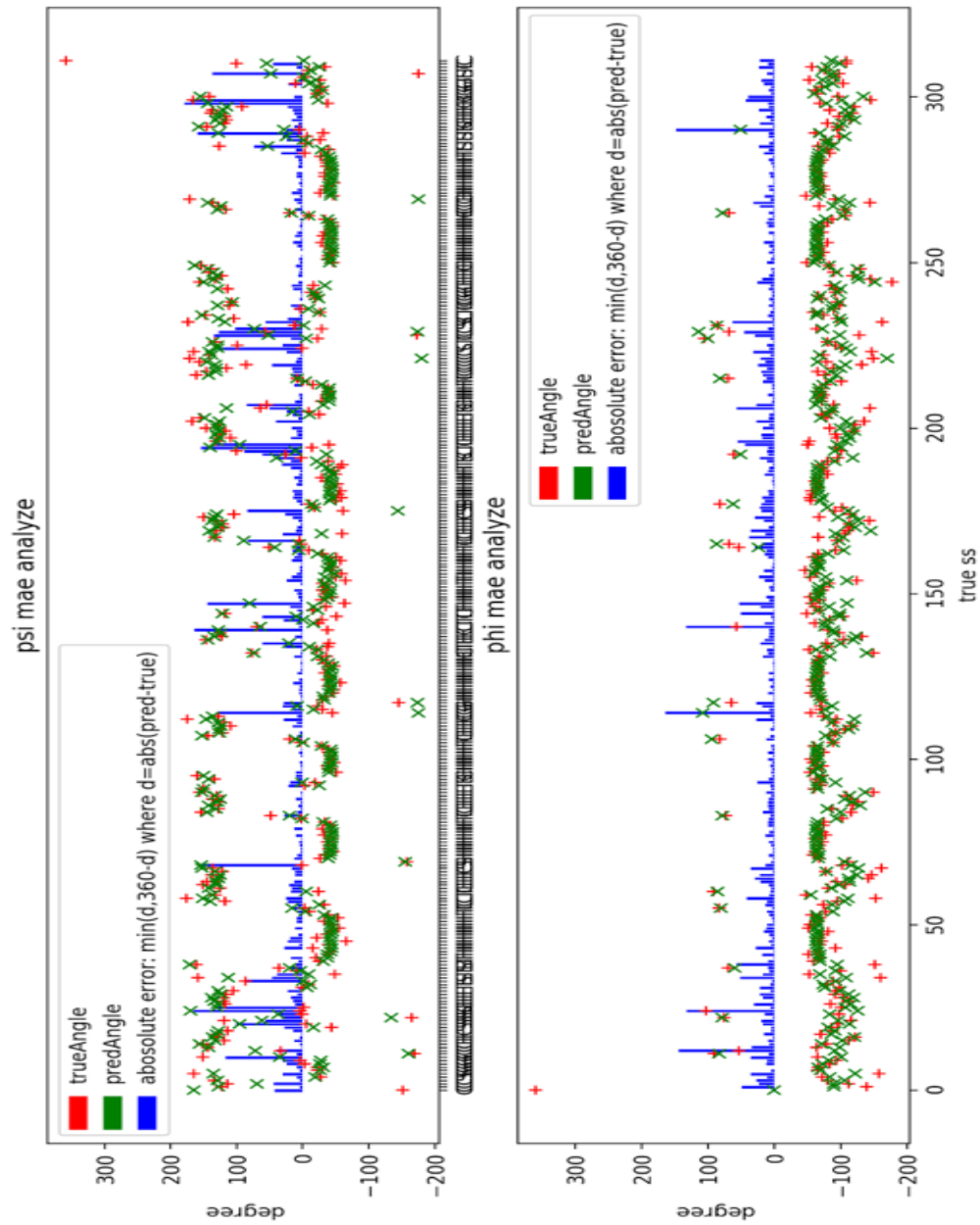


Figure 5-7 Psi-Phi angle prediction results of two proteins in CASP12, T0860 (top) and T0861 (bottom). Predicted angle value, true angle value, and absolute error are plotted for each amino acid position, which is labelled by its true secondary structure type. The low blue bars, which denote the error between predicted angles and truth angels.



Table 5.4 Comparison of mean absolute errors (MAE) of Psi-Phi angle prediction between DeepRIN and SPIDER3 using the same training dataset (SPIDER's training set) and the same test dataset.

	Angle	CASP10 (98 out of 103)	CASP11 (83 out of 85)	CASP12 (40 out of 40)	SPIDER3's test set (1174 out of 1199)	Recent PDB easy cases (226)	Recent PDB hard cases (94)
SPIDER3	Psi	31.17	33.05	35.67	27.33	24.93	29.53
	Phi	20.41	21.38	21.12	18.73	17.49	19.35
DeepRIN	Psi	<b>25.64</b>	<b>28.27</b>	<b>30.93</b>	<b>22.74</b>	<b>23.25</b>	<b>28.78</b>
	Phi	<b>17.22</b>	<b>18.99</b>	<b>19.72</b>	<b>16.40</b>	<b>16.04</b>	<b>18.01</b>

\*T0675, T0677 and T0754 could not generate DSSP results. T0709, T07111, T0816 and T0820 are too short and PSI-BLAST did not have a hit. The SPIDER3's training set (sequences with length less than 700) 4532 out of 4590 proteins in total were used to train our model and the SPIDER3's test set (sequences with length less than 700) 1174 out of 1199 proteins in total were used for testing on both tools.

# CHAPTER 6 PROTEIN BETA TURN PREDICTION USING DEEP DENSE INCETPION NETWORKS

## 6.1 Methods and Materials

### 6.1.1 Preliminaries and Problem Formulation

To make an accurate prediction, it is important to provide useful input features to machine learning models. In our method, we carefully designed feature matrices corresponding to the primary amino acid sequence of a protein. Specifically, there are four features involved: physicochemical feature, HHBlits profile, predicted eight state secondary structure from MUFold-SS (Fang et al., 2018) and predicted shape string from Frag1D (Zhou et al., 2009).

The first set of features used is called physico-chemical features, which describe hydrophobic, steric, and electric properties of amino acids and provide useful information for protein sequence analysis and prediction. By using physico-chemical features, the protein sequences are represented as an informative dense matrix. The physico-chemical feature matrix consists of the sever physico-chemical properties as in (Heffernan et al., 2017) plus a number 0 or 1 representing the existence of an amino acid at this position as an input (called NoSeq label). The reason of adding the NoSeq label is because the proposed deep neural networks are designed to take a fixed size input, such as a sequence of length 700 residues in our experiment. To run a protein sequence shorter than 700 through the network, the protein sequence will be padded at the end with 0 values and the NoSeq label is set to 1. If the protein is longer than 700 residues, it can be split into multiple segments, each shorter than 700 residues. Hence, a protein sequence will be represented as a 700-by-8 matrix, which is the first input feature for DeepDIN.

The second set of useful features comes from the protein profiles generated using HHBlits (Remmert et al., 2012). In our experiments, the HHBlits software used the database uniprot20\_2013\_03, which can be downloaded from [http://wwwuser.gwdg.de/~compbiol/data/hhsuite/databases/hhsuite\\_dbs/](http://wwwuser.gwdg.de/~compbiol/data/hhsuite/databases/hhsuite_dbs/). The profile values were transformed by the sigmoid function into the range (0, 1). Each amino acid in the protein sequence is represented as a vector of 31 real numbers, of which 30 from amino acids HHBlits profile values and 1 NoSeq label in the last column. The HHBlits, the names of the parameters are amino acids and some transition probabilities: “A, C, D, E, F, G, H, I, K, L, M, N, P, Q, R, S, T, V, W, Y, M->M, M->I, M->D, I->M, I->I, D->M, D->D, Neff, Neff\_I, and Neff\_D”. HHBlits generates profiles which is more sensitive than PSI-BLAST profile and provides useful evolutionary features for protein sequence. Hence, a HHBlits profile will be represented as a 700-by-30 matrix, which is the second input feature for DeepDIN.

The third set of useful features, predicted shape string, comes from Frag1D (Zhou et al., 2009). For each protein sequence, the Frag1D can generate useful predicted protein 1D structure features: the classical three-state secondary structure, three- and eight-state shape string. Classical three state secondary structure contains H (helix), S (sheet), and R (random loop). Eight state shape string label contains R (polyproline type alpha structure), S (beta sheet), U, V (bridging regions), A (alpha helices), K (310 helices), G (almost entirely glycine), and T (turns). The prediction of protein secondary structure has been used as an important feature for protein structure prediction. However, for an average of 40% of all residues in loop regions, the classical secondary structure does not carry useful structure information. On the other hand, the protein structure can be described by pairs of psi phi

torsion angles. Ison et al. (2005) proposed Shape Strings, which can accurately describe a 1D string of symbols representing the protein backbone psi phi torsion angles. The shape strings can describe the conformations of residues in regular secondary structure elements, e.g. shape 'A' corresponds to alpha helix and shape 'S' corresponds to beta sheets. Besides, shape strings classify the random loop regions into several states that can contain much more conformation information, which is particularly useful for gamma-turn prediction problem. For the Frag1D predicted result, each amino acid in the protein sequence is represented as a vector of 15 numbers, of which 3 from the classical three-state secondary structure, 3 from the three-state shape string, 8 from the eight-state shape string and 1 NoSeq label in the last column. The predicted classical three-state secondary structure feature is represented as one-hot encoding as followed: helix: (1,0,0), strand: (0,1,0), and loop: (0,0,1). The same rule applies to three- and eight-state shape string features. Hence, a Frag1D result will be represented as a 700-by-15 matrix, which is the third input feature for DeepDIN.

The fourth set of useful features comes from our previous designed secondary structure prediction tool: MUFold-SS (Fang et al., 2018). MUFold-SS achieved state-of-the-art performance in eight state secondary structure prediction and it should provide useful features in beta-turn prediction tasks. The eight-state secondary structure are: H (alpha helix), B (beta bridge), E (extended strand), G (3-helix), I (5 helix), T (hydrogen bonded turn), and S (bend). Hence, an eight-state predicted secondary structure will be represented as a 700-by-8 matrix, which is the fourth input feature for DeepDIN.

Protein beta-turn prediction is a classification problem. To be specific, it can be formulated as residue-level prediction or turn-level prediction as first proposed by (Singh et al., 2015).

Residue-level prediction: To predict each amino acid is a turn or non-turn. The class label is either turn or non-turn. Here, the predicted output is a 700-by-3 matrix, where '700' is the sequence length 700 and '3' stands for two-state labels plus 1 NoSeq label.

Turn-level prediction: At the turn-level, a sliding window of four residues was used to generate the turn-level data sets. And the overall predicted beta-turn output of a protein sequence is represented as a fixed-size matrix, with a (700-4+1) dimension by 3 for two-state labels plus 1 NoSeq label matrix. For nine-class classification problem, the label is: turn of the specific type or others.

The evaluation metric for beta-turn prediction typically uses MCC more often than accuracy, since the accuracy only considers the true positive and false positive without the true negative and false negative, and non-beta-turns (negative data) dominate the data. MCC can be calculated as follows:

$$MCC = \frac{TP * TN - FP * FN}{\sqrt{(TP + FP)(TP + FN)(TN + FP)(TN + FN)}} \quad 1)$$

where TP is the number of true positives, TN is the number of true negatives, FP is the number of false positives and FN is the number of false negatives.

### **6.1.2 New Deep Dense Inception Networks for Protein Beta-turn Prediction (DeepDIN)**

In this section, a new deep dense inception network architecture (DeepDIN) is presented. The architecture makes use of deep inception (Szegedy et al., 2017) networks and dense

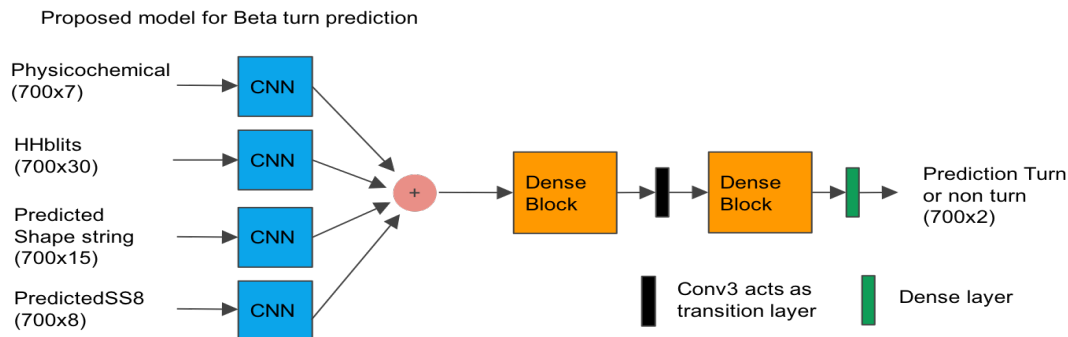
network (Huang et al., 2017). Figure 6-1 (A) presents our proposed network design. It shows the beta-turn prediction:

1. Given a protein sequence, the system will generate four features: physico-chemical feature, profile features from HHBlits, predicted shape string (using Frag1D) and predicted eight-state secondary structure (using MUFold-SS).
2. The convolutional layer will then perform convolution operation on each feature to get the coevolved feature map.
3. Concatenate four convolved feature maps along feature dimension.
4. Feed the concatenated feature map into stringed dense inception blocks (See Figure 2 (B) for illustration). In between there is a convolutional layer acting as transition layer.
5. Predict beta-turn (either turn or non-turn) in the last dense layer which uses Softmax as activation function.

Figure 6-1 (B) shows details of a dense inception block. It consists of four small version of inception blocks and each inception block is fully connected with other inception blocks. In other words, a dense inception module is constituted by connecting each inception layer to every other inception layer in a feed-forward fashion. The design of dense inception modules can extract non-local interactions of residues over a diverse range in a more effective way. Adding more dense inception blocks is possible but requires more memory. Each convolution layer, such as ‘Conv (3)’ in Figure 6-1, consists of four operations sequentially: 1) A one-dimensional convolution operation using the kernel size of three; 2) the Batch normalization technique (Ioffe and Szegedy, 2015) for speeding up the training process and acting as a regularizer; 3) the activation operation, ReLU (Radford et al.,

2015); and 4) the dropout operation (Srivastava et al., 2014) to prevent the neural network from overfitting by randomly dropping neurons during the deep network training process so that the network can avoid or reduce co-adapting. DeepDIN was implemented, trained, and tested using TensorFlow and Keras. In our experiments, a large number of network parameters and training parameters were tried. For the results reported, the dropout rate was set at 0.4. The optimizer used during training is Adam (Kingma and Ba, 2014), which can control the learning rate dynamically for network weight updates. There are nine class beta-turn classification and the observations for a certain class can be as many as 40,000 or as little as 100. In different classification tasks, the batch size varies from 50-200. The Max epochs is set up to 100. The training time varies from 2 hours up to 5 hours depending on the data size when training different classification models.

In our previous study (Fang et al, 2018; Fang et al., 2017; Fang et al., 2018) and (Wang et al., 2017) have successfully applied the stacked convolutional neural network (CNN), inception (Szegedy et al., 2017) module, deep residual (He et al., 2016) module to protein sequence analysis and prediction problems. Inspired by our previous work, here we propose a new deep neural network architecture called: dense inception network (DeepDIN) for beta-turn prediction.



(A)

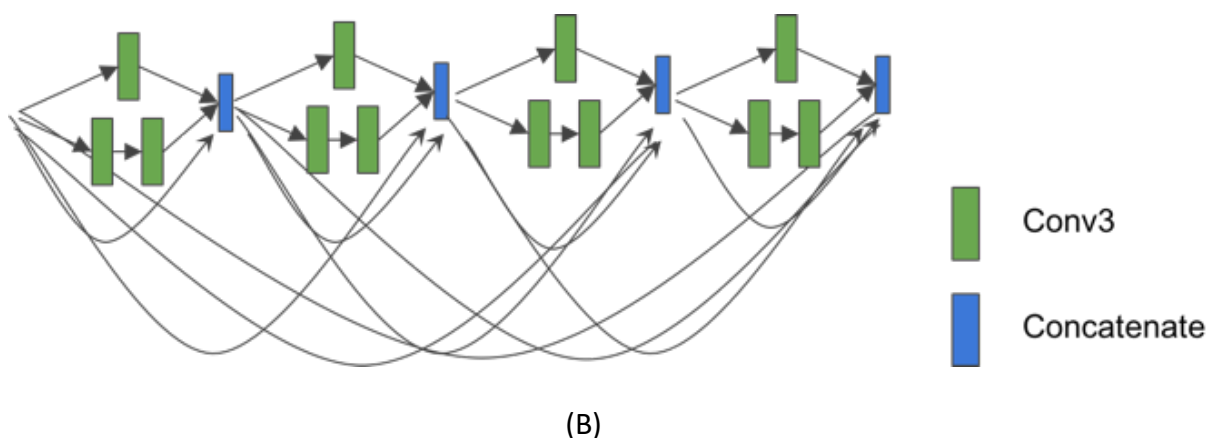


Figure 6-1 (A) shows the overall proposed model for beta-turn prediction. (B) shows the details of a dense inception module that consists of four inception modules, each of which is fully connected in a feed forward fashion.

### 6.1.3 Apply Transfer Learning and Balanced Learning to DeepDIN to Handle Imbalanced Dataset

It is often unsuitable for tackling the problem of small sample sizes for deep learning. In this work, in order to enable the deep neural networks to handle small classes, the following deep learning strategies were used to address the small classes classification problem.

**Balanced learning:** Many previous researchers have studied the problem of imbalanced data learning and proposed ways of balancing the data set by using either over-sampling like SMOTE (Han et al., 2015) or under-sampling like Tomek Links (Tomek, 1976). The beta-turn data is highly unbalanced, and this would cause the deep neural network like DeepDIN prone to predict everything as the negative class. In this experiment, the protein beta-turns as positive data are not very large, any up-sampling or down-sampling may cause loss of useful information. Rather than re-sampling the training data points, a balanced learning approach was adapted to handle the problem. The weighted cross entropy was used as the loss function, which is defined as the following functions:



$$\forall i \in [0, N), H(i) = - \sum_l y_{i,l} * \log \hat{y}_{i,l} \quad (2)$$

$$H = \sum_l W * y_l * H(i) \quad (3)$$

where  $l$  is the number of classes;  $W = (w_1, w_2, \dots, w_l)$  is the weight for each class;  $N$  is the total number of data points;  $y_i$  is the one-hot ground truth label;  $\hat{y}_i$  is the predicted probability distribution of a data point;  $H(i)$  is the cross-entropy loss of one data; and  $H$  is the weighted cross-entropy. The weighted cross entropy as the loss function was able to address the issue caused by the small sample size by re-scaling the prediction of each class by its weight. In this implementation, the class weights were calculated using training data and assigned using the Scikit-learn (Pedregosa et al., 2011) toolbox. The balanced class weights are given by  $n\_samples / (n\_classes * \text{bincount}(y))$ , where  $y$  is array of original class labels per sample, “bincount” is a built-in function from Scikit-learn toolbox to calculate the number of bins.

**Transfer Learning:** We applied transfer learning to handle the limited number of beta-turn data used in the training set. The idea of transfer learning originally came from the image classification problem (Raina et al., 2007). This technique was proposed to handle the insufficient size of a data set that can be used to train the deep neural network. In our study, since there are nine classes of beta-turns, and especially those in VIa1, VIa2, and VIb contains a few hundred of data points, the amount of data belonging to each class may not produce a model with the ability to extract features and being generalized well. To solve this problem, the pre-trained weights from DeepDIN used to classify two-class beta-turns was loaded into each separate nine-class classification model as initial weight. In

particular, the pre-trained model here is the beta-turn model used to classify the two-class beta-turn problem. Since that model has “observed” some generic features of what a beta-turn is, it should be useful to many specific nine-class beta-turn classification tasks. Then for training each individual class model, the specific subset of the training set for each individual class was fed into and the overall network weights were fine-tuned. The weights of the pre-trained networks were fine-tuned by continuing the backpropagation. It is possible to fix the earlier layer of the deep networks due to the overfitting issue and only fine-tune the high-level portion of the network. After the trials, the overall network was fine-tuned without freezing the lower level features.

For the learning rates during the transfer learning, a smaller learning rate (0.005) and batch size (10) were used to train the network and fine-tune the network weights in the fine-tuning. The reason is that the pre-trained network weights are relative good, a slower and smaller learning rate will not distort them too quickly and too much before it converges.

#### **6.1.4 Benchmark datasets**

The following two publically available benchmark data sets were used in our experiments: BT426 (Guruprasad and Rajkumar, 2000) is a data set commonly used for benchmarking beta-turn prediction methods. BT426 contains 426 protein chains in total with 25 percentage sequence identity cutoffs, and resolution better than 2.0 Å. This benchmark was used to compare the performance of many previous predictors, such as BetaTPred3 (Singh et al., 2015) and NetTurnP (Petersen et al., 2010). In this work, five-fold cross-validation experiments on BT426 were performed and results were compared against other predictors.

BT6376 (Singh et al., 2015) is a public benchmark containing 6376 non-homologous protein chains. No two protein chains have more than 30% sequence identity. The structures of these proteins were determined by X-ray crystallography at 2.0 Å resolution or better. Each chain contains at least one beta-turn. The beta-turn labels were assigned by PROMOTIF (Hutchinson and Thornton, 1996) program. This benchmark provides data sets for both two-class beta-turn classification and nine-class beta-turn classification. For the nine-class beta-turn labels were annotated by using PROMOTIF, too.

## **6.2 Results and Discussion**

In this section, extensive experimental results of the proposed deep neural networks on the benchmark data sets and performance comparison with existing methods are presented. To evaluate the performance of our tool, a five-fold cross validation technique was used on all data sets.

### **6.2.1 How Feature Affects the DeepDIN Performance**

Since we used four features for our proposed DeepDIN architecture, it is important to quantitatively determine how much improvement the proposed DeepDIN can make by using single, some, or all of the features (See Table 6.2). We used TypeI beta-turns for experiments. This dataset has 6039 proteins containing total of 42,393 TypeI beta-turns. In each experiment, a five-fold cross-validation was performed. The running time for each experiment is about 3-4 hours.

It can be found that the predicted shape string feature either used alone or used in combined with other features can highly improve the prediction performance. However, it

suffers from high variance compared with other features. Using predicted shape string can improve the prediction but the performance is not as stable as using other features.

Another observation is that some combined features have better prediction results than those features used alone, which means features in-between can have some complementary affect. For instance, when the predicted shape string is combined with the predicted secondary structure as input, the prediction performance is much better than just using predicted shape string. Although both features are related to protein secondary structure, they may capture different aspect of features for a protein. Shape string combined with secondary structure can achieve better results than shape string combined with physicochemical feature.

From Table 6.1, it shows that if all four features were used, the prediction result is much better and stable. We used all four features together in the other experiments.

*Table 6.1 Different feature combinations will affect prediction performance*

physicochemical	SS8	Shape string	HHBlits profile	MCC
x				0.183(±0.013)
	x			0.311(±0.018)
		x		0.364(±0.058)
			x	0.321(±0.014)
x	x			0.401(±0.002)
x		x		0.391(±0.052)
x			x	0.365(±0.011)
	x	x		0.423(±0.031)
	x		x	0.357(±0.014)
		x	x	0.422(±0.042)
x	x	x		0.472(±0.040)
x		x	x	0.454(±0.051)
x	x		x	0.455(±0.037)
	x	x	x	0.446(±0.035)
x	x	x	x	0.462(±0.027)

## 6.2.2 Residue-Level and Turn-Level Two-Class Prediction on BT426

Table 6.2 Residue-Level Prediction on BT426

Predictor	MCC
BTPRED (Shepherd <i>et al.</i> , 1999)	0.35
BetaTPred2 (Kaur and Raghava, 2002, 2004)	0.43
Hu and Li (2008)	0.47
NetTurnP (Petersen <i>et al.</i> , 2010)	0.50
BetaTPred3-Tweak (Singh <i>et al.</i> , 2015)	0.50
BetaTPred3-7Fold (Singh <i>et al.</i> , 2015)	0.51
BetaTPred3 (Singh <i>et al.</i> , 2015)	0.51
DeepDIN	<b>0.647(±0.016)</b>

Table 6.3 Turn-level Prediction on BT426

Features	MCC
BetaTPred3 (Singh <i>et al.</i> , 2015)	0.43
DeepDIN	<b>0.550(±0.019)</b>

Table 6.2 and 6.3 shows experiment results of comparing DeepDIN with existing methods at residue-level and turn-level on benchmark BT426. At both residue-level or turn-level, the DeepDIN outperformed all existing methods. In (Singh *et al.*, 2015), they proposed a “turn-level prediction formulation”, which predicts the complete beta-turn rather than focusing on the residues in a beta-turn.

It is worth mentioning that in (Tang *et al.*, 2011). They reported their turn-level MCC around 0.66 on benchmark BT426. Actually, they preprocessed the dataset in a way that the negative (non-turn) samples was randomly selected when the ratio of positive to negative as 1:3 (Tang *et al.*, 2011). In real world scenario, it is not possible to sample the data this way. Our system can handle the original BT426 dataset (the ratio of positive to

negative as high as 1:9). Also, results comparison should be under same condition. In (Tang *et al.*, 2011), they compared their results using the preprocessed dataset with other predictors using original BT426 dataset, which is not fair and objective comparison.

### **6.2.3 Turn-level Nine-Class Prediction on BT6376**

Table 6.4 show a list of class sizes information on the concrete sample and class sizes. The purpose of this table is to give reader information on how small the positive turn samples among all samples in each class. As one can see, for each beta-turn class, the dataset is very imbalanced, as non-turn occupy majority of the data samples.

Table 6.5 shows the nine-class beta-turn prediction results. The average MCC results of DeepDIN for large class beta-turns such as I, I', II, II', IV, outperformed BetaTPred3 at least seven percentage points, which is a significant improvement. For some small classes such as VIa1, VIb the improvement is about three percentage points. DeepDIN performs not as good as BetaTPred3 in small classes such as VIa2 in average MCC, particularly because of the small amount of training data points available. Generally speaking, deep neural networks are always biased to predicted negative classes if a very small amount of imbalanced observations are given. However, by applying balanced learning and transfer learning, this issue can be alleviated or overcome.

Since the beta-turn dataset is very imbalanced, during training, different class weights were calculated using the Scikit-learn (Pedregosa *et al.*, 2011) toolbox and then assigned to the loss function during the model training process. The experiments were performed on an Alienware Area-51 desktop computer equipped with Nvidia Titan-X GPU (11 GB memory). A five-fold cross-validation evaluation was performed on each of nine-class

beta-turn classification tasks. The average experiment time ranges from 2 to 4 hours due to the different amount of observations for each class.

Table 6-4 Nine-class beta-turn and non-turn class sizes in BT6376

Beta-turn types	# of proteins	# of turns	# of non-turns	turns / non-turns
Type I	6039	42,393	1,366,911	0.031
Type I'	2786	4353	747,596	0.005
Type II	4750	13,559	1,183,457	0.011
Type II'	1995	2643	545,300	0.004
Type IV	5950	38,201	1,360,907	0.028
Type VIa1	600	654	182,122	0.003
Type VIa2	177	188	56,761	0.003
Type VIb	914	1082	263,099	0.004
Type VIII	4257	10,111	1,114,707	0.009

Table 6.5 Nine-class beta-turn during balance learning, the performance was evaluated at turn-level on BT6376

Beta-turn types	BetaTPred3 average MCC	DeepDIN Average MCC
Type I	0.30	0.462(±0.027)
Type I'	0.45	0.645(±0.057)
Type II	0.35	0.569(±0.050)
Type II'	0.33	0.564(±0.061)
Type IV	0.20	0.292(±0.016)
Type VIa1	0.33	0.395(±0.023)
Type VIa2	0.25	0.262(±0.121)
Type VIb	0.35	0.465(±0.023)
Type VIII	0.17	0.234(±0.015)

# CHAPTER 7 PROTEIN GAMMA TURN PREDICTION USING DEEP DENSE INCETPION NETWORKS

## 7.1 Materials and Methods

### 7.1.1 Problem formulation

A protein gamma-turn prediction is a binary classification problem, which can be formulated as followed: given a primary sequence of a protein, a sliding window of  $k$  residues were used to predict the central residue turn or non-turn. For example, if  $k$  is 17, then each protein is subsequently sliced into fragments of 17 amino acids with a sliding window.

To make accurate prediction, it is important to provide useful input features to machine-learning methods. We carefully designed a feature matrix corresponding to the primary amino acid sequence of a protein, which consists of a rich set of information derived from individual amino acid, as well as the context of the protein sequence. Specifically, the feature matrix is a composition of HHBlits profile (Remmert *et al.*, 2012), and predicted protein shape string using Frag1D (Zhou *et al.*, 2009).

The first set of useful features comes from the protein profiles generated using HHBlits (Remmert *et al.*, 2012). In our experiments, the HHBlits software used database uniprot20\_2013\_03, which can be downloaded from [http://wwwuser.gwdg.de/~compbiol/data/hhsuite/databases/hhsuite\\_dbs/](http://wwwuser.gwdg.de/~compbiol/data/hhsuite/databases/hhsuite_dbs/). A HHBlits profile can reflect the evolutionary information of the protein sequence based on a search of the given protein sequence against a sequence database. The profile values were scaled



by the sigmoid function into the range (0, 1). Each amino acid in the protein sequence is represented as a vector of 31 real numbers, of which 30 from HHM Profile values and 1 *NoSeq* label (representing a gap) in the last column. The HHBlits profile corresponds to amino acids and some transition probabilities, i.e., A, C, D, E, F, G, H, I, K, L, M, N, P, Q, R, S, T, V, W, Y, M->M, M->I, M->D, I->M, I->I, D->M, D->D, Neff, Neff\_I, and Neff\_D.

The second set of useful features, predicted shape string, comes from Frag1D (Zhou *et al.*, 2009). For each protein sequence, Frag1D can generate useful predicted protein 1D structure features: classical three-state secondary structures, and three- and eight-state shape strings. Classical three-state secondary structures and three-state shape string labels both contain H (helix), S (sheet), and R (random loop), but they are based on different methods so that they have small differences. In this experiment, we used all the features from Frag1D. Eight-state shape string labels contain R (polyproline type alpha structure), S (beta sheet), U/V (bridging regions), A (alpha helices), K ( $3_{10}$  helices), G (almost entirely glycine), and T (turns). The classical prediction of three-state protein secondary structures has been used as an important feature for protein structure prediction, but it does not carry further structural information for the loop regions, which account for an average of 40% of all residues in proteins. Ison *et al.* (2005) proposed Shape Strings, which give a 1D string of symbols representing the distribution of protein backbone psi-phi torsion angles. The shape strings include the conformations of residues in regular secondary structure elements; in particular, shape 'A' corresponds to alpha helix and shape 'S' corresponds to beta strand. Besides, shape strings classify the random loop regions into several states that contain much more conformational information, which we found particularly useful for

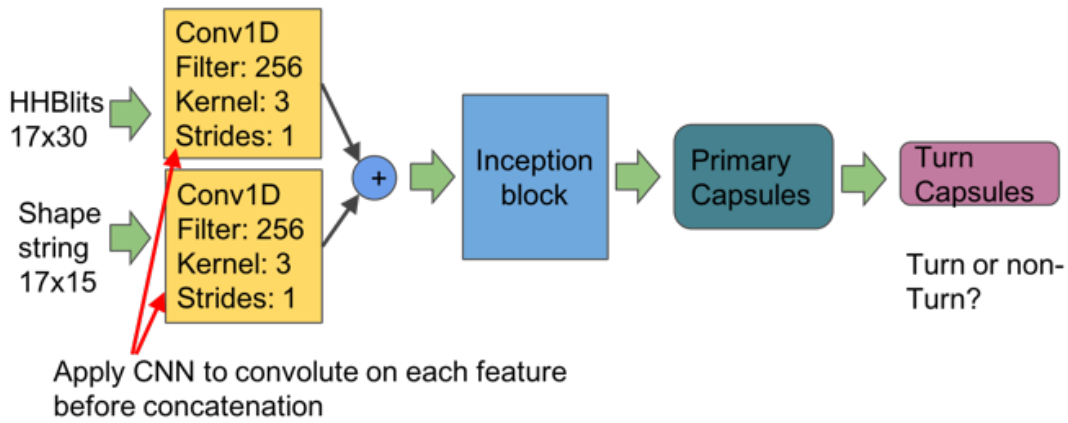
gamma-turn prediction problem. For the Frag1D prediction result, each amino acid in the protein sequence is represented as a vector of 15 numbers, of which 3 from the classical three-state secondary structures, 3 from the three-state shape strings, 8 from the eight-state shape strings and 1 *NoSeq* label in the last column. The predicted classical three-state secondary structure feature is represented as one-hot encoding as followed: helix: (1,0,0), strand: (0,1,0), and loop: (0,0,1). The same rule applies to three- and eight-state shape string features. In this work, we also tried the traditional eight-state protein secondary structures. However, the prediction result was not as good as the one from the eight-state shape strings. This is probably because the traditional eight-state secondary structures contain much less structural information for the gamma-turn prediction problem.

### 7.1.2 Model Design

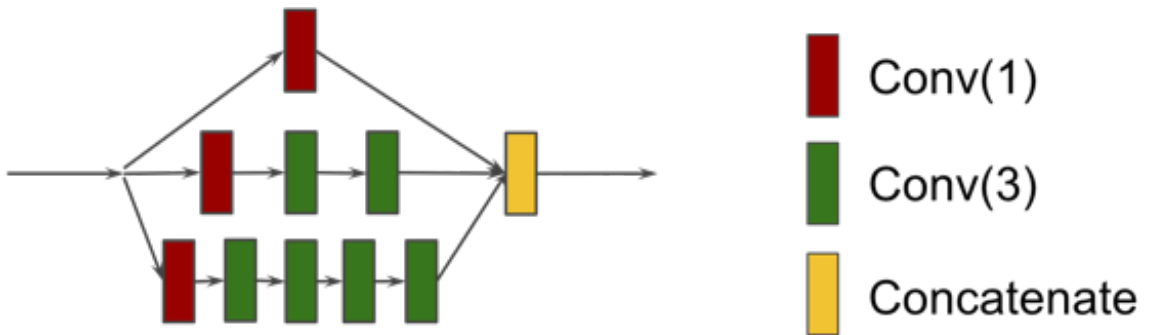
In this section, a new deep inception capsule network (DeepICN) is presented. Figure 7-1 A shows the model design. The input features for DeepICN are HHBlits profiles and predicted shape strings. Since the distributions of HHBlits profiles and predicted shape strings are different, we applied convolutional filters separately on the two features, then concatenated them. The CNN is used to generate the convolved features. We first applied CNN to extract local low-level features from protein profiles and predicted shape strings features. This CNN layer will extract local features similar to a CNN used to extract “edge” features of objects in an image (Xie and Tu, 2015).

After the convoluted feature concatenation, the merged features are fed into the inception module (See Figure 7-1 B for details). The inception network (Szegedy *et al.*, 2017) was then applied to extract low-to-intermediate features for CapsuleNet. In (Sabour

*et al.*, 2017), CapsuleNet was used for digital image classification and the primary capsule layers were placed after a convolutional layer. Their network design worked well for digital image recognition with the image dimension 28-by-28. Considering the complex features of protein HHblits profile and shape strings, it is reasonable to apply a deeper network to extract local to medium level features so that CapsuleNet can work well on top of those features and extract high-level features for gamma-turn classification. The purpose of setting up an inception block right after CNN is to extract intermediate-level features.



(A)



(B)

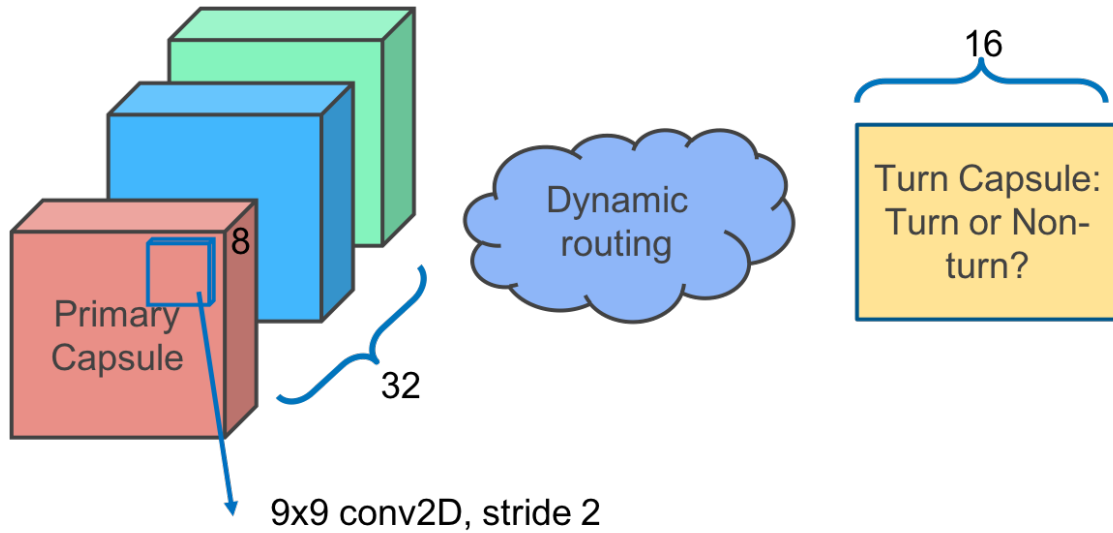


Figure 7-1 (A) A deep inception capsule network design. The input features are HHBlits profile (17-by-30 2D array) and predicted shape string using Frag1D (17-by-15 2D array). Each feature is convolved by a convolutional layer. Both convolved features then get concatenated. An inception block is followed to extract low to medium features. A primary capsule layer then extracts higher level features. The final turn capsule layer makes predictions. (B) An inception block. Inside this inception block: Red square Conv(1) stands for convolution operation with kernel size 1. Green square Conv(3) stands for convolution operation with kernel size 3. Yellow square stands for feature map concatenation. (C) Zoom-in between primary capsules and turn capsules. The primary capsule layer contains 32 channels of convolutional 8D capsules. The final layer turn capsule has two 16D capsules to represent two states of the predicted label: gamma-turn or non-gamma-turn. The computation between those two layers is dynamic routing.

Each convolution layer, such as ‘Conv (3)’ in Figure 7-1 B, consists of four operations in sequential order: (1) a one-dimensional convolution operation using the kernel size of three; (2) the batch normalization technique (Ioffe and Szegedy, 2015) for speeding up the training process and acting as a regularizer; (3) the activation operation, ReLU (Radford *et al.*, 2015); and (4) the dropout operation (Srivastava *et al.*, 2014) to prevent the neural network from overfitting by randomly dropping neurons during the deep network training process so that the network can avoid co-adapting.

The capsule layers are placed after the inception module to extract high-level features or explore the spatial relationship among the local features that are extracted in the above-

mentioned layers. The primary capsule layer (See Figure 7-1 C) is a convolutional capsule layer as described in (Sabour *et al.*, 2017). It contains 32 channels of convolutional 8D capsules, with a 9 x 9 kernel and a stride of 2. The final layer (turn capsule) has two 16D capsules to represent two states of the predicted label: gamma-turn or non-gamma-turn. This layer receives the inputs from all the primary capsules output through the dynamic routing algorithm (Sabour *et al.*, 2017), which is an effective way to implement the explaining away that is needed to segment highly overlapping objects (features). The squashing activation function (Sabour *et al.*, 2017) was applied in the computation between the primary capsule layer and the turn capsule layer as follows:

$$v_j = \frac{\|s_j\|}{1 + \|s_j\|^2} \frac{s_j}{\|s_j\|}$$

where  $v_j$  is the vector output of capsule  $j$  and  $s_j$  is its total output.

The dynamic routing algorithm (Sabour *et al.*, 2017) is as follows:

---

Routing Algorithm:

---

Routing ( $\widehat{u}_{j|i}$ ,  $r$ ,  $l$ )

For all capsule  $i$  in layer  $l$  and capsule  $j$  in layer  $(l+1)$ :  $b_{i,j} \leftarrow 0$

For  $r$  iteration do

For all capsule  $i$  in layer  $l$ :  $c_i \leftarrow \text{softmax}(b_i)$

For all capsule  $j$  in layer  $(l + 1)$ :  $s_j \leftarrow \sum_i c_{ij} \widehat{u}_{j|i}$

For all capsule  $j$  in layer  $(l + 1)$ :  $v_j \leftarrow \text{squash}(s_j)$

For all capsule  $i$  in layer  $l$  and capsule  $j$  in layer  $(l + 1)$ :  $b_{ij} \leftarrow b_{ij} + \widehat{u}_{j|i} \cdot v_j$

---

The evaluation metric for gamma-turn prediction more commonly uses Matthew Correlation Coefficient (MCC) than percentage accuracy since the accuracy only considers the true positives and false positives without the true negatives and false negatives. Another reason is that the gamma-turn dataset is very imbalanced, where MCC can evaluate how well the classifier performs on both positive and negative labels. MCC can be calculated from the confusion matrix as follows:

$$MCC = \frac{TP * TN - FP * FN}{\sqrt{(TP + FP)(TP + FN)(TN + FP)(TN + FN)}}$$

where TP is the number of true positives, TN is the number of true negatives, FP is the number of false positives and FN is the number of false negatives.

### 7.1.3 Model Training

DeepICN was implemented, trained, and tested using TensorFlow and Keras. Different sets of hyper-parameters (dynamic routing iteration times, training data sample size, convolution kernel size, and sliding window size) of DeepICN were explored. An early stopping strategy was used when training the models and if the validation loss did not reduce in 10 epochs, the training process stopped. The Adam optimizer was used to dynamically change the learning rate during model training. All the experiments were performed on an Alienware Area-51 desktop equipped with a Nvidia Titan X GPU (11 GB graphic memory).

### 7.1.4 Experiment Dataset

1) **CullPDB** (Wang and Dunbrack, 2003) was download on November 2, 2017. It originally contained 20,346 proteins with percentage cutoff 90% in sequence identity,

resolution cutoff 2.0 Å, and R-factor cutoff 0.25. This dataset was preprocessed and cleaned up by satisfying all the following conditions: with length less than 700 amino acids; with valid PSIBLAST profile, HHblits profile; with shape strings predicted by Frag1D (Zhou *et al.*, 2009); and with gamma-turn labels retrieved by PROMOTIF (Hutchinson and Thornton, 1996). After this, 19,561 proteins remained and CD-Hit (Li and Godzik, 2006) with 30% sequence identity cutoff was applied on this dataset resulting in 10,007 proteins. We removed proteins with sequence identity more than 30% for an objective and strict test in terms of model generalization. This dataset was mainly used for deep neural network hyper-parameter tuning and the exploration of CapsuleNet configurations. It was also used to compare the proposed inception capsule model with other deep-learning models. For these purposes, a balanced dataset was built: all positive gamma-turn labels and an equal size of negative non-gamma-turn labels were selected to form a balanced dataset.

**2)** The benchmark **GT320** (Guruprasad and Rajkumar, 2000) is a common data set used for benchmarking gamma-turn prediction methods. GT320 contains 320 non-homologous protein chains in total with 25% sequence identity cutoffs, and resolution better than 2.0 Å resolution. This benchmark was used to compare the performance with previous predictors. Each chain contains at least one gamma-turn. The gamma-turns were assigned by PROMOTIF (Hutchinson and Thornton, 1996). In this work, five-fold cross-validation experiments on GT320 was performed and results were compared against other predictors.

## 7.2 Experimental Results

In this section, extensive experimental results of the proposed deep CapsuleNets with different hyper-parameters were tuned and tested using CullPDB and five-fold cross-validation results on GT320. The performance comparison with existing methods is presented.

### 7.2.1 Hyper-parameter Tuning and Model Performance

Tables 7.1-4 show the exploration of the inception capsule network with different hyper-parameters. This set of experiments was to find out a better configuration of hyper-parameters for the deep networks using the CullPDB dataset. Since this network involves many hyper-parameters, only the major ones were explored. Table 1 shows how the sliding window size affects the model performance. In this experiment, 1000 proteins were randomly selected to form the training set, 500 for the validation set and 500 for the test set. Each experiment was performed with five times of data randomization.

Table 7.1 shows how the sliding window size of input affects the deep capsule network performance. The larger the window size, the more training time it took for CapsuleNet. However, MCC may not grow as the window size increases. We chose the window size of 17 amino acids based on its peak MCC performance in the experiments. The t-test p-values show that the window size 17 test MCC compared to other window sizes is statistically significant.

Table 7.2 shows the dropout rate's effects on the performance of the deep capsule network. If a dropout was not used, the network had very high over-fitting. The dropout rate 0.4-0.5 is reasonable as it is a compromise between the training and test prediction performance. We chose dropout 0.5 in our study. The P-value between the dropout of 0.5



and any of others was insignificant. Although The dropout of 0.8 had the highest test average MCC, its standard deviation ( $\pm 0.0249$ ) is also high, and hence, we did not use it.

Table 7.1 Effect of window size on MCC performance

Window size	Test average MCC	Time (hr)	P-value on MCC
15	0.4458( $\pm 0.0107$ )	0.18( $\pm 0.11$ )	0.0115
17	0.4645( $\pm 0.0062$ )	0.24( $\pm 0.15$ )	-
19	0.4442( $\pm 0.0049$ )	0.37( $\pm 0.18$ )	0.0010
21	0.4548( $\pm 0.0055$ )	0.43( $\pm 0.20$ )	0.0499
23	0.4227( $\pm 0.0076$ )	0.37( $\pm 0.23$ )	0.0001
25	0.4369( $\pm 0.0076$ )	0.45( $\pm 0.25$ )	0.0005

Table 7.2 Effect of dropout on MCC performance

Dropout	Train average MCC	Test average MCC	P-value on test MCC
No	0.9974( $\pm 0.0015$ )	0.4439( $\pm 0.0101$ )	0.1236
0.3	0.9857( $\pm 0.0154$ )	0.4454( $\pm 0.0049$ )	0.0843
0.4	0.9010( $\pm 0.1457$ )	0.4515( $\pm 0.0047$ )	0.4294
0.5	0.9377( $\pm 0.0598$ )	0.4558( $\pm 0.0092$ )	-
0.6	0.9159( $\pm 0.0688$ )	0.4525( $\pm 0.0111$ )	0.6647
0.7	0.8371( $\pm 0.0920$ )	0.4604( $\pm 0.0063$ )	0.4318
0.8	0.6072( $\pm 0.1033$ )	0.4646( $\pm 0.0249$ )	0.5228

Table 7.3 Effect of training size on training time and MCC performance

Training size	Test average MCC	Time (hr)
500	0.4224( $\pm 0.0035$ )	0.23( $\pm 0.17$ )
1000	0.4553( $\pm 0.0098$ )	0.87( $\pm 0.03$ )
2000	0.4422( $\pm 0.0204$ )	1.59( $\pm 0.07$ )
3000	0.4752( $\pm 0.0111$ )	2.38( $\pm 0.09$ )
4000	0.4787( $\pm 0.0147$ )	3.13( $\pm 0.12$ )
5000	0.4717( $\pm 0.0165$ )	3.91( $\pm 0.14$ )

Table 7.4 Effect of dynamic routing on MCC performance

dynamic routing times	Test average MCC	Time (hr)	P-value on MCC
1	0.4454( $\pm 0.0049$ )	0.44( $\pm 0.16$ )	0.4644
2	0.4492( $\pm 0.0086$ )	0.31( $\pm 0.17$ )	-
3	0.4407( $\pm 0.0032$ )	0.37( $\pm 0.15$ )	0.1017
4	0.4497( $\pm 0.0045$ )	0.32( $\pm 0.18$ )	0.9276
5	0.4487( $\pm 0.0061$ )	0.41( $\pm 0.14$ )	0.9502

Table 7.3 shows the effects of the training sample size on the deep capsule network training speed and performance. More training data increased training time and the model performance. However, after 3000 samples, the MCC performance did not improve significantly with more training data. This is consistent with the observation in (Sabour et al., 2017) that CapsuleNet did not need a large dataset for training.

Table 7.4 shows the effect of number of dynamic routing on the performance. Dynamic routing is used in CapsuleNet similar to max-pooling in a CNN, but it is more effective than max-pooling in that it allows neurons in one layer to ignore all but the most active feature detector in a local pool in the previous layer. In this experiment, we fixed the other hyper-parameters searched in the above-mentioned experiments and studied how number of dynamic routing affected the performance. Considering the training time and the MCC performance, 2 routings are suitable, as more dynamic routing does not have significant improvement. The training time did not show large variations as the number of dynamic routings increases. This may be because our experiments used early stopping.

### **7.2.2 Prediction confidence: the capsule length**

According to (Sabour *et al.*, 2017), the capsule length indicates the probability that the entity represented by the capsule is present in the current input. In other words, the capsule length in the last layer can be used for prediction of gamma-turn and assessment of prediction confidence. The longer the turn capsule length is, the more confident the prediction of a turn capsule will be. Here, the capsule length in Turn Capsules can be used to show how confidence a gamma-turn is predicted. Specifically, a test set (with 5000 proteins containing 19,594 data samples) was fed into the trained inception capsule network to get a capsule length vector. Then the capsule length vector that represents

positive capsules were kept. Since all the capsule length values fall into the range between 0 and 1, they were grouped into bins with the width of 0.05, so that there are totally 20 bins. The precision of each bin can be calculated to represent the prediction confidence. Figure 7-2 shows the fitting curve of precision (percentage of correctly predicted gamma-turns, i.e., true positives in the bin) versus the capsule length. A nonlinear regression curve was used to fit all the points, yielding the following equation:

$$y = 1.084x^2 - 0.203x + 0.147$$

where  $x$  is the capsule length and  $y$  is the precision.

The fitting-curve can be further used for prediction confidence assessment: given a capsule length, its prediction confidence can be estimated using the above equation.

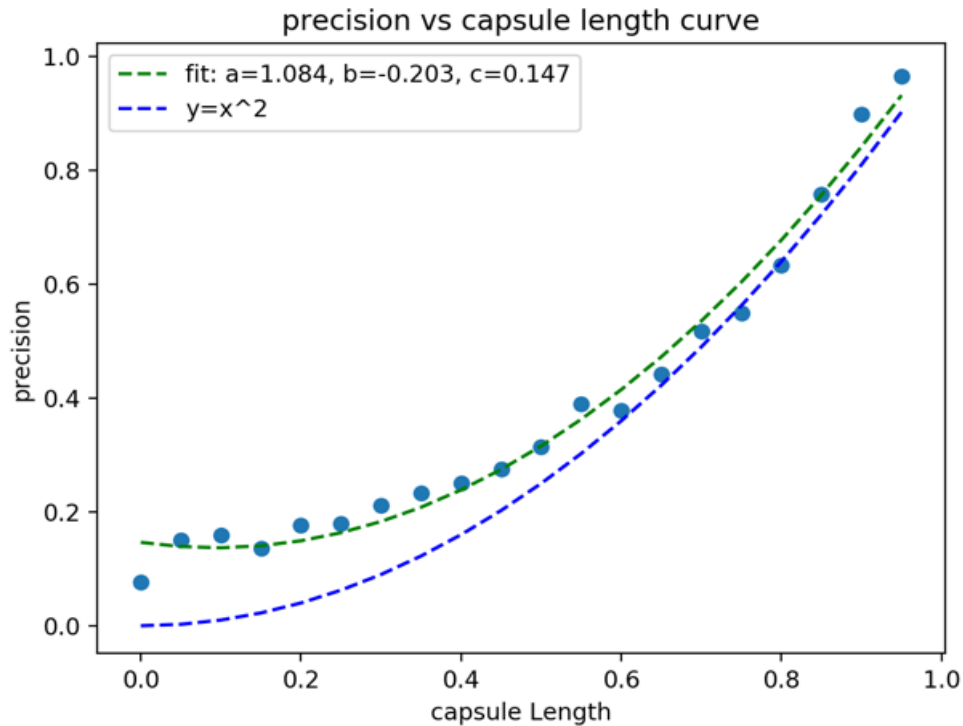


Figure 7-2 The fitting curve of precision (percentage of true positive in the bin) versus the capsule length. The green line is the fitting curve and the blue line ( $y=x^2$ ) is for reference.

### 7.2.3 Proposed model performance compared with previous predictors

For comparing with other predictors, the public benchmark GT320 was used. Following the previous studies, a five-fold cross validation results were reported, as shown in Table 7.5. This GT320 is an imbalanced dataset, but for objective evaluation, we did not sample any balanced data from training or testing, as done in previous studies. Table 7.5 shows that the proposed inception capsule network outperformed all the previous methods by a significant margin.

Table 7.5 Performance comparison with previous predictors using GT320 benchmark.

Methods	MCC
Our Approach	0.45
Zhu <i>et al.</i> , 2012	0.38
Hu's SVM	0.18
SNNS	0.17
GTSVM	0.12
WEKA-logistic regression	0.12
WEKA-naïve Bayes	0.11

\*The results of WAKA, SNNS were obtained from (Kaur and Raghava, 2002), the result of GTSVM was obtained from (Pham *et al.*, 2005) and result of Hu's SVM was from (Hu and Li, 2008). Zhu *et al.*, (2012) is the previous best predictor result.

### 7.2.4 Extend CapsuleNet for classic and inverse gamma-turn prediction

Many previous gamma-turn predictors only predict whether a turn is gamma-turn or not. Here, we also extended our deep inception capsule model for classic and inverse gamma-turn prediction. The experiment dataset is still CullPDB, and inverse and classic labels were assigned using PROMOTIF (Hutchinson and Thornton, 1996). The same deep inception capsule network (shown in Figure 7-1 A) was applied except the last turn capsule layer now has three capsules to predict non-turn, inverse turn or classic turn as a three-class classification problem. The performance metric Q3 is used which is the accuracy of correct prediction for each class. The prediction results are shown in Table 6. Different numbers of proteins were used to build the training set. The validation and test set contain 500

proteins each. The CullPDB dataset contains 10,007 proteins which have 1383 classic turns, 17,800 inverse turns, and 2,439,018 non-turns in total. This is a very imbalanced dataset. In this experiment, the balanced training set, validation set, and test set were generated as follows: The inverse turn samples were randomly drawn as much as classic turn sample size. For the non-turn samples, they were randomly drawn twice as much as classic turn sample size, i.e. the sum of inverse turn samples and classic turn samples. The training loss and validation loss curves are shown in Figure 7-3. From the loss curve, it shows that after about 75 epochs, the model learning process was converging. Since the model hyper-parameters had been explored in the earlier experiments, during this experiment, we adopted similar values, i.e., the window size was chosen 17 amino acids, the filter size is 256, the convolution kernel size was chosen 3, the dynamic routing was chosen 3 iterations and dropout ratio was 0.3.

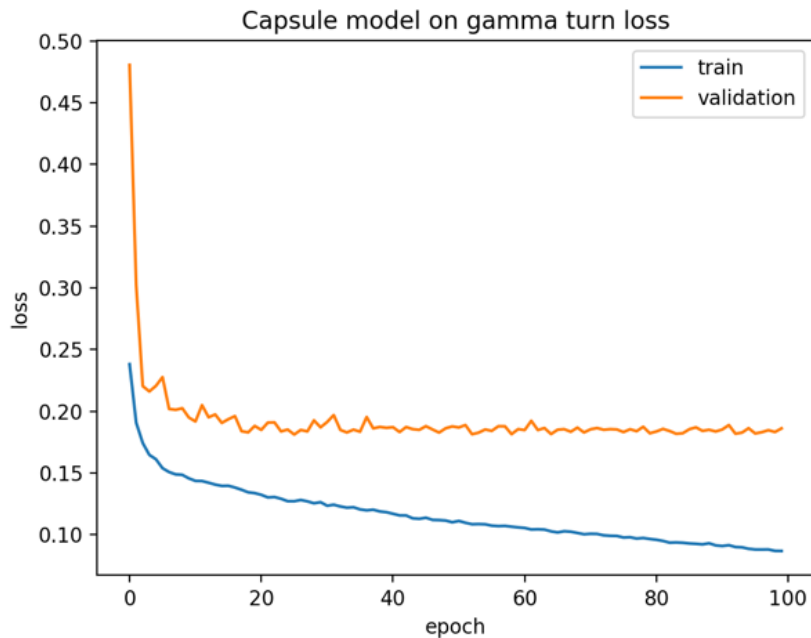


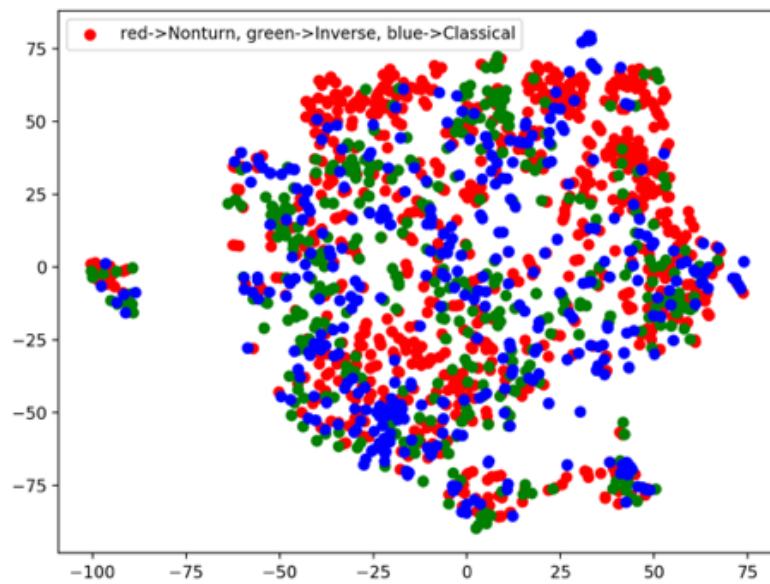
Figure 7-3 Training loss and validation loss curve of deep inception capsule network for classic and inverse gamma-turn.

Table 7.6 Non-turn, inverse and classic turn prediction results.

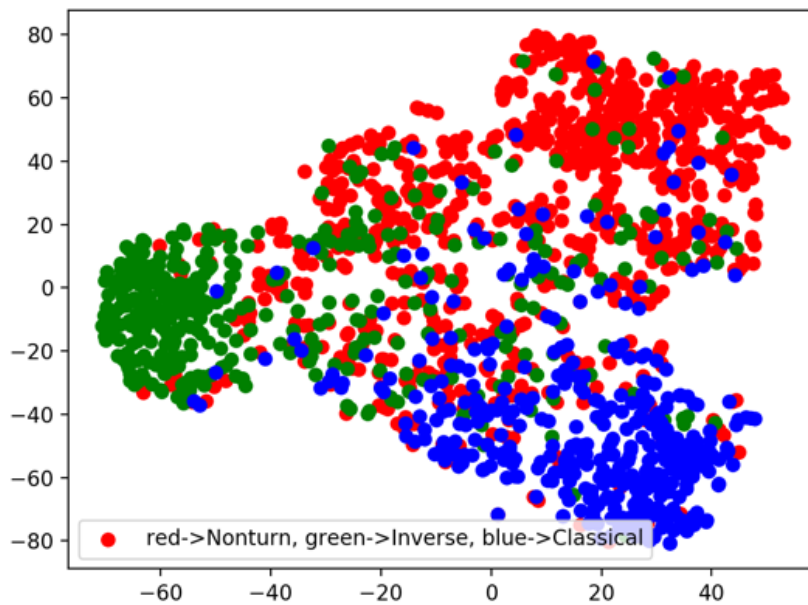
Training size	Test average Q3	Time (hr)	P-value
5000	0.6839( $\pm 0.0053$ )	0.25( $\pm 0.20$ )	-
6000	0.6783( $\pm 0.0076$ )	0.38( $\pm 0.22$ )	0.2706
7000	0.6864( $\pm 0.0124$ )	0.34( $\pm 0.16$ )	0.3057

### 7.2.5 Visualization of the features learnt by capsules

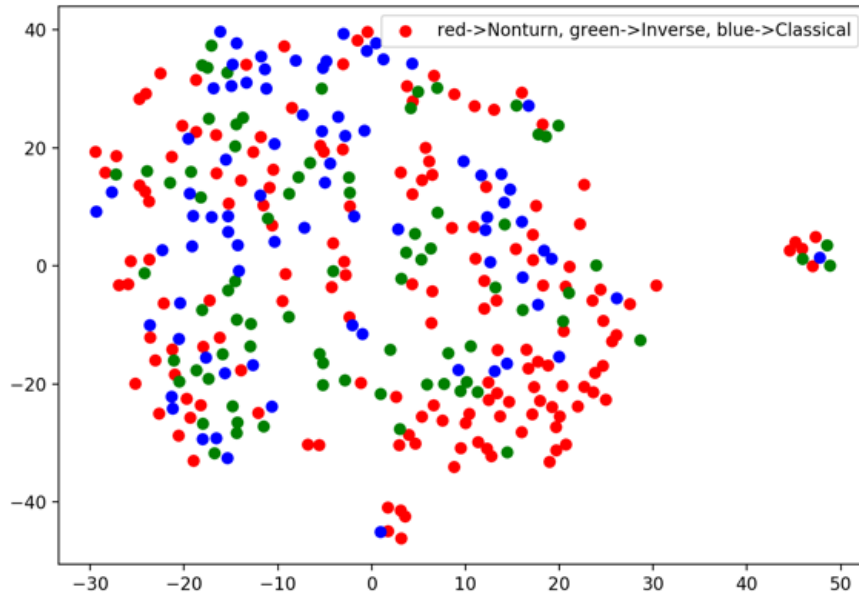
In order to verify whether the extract high-level features learnt/extracted from the input data have the prediction power and are generalizable, t-SNE (Maaten and Hinton, 2008) was applied to visualize the input features and the capsule features for both the training data and the test data. Figure 7-4 (A) shows the t-SNE plot of the input features from the training data before the training. The input data has 45 features (i.e. 45 dimensions), and t-SNE can project 45 dimensions onto two principal dimensions and visualize it. There was no clear cluster in the training data. Figure 7-4 (B) shows the t-SNE plot of the capsule features from the training data. The turn capsule contains 16 dimensions, and the t-SNE can similarly project the capsule features to two major principal features and visualize it. The clusters were obviously formed after the training. Figure 7-4 (C) and (D) show the t-SNE plots for the input features and the capsule features of the test data. There was no clear cluster for the input features in the test data either. The capsule features still tend to be clustered together in the test data, although to less extent than the training data.



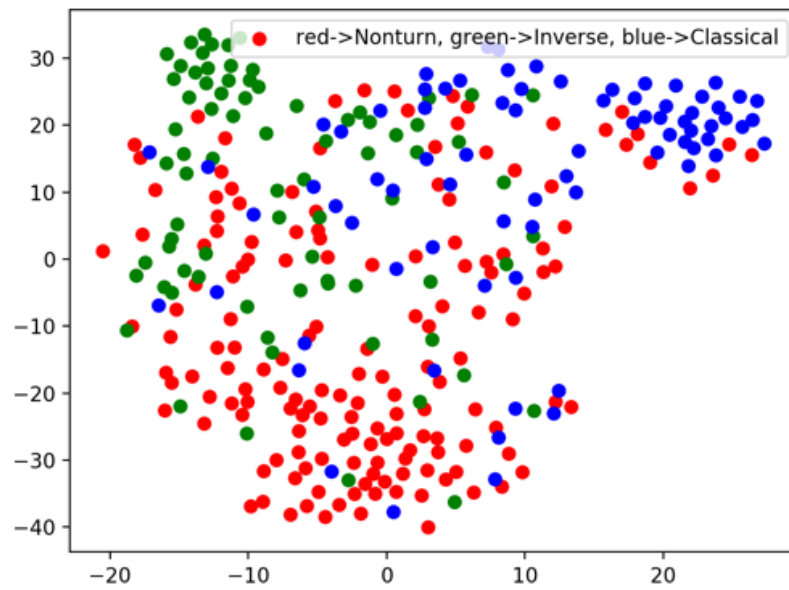
(A)



(B)



(C)

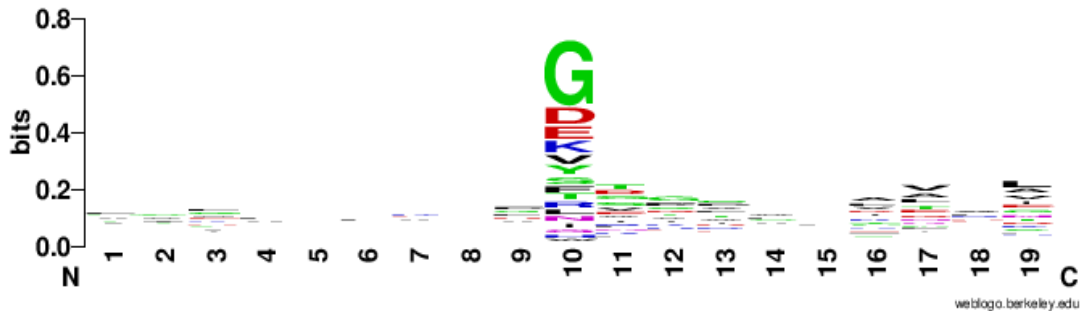


(D)

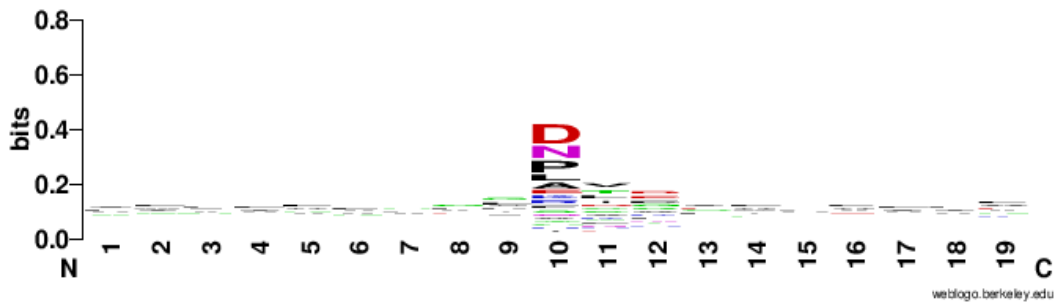


Figure 7-4 t-SNE plots of capsule network features. (A) and (B) are plots of the input features and the capsule features, respectively for training dataset (3000 proteins with 1516 turn samples). (C) and (D) are plots of the input features and the capsule features, respectively for the test dataset (500 proteins with 312 turn samples). Red dots represent non-turns, green dots represent inverse turns and blue dots represent classic turns.

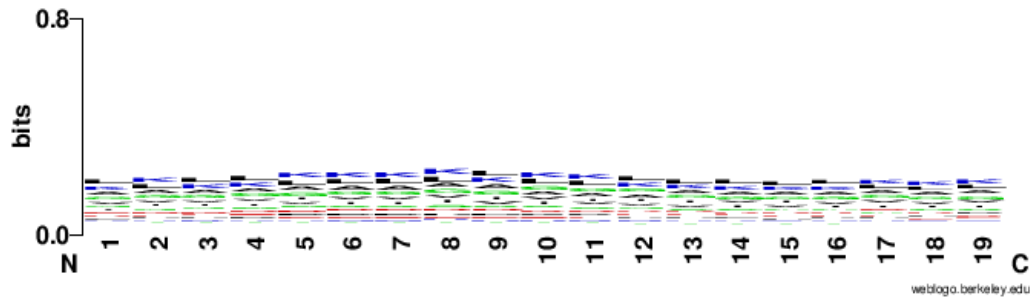
Figure 7-5 (A) shows the classic turn Weblogo and Figure 7-5 (B) shows the inverse turn Weblogo (Crooks et al., 2004). In the two plots, the y axis has the same height of 0.8 bits. Both types of turns have some visible features and the classic turn Weblogo contains more information content than the inverse turn.



(A)



(B)



(C)

Figure 7-5 (A) Classic turn Weblgo; (B) inverse turn Weblgo; and (C) Non-turn Weblgo

### 7.2.6 Ablation study

To discover the important elements in our proposed network, an ablation study was performed by removing or replacing different components in the deep inception capsule network. In particular, we tested the performance of the proposed models without the capsule component, replacing the capsule component with CNN, or replacing inception component with CNN. These sets of experiments were performed using the same amount of data (3000 proteins for training, 500 proteins for validation, and 500 for test) and the same parameter setting: dropout ratio 0.5 and window size 17. From the ablation test result presented in Table 7.7, we found that the capsule component is the most effective component in our network, since the performance dropped significantly when removing or replacing the capsule component. The inception component also acts as an important component as it can effectively extract feature maps for capsule components compared to CNN.

Table 7.7 Ablation test.

Model	MCC
Replace inception component with CNN	0.4544( $\pm 0.0106$ )
Replace capsule component with CNN	0.4485( $\pm 0.0056$ )
Without capsule component	0.4551( $\pm 0.0059$ )
Proposed Design	0.4752( $\pm 0.0111$ )

### 7.3 Conclusion and Discussion

In this work, the latest deep-learning framework, CapsuleNet, was applied to protein gamma-turn prediction. Instead of applying capsule network directly, a new model called inception capsule network was proposed and has shown improved performance comparing to previous predictors. This work has several innovations.

First of all, this work is the first application of deep neural networks to protein gamma-turn prediction. Compared to previous traditional machine-learning methods for protein gamma-turn prediction, this work uses a more sophisticated, yet efficient, deep-learning architecture, which outperforms previous methods. A software tool has been developed and it will provide the research community a powerful deep-learning prediction tool for gamma-turn prediction. The ablation test was performed, and the importance of capsule component was verified.

Second, this work is the earliest application of CapsuleNet to protein structure-related prediction, and possibly to any bioinformatics problems to our knowledge, as CapsuleNet was just published in 2017. Here, we proposed an inception capsule network for protein gamma-turn prediction and explored some unique characters of capsules. To explore the capsule length, we designed an experiment of grouping each capsule length into several bins and discovered the relationship between prediction precision and capsule length. A

nonlinear curve can be applied to fit the data and further used for estimating the prediction confidence. In addition, the network was extended to inverse turn and classical turn prediction. The inverse turn capsule and classical turn capsule were further explored by showing the t-SNE visualization of the learnt capsule features. Some interesting motifs were visualized by Weblogo.

Third, new features have been explored and applied to gamma-turn prediction. The features used for network training, namely HHBlits profiles and predicted shape string, contain high information content making deep learning very effective. The HHBlits profiles provide evolutionary information while shape strings provide complementary structural information for effectively predicting gamma turns.

Last but not least, previous gamma-turn resources are very limited and outdated. A few servers are not maintained, and no downloadable executable of gamma-turn is available. Here a free tool with source code utilizing deep learning and state-of-the-art CapsuleNet will be ready for researchers to use.

## CHAPTER 8 SUMMARY

Protein secondary structure and super-secondary structure are providing useful features for protein tertiary structure prediction. Deep learning can lead to significant improvement to these problems. In this dissertation, several novel deep neural networks were proposed for protein secondary structure and super-secondary structure prediction:

In the work of Deep Inception-Inside-Inception, a new deep neural network architecture Deep3I was proposed for protein secondary structure prediction and other protein structural feature prediction, such as Psi-Phi angle prediction. Extensive experimental results show that Deep3I obtained more accurate predictions than the best state-of-the-art methods and tools. The experiments were designed carefully, and the datasets used in training, e.g., the CullPDB dataset, were processed to remove any significantly similar sequences with the test sets using CD-HIT to avoid any bias. Compared to previous deep-learning methods for protein secondary structure prediction and Psi-Phi angle prediction, this work uses a more sophisticated, yet efficient, deep-learning architecture. Deep3I utilizes hierarchical deep Inception blocks to effectively process local and non-local interactions of residues. An open source software has been developed based on Deep3I. It will provide the research community a powerful prediction tool for secondary structures and Psi-Phi angles. A URL for downloading the tool will be provided upon acceptance of publication.

In the work of Deep neighbor residual network: Compared with previous deep-learning methods for protein secondary structure prediction, the new method consists of two types of networks: a new deep neighbor residual network (DeepNRN) for predicting secondary structures and a Struct2Struct network for making the predictions more protein-like.

Extensive experimental results show the new method achieved better Q3 and Q8 prediction accuracies than existing state-of-the-art methods.

In the work of deep residual inception network, a new deep neural network architecture DeepRIN was proposed for protein Psi-Phi angle prediction. Extensive experimental results show that DeepRIN consistently generated more accurate predictions than the best state-of-the-art methods. The experiments were designed carefully, and the datasets used in training, e.g., the CullPDB dataset, were processed to remove any significantly similar sequences with the test sets using CD-HIT to avoid any bias. Compared to previous deep-learning methods for Psi-Phi angle prediction, this work developed a more sophisticated, yet efficient, deep-learning architecture. DeepRIN utilized hierarchical deep Inception blocks to effectively process local and non-local interactions between residues and the residual shortcuts help propagate high-level features into deep networks. A software tool has been developed based on DeepRIN and is made available to the research community for download at <http://dlsrv8.cs.missouri.edu/~cf797/MUFoldAngle/>.

In the work of deep dense inception network, a new a new deep neural network architecture DeepDIN was proposed for protein beta-turn prediction. Extensive experimental results show that DeepDIN obtained more accurate predictions than the best state-of-the-art methods and tools. Compared to previous machine-learning methods for protein beta-turn prediction, this work uses a more sophisticated, yet efficient, deep-learning architecture. The proposed DeepDIN takes input of the entire protein sequence as the input feature, whereas all previous predictors rely on a fix-sized sliding window, which is more effective and efficient to extract long-range residue interactions. DeepDIN utilizes densely connected inception blocks to effectively process local and non-local interactions

of residues. Second, since the beta-turn dataset is very imbalanced (the ratio of positive samples over negative samples is about 1:9), balanced learning and transfer learning were applied to overcome the problem. It is worth mentioning that the transfer learning was originally applied to image recognition tasks, here we apply similar method to training models for small beta-turn classification tasks. The pre-trained base network is effective in learning some more general beta-turn features, then the transfer learning technique can transfer the base network to some more specific models that can classify nine-class beta-turns. This demonstrates some good examples of handling imbalanced datasets in protein sequence analysis. Third, this work quantitatively discovered how different input features can affect the beta-turn prediction. For example, some good features such as shape string and HHBlits profile can improve beta-turn classification effectively. In future work, the small beta-turn classes still have room for further improvement. Also, those features can be useful for other turn prediction problems, such as gamma-turn prediction (Pham *et al.*, 2005). Last but not least, we have implemented a tool called MUFold-BetaTurn which utilizes the proposed DeepDIN architecture for beta-turn prediction. This tool is ready for the research community to use freely.

In this work of deep inception capsule network, the latest deep-learning framework, CapsuleNet, was applied to protein gamma-turn prediction. Instead of applying capsule network directly, a new model called inception capsule network was proposed and has shown improved performance compared to previous predictors. This work has several innovations. First of all, this work is the first application of deep neural networks to protein gamma-turn prediction. Compared to previous traditional machine-learning methods for protein gamma-turn prediction, this work uses a more sophisticated, yet efficient, deep-

learning architecture, which outperforms previous methods. A software tool has been developed and it will provide the research community a powerful deep-learning prediction tool for gamma-turn prediction. The ablation test was performed, and the importance of capsule component was verified. Second, this work is the earliest application of CapsuleNet to protein structure-related prediction, and possibly to any bioinformatics problems to our knowledge, as CapsuleNet was just published in 2017. Here, we proposed an inception capsule network for protein gamma-turn prediction and explored some unique characters of capsules. To explore the capsule length, we designed an experiment of grouping each capsule length into several bins and discovered the relationship between prediction precision and capsule length. A nonlinear curve can be applied to fit the data and further used for estimating the prediction confidence. In addition, the network was extended to inverse turn and classical turn prediction. The inverse turn capsule and classical turn capsule were further explored by showing the t-SNE visualization of the learnt capsule features. Some interesting motifs were visualized by Weblogo. Third, new features have been explored and applied to gamma-turn prediction. The features used for network training, namely HHBlits profiles and predicted shape string, contain high information content making deep learning very effective. The HHBlits profiles provide evolutionary information while shape strings provide complementary structural information for effectively predicting gamma turns. Last but not least, previous gamma-turn resources are very limited and outdated. A few servers are not maintained, and no downloadable executable of gamma-turn is available. Here a free tool with source code utilizing deep learning and state-of-the-art CapsuleNet will be ready for researchers to use.



Last but not least, we built a web server called MUFold-SS-Angle that predicts protein secondary structure and backbone torsion angle from the protein sequence. This server employs MUFold-SS and MUFold-Angle, which are two standalone tools we recently developed to predict secondary structure and backbone torsion angles, respectively. Both tools outperform other predictors/servers in both easy cases (proteins with similar sequences in PDB) or hard cases (proteins without detectable similarity in PDB) on extensive test cases.

**The major achievements and contributions are:**

- 1) A new very deep learning network architecture, Deep3I, was proposed to effectively process both local and global interactions between amino acids in making accurate secondary structure prediction and Psi-Phi angle prediction. Extensive experimental results show that the new method outperforms the best existing methods and other deep neural networks significantly. An open-source tool Deep3I-SS was implemented based on the new method. This tool can predict the protein secondary structure and the Psi-Phi angles fast and accurately.
- 2) DeepNRN, a new deep-learning network with new architecture, is proposed for protein secondary structure prediction; and experimental results on the CB513, CASP10, CASP11, CASP12 benchmark data sets show that DeepNRN outperforms existing methods and obtains the best results on multiple data sets.
- 3) A new deep neural network architecture, DeepRIN, is proposed to effectively capture and process both local and global interactions between amino acids in a protein sequence. Extensive experiments using popular benchmark datasets were conducted to demonstrate that DeepRIN outperformed the best existing tools significantly. A

- software tool based on DeepRIN is made available to the research community for download.
- 4) A new deep neural network architecture, DeepDIN, is proposed to beta-turn classification problem. In addition, balanced learning and transfer learning techniques were applied overcome the problem of imbalanced dataset. Several new features were explored quantitatively for beta turn prediction effectively.
  - 5) A new deep neural network architecture, DeepICN, is proposed to gamma-turn classification problem. Also, capsule length, representing the confidence of prediction, was further explored. This is the first application of capsule networks to biological sequence analysis.
  - 6) A new web server, called MUFold-SS-Angle, is a combined web service of both MUFold-SS and MUFold-Angle tools and will provide the community a better usage of the software.

## Refereed publication:

- Fang, Chao, Yi Shang, and Dong Xu. "A New Deep Neighbor-Residual Neural Network for Protein Secondary Structure Prediction." *Tools with Artificial Intelligence (ICTAI), 2017 IEEE 29th International Conference on.* IEEE, 2017.
- Fang, Chao, Yi Shang, and Dong Xu. "MUFOLD-SS: New deep inception-inside-inception networks for protein secondary structure prediction." *Proteins: Structure, Function, and Bioinformatics* 86.5 (2018): 592-598.
- Fang, Chao, Yi Shang, and Dong Xu. "Prediction of Protein Backbone Torsion Angles Using Deep Residual Inception Neural Networks." *IEEE/ACM Transactions on Computational Biology and Bioinformatics* (2018).
- Fang, Chao, Yi Shang, and Dong Xu. (2018). "Improving Protein Gamma-Turn Prediction Using Inception Capsule Networks." (submitted)
- Fang, Chao, Yi Shang, and Dong Xu. (2018). "MUFold-BetaTurn: A Deep Inception Network for Protein Beta-Turn Prediction" (submitted)
- Fang, Chao, Zhaoyu Li, Dong Xu and Yi Shang. (2018) "MUFold-SS-Angle: A Web Server for Protein Secondary Structure and Backbone Torsion Angle Prediction." *Bioinformatics*, (submitted).

## REFERENCE

- Abadi, M., Agarwal, A., Barham, P., Brevdo, E., Chen, Z., Citro, C., Corrado, G.S., Davis, A., Dean, J., Devin, M. and Ghemawat, S., (2016). Tensorflow: Large-scale machine learning on heterogeneous distributed systems. *arXiv preprint arXiv:1603.04467*.
- Adamczak, R., Porollo, A. and Meller, J., (2004). Accurate prediction of solvent accessibility using neural networks–based regression. *Proteins: Structure, Function, and Bioinformatics*, 56(4), pp.753-767.
- Altschul, S.F., Madden, T.L., Schäffer, A.A., Zhang, J., Zhang, Z., Miller, W. and Lipman, D.J., (1997). Gapped BLAST and PSI-BLAST: a new generation of protein database search programs. *Nucleic acids research*, 25(17), pp.3389-3402.
- Alkorta, I., Suarez, M. L., Herranz, R., González-Muñiz, R., and García-López, M. T. (1996). Similarity study on peptide  $\gamma$ -turn conformation mimetics. *Molecular modeling annual*, 2(1), 16-25.
- Anfinsen, C. B. (1973). Principles that govern the folding of protein chains. *Science*, 181(4096), 223-230.
- Asgari, E. and Mofrad, M.R., (2015). Continuous distributed representation of biological sequences for deep proteomics and genomics. *PloS one*, 10(11), p.e0141287.
- Bahdanau, D., Cho, K., and Bengio, Y. (2014). Neural machine translation by jointly learning to align and translate. *arXiv preprint arXiv:1409.0473*.
- Berman, H. M., Westbrook, J., Feng, Z., Gilliland, G., Bhat, T. N., Weissig, H., ... & Bourne, P. E. (2006). The Protein Data Bank, 1999–. In *International Tables for Crystallography Volume F: Crystallography of biological macromolecules* (pp. 675-684). Springer Netherlands.

- Biegert, A. and Söding, J., (2009). Sequence context-specific profiles for homology searching. *Proceedings of the National Academy of Sciences*, 106(10), pp.3770-3775.
- Bjorkman, P. J., & Parham, P. (1990). Structure, function, and diversity of class I major histocompatibility complex molecules. *Annual review of biochemistry*, 59(1), 253-288.
- Boratyn, G.M., Schäffer, A.A., Agarwala, R., Altschul, S.F., Lipman, D.J. and Madden, T.L., (2012). Domain enhanced lookup time accelerated BLAST. *Biology direct*, 7(1), p.12.
- Bragg, W. L., Phillips, D. C., & Lipson, H. (1975). *development of X-ray analysis*. G. Bell.
- Busia, A. and Jaitly, N., (2017). Next-Step Conditioned Deep Convolutional Neural Networks Improve Protein Secondary Structure Prediction. *arXiv preprint arXiv:1702.03865*.
- Bystrov, V. F., Portnova, S. L., Tsetlin, V. I., Ivanov, V. T., and Ovchinnikov, Y. A. (1969). Conformational studies of peptide systems: The rotational states of the NH-CH fragment of alanine dipeptides by nuclear magnetic resonance. *Tetrahedron*, 25(3), 493-515.
- Cheng, J., Randall, A.Z., Sweredoski, M.J. and Baldi, P., (2005). SCRATCH: a protein structure and structural feature prediction server. *Nucleic acids research*, 33(Suppl. 2), pp.W72-W76.
- Chollet, F., (2015). Keras.
- Chollet, F. (2016). Xception: Deep Learning with Depthwise Separable Convolutions. *arXiv preprint arXiv:1610.02357*.

- Ciregan, D., Meier, U., & Schmidhuber, J. (2012, June). Multi-column deep neural networks for image classification. In *Computer Vision and Pattern Recognition (CVPR), 2012 IEEE Conference on* (pp. 3642-3649). IEEE.
- Collobert, R., & Weston, J. (2008, July). A unified architecture for natural language processing: Deep neural networks with multitask learning. In *Proceedings of the 25th international conference on Machine learning* (pp. 160-167). ACM.
- Chou, P. Y., and Fasman, G. D. (1979). Prediction of beta-turns. *Biophysical Journal*, 26(3), 367-383.
- Chou, K. C., and Blinn, J. R. (1997). Classification and prediction of  $\beta$ -turn types. *Journal of protein chemistry*, 16(6), 575-595.
- Chou, P. Y., and Fasman, G. D. (1974). Conformational parameters for amino acids in helical,  $\beta$ -sheet, and random coil regions calculated from proteins. *Biochemistry*, 13(2), 211-222.
- Chou, K. C. (1997). Prediction of beta-turns in proteins. *J Pept Res*, 49(2), 120-44.
- Cole, C., Barber, J. D., and Barton, G. J. (2008). The Jpred 3 secondary structure prediction server. *Nucleic acids research*, 36(suppl\_2), W197-W201.
- Crooks, G. E., Hon, G., Chandonia, J. M., and Brenner, S. E. (2004). WebLogo: a sequence logo generator. *Genome research*, 14(6), 1188-1190.
- Dai, L. and Zhou, Y., 2011. Characterizing the existing and potential structural space of proteins by large-scale multiple loop permutations. *Journal of molecular biology*, 408(3), pp.585-595.

- Deng, J., Dong, W., Socher, R., Li, L. J., Li, K., & Fei-Fei, L. (2009, June). Imagenet: A large-scale hierarchical image database. In *Computer Vision and Pattern Recognition, 2009. CVPR 2009. IEEE Conference on* (pp. 248-255). IEEE.
- Dill, K. A. (1990). Dominant forces in protein folding. *Biochemistry*, 29(31), 7133-7155.
- Dill, K. A., & MacCallum, J. L. (2012). The protein-folding problem, 50 years on. *science*, 338(6110), 1042-1046.
- Dor, O., & Zhou, Y. (2007). Achieving 80% ten-fold cross-validated accuracy for secondary structure prediction by large-scale training. *Proteins: Structure, Function, and Bioinformatics*, 66(4), 838-845.
- Dor, O., & Zhou, Y. (2007). Real-SPINE: An integrated system of neural networks for real-value prediction of protein structural properties. *PROTEINS: Structure, Function, and Bioinformatics*, 68(1), 76-81.
- Drozdetskiy, A., Cole, C., Procter, J. and Barton, G.J., (2015). JPred4: a protein secondary structure prediction server. *Nucleic acids research*, 43(W1), pp.W389-W394.
- Fang, C., Shang, Y., and Xu, D. (2018). MUFOLD-SS: New Deep Inception-Inside-Inception Networks for Protein Secondary Structure Prediction. *Proteins: Structure, Function, and Bioinformatics*.
- Fang, C., Shang, Y., and Xu, D. (2017). A New Deep Neighbor-Residual Neural Network for Protein Secondary Structure Prediction. *29th IEEE International Conference on Tools with Artificial Intelligence (ICTAI)*, IEEE.
- Fang, C., Shang, Y., and Xu, D. (2018). Prediction of Protein Backbone Torsion Angles Using Deep Residual Inception Neural Networks. *IEEE/ACM Transactions on*

- Computational Biology and Bioinformatics*, vol. PP, no. 99, pp. 1-1. doi: 10.1109/TCBB.2018.2814586.
- Faraggi, E., Xue, B., & Zhou, Y. (2009). Improving the prediction accuracy of residue solvent accessibility and real-value backbone torsion angles of proteins by guided-learning through a two-layer neural network. *Proteins: Structure, Function, and Bioinformatics*, 74(4), 847-856.
- Faraggi, E., Yang, Y., Zhang, S., & Zhou, Y. (2009). Predicting continuous local structure and the effect of its substitution for secondary structure in fragment-free protein structure prediction. *Structure*, 17(11), 1515-1527.
- FAUCHÈRE, J. L., Charton, M., Kier, L. B., Verloop, A., & Pliska, V. (1988). Amino acid side chain parameters for correlation studies in biology and pharmacology. *Chemical Biology & Drug Design*, 32(4), 269-278.
- Fu, L., Niu, B., Zhu, Z., Wu, S. and Li, W., 2012. CD-HIT: accelerated for clustering the next-generation sequencing data. *Bioinformatics*, 28(23), pp.3150-3152.
- Fuchs, P. F., and Alix, A. J. (2005). High accuracy prediction of  $\beta$ -turns and their types using propensities and multiple alignments. *Proteins: Structure, Function, and Bioinformatics*, 59(4), 828-839.
- Garnier, J., Osguthorpe, D. J., and Robson, B. (1978). Analysis of the accuracy and implications of simple methods for predicting the secondary structure of globular proteins. *Journal of molecular biology*, 120(1), 97-120.



- Gibson, K. D., & Scheraga, H. A. (1967). Minimization of polypeptide energy. I. Preliminary structures of bovine pancreatic ribonuclease S-peptide. *Proceedings of the National Academy of Sciences*, 58(2), 420-427.
- Gibrat, J. F., Garnier, J., and Robson, B. (1987). Further developments of protein secondary structure prediction using information theory: new parameters and consideration of residue pairs. *Journal of molecular biology*, 198(3), 425-443.
- Gregor, K., Danihelka, I., Graves, A., Rezende, D. J., & Wierstra, D. (2015). DRAW: A recurrent neural network for image generation. *arXiv preprint arXiv:1502.04623*.
- Gehring, J., Auli, M., Grangier, D., Yarats, D., and Dauphin, Y. N. (2017). Convolutional Sequence to Sequence Learning. *arXiv preprint arXiv:1705.03122*.
- Guruprasad, K., and Rajkumar, S. (2000). Beta-and gamma-turns in proteins revisited: a new set of amino acid turn-type dependent positional preferences and potentials. *Journal of biosciences*, 25(2), 143-156.
- Guruprasad, K., M. J. Rao, S. Adindla, and L. Guruprasad. "Combinations of turns in proteins." *Chemical Biology and Drug Design* 62, no. 4 (2003): 167-174.
- Han, H., Wang, W. Y., and Mao, B. H. (2005). Borderline-SMOTE: a new over-sampling method in imbalanced data sets learning. *Advances in intelligent computing*, 878-887.
- He, K., Zhang, X., Ren, S., & Sun, J. (2016). Deep residual learning for image recognition. In *Proceedings of the IEEE conference on computer vision and pattern recognition* (pp. 770-778).
- Heffernan, R., Dehzangi, A., Lyons, J., Paliwal, K., Sharma, A., Wang, J., ... & Yang, Y. (2015). Highly accurate sequence-based prediction of half-sphere exposures of amino acid residues in proteins. *Bioinformatics*, 32(6), 843-849.

- Heffernan, R., Yang, Y., Paliwal, K., & Zhou, Y. (2017). Capturing Non-Local Interactions by Long Short Term Memory Bidirectional Recurrent Neural Networks for Improving Prediction of Protein Secondary Structure, Backbone Angles, Contact Numbers, and Solvent Accessibility. *Bioinformatics*, btx218.
- Hochreiter, S., & Schmidhuber, J. (1997). Long short-term memory. *Neural computation*, 9(8), 1735-1780.
- Hu, X., and Li, Q. (2008). Using support vector machine to predict  $\beta$ - and  $\gamma$ -turns in proteins. *Journal of computational chemistry*, 29(12), 1867-1875.
- Huang, Y. M., & Bystroff, C. (2005). Improved pairwise alignments of proteins in the Twilight Zone using local structure predictions. *Bioinformatics*, 22(4), 413-422.
- Huang, G., Liu, Z., Weinberger, K.Q. and van der Maaten, L., (2016). Densely connected convolutional networks. *arXiv preprint arXiv:1608.06993*.
- Hutchinson, E. G., and Thornton, J. M. (1994). A revised set of potentials for  $\beta$ -turn formation in proteins. *Protein Science*, 3(12), 2207-2216.
- Ioffe, S. and Szegedy, C., 2015, June. Batch normalization: Accelerating deep network training by reducing internal covariate shift. In *International Conference on Machine Learning* (pp. 448-456).
- Ison, R. E., Hovmoller, S., and Kretsinger, R. H. (2005). Proteins and their shape strings. *IEEE engineering in medicine and biology magazine*, 24(3), 41-49.
- Jacobson, M., & Sali, A. (2004). Comparative protein structure modeling and its applications to drug discovery. *Annual reports in medicinal chemistry*, 39, 259-276.

- Jahandideh, S., Sarvestani, A. S., Abdolmaleki, P., Jahandideh, M., and Barfeie, M. (2007).  $\gamma$ -Turn types prediction in proteins using the support vector machines. *Journal of theoretical biology*, 249(4), 785-790.
- Jones, D. T. (1999). Protein secondary structure prediction based on position-specific scoring matrices. *Journal of molecular biology*, 292(2), 195-202.
- Kang, H. S., Kurochkina, N. A., & Lee, B. (1993). Estimation and use of protein backbone angle probabilities. *Journal of molecular biology*, 229(2), 448-460.
- Kabsch, W., & Sander, C. (1983). Dictionary of protein secondary structure: pattern recognition of hydrogen-bonded and geometrical features. *Biopolymers*, 22(12), 2577-2637.
- Kaur, H., Garg, A., and Raghava, G. P. S. (2007). PEPstr: a de novo method for tertiary structure prediction of small bioactive peptides. *Protein and peptide letters*, 14(7), 626-631.
- Kaur, H., and Raghava, G. P. S. (2002). BetaTPred: prediction of  $\beta$ -turns in a protein using statistical algorithms. *Bioinformatics*, 18(3), 498-499.
- Kaur, H., and Raghava, G. P. S. (2004). A neural network method for prediction of  $\beta$ -turn types in proteins using evolutionary information. *Bioinformatics*, 20(16), 2751-2758.
- Kim, S. (2004). Protein  $\beta$ -turn prediction using nearest-neighbor method. *Bioinformatics*, 20(1), 40-44.
- Kingma, D. P., & Ba, J. (2014). Adam: A method for stochastic optimization. *arXiv preprint arXiv:1412.6980*.

- Karchin, R., Cline, M., Mandel-Gutfreund, Y., & Karplus, K. (2003). Hidden Markov models that use predicted local structure for fold recognition: alphabets of backbone geometry. *Proteins: Structure, Function, and Bioinformatics*, 51(4), 504-514.
- Kendrew, J. C., Dickerson, R. E., Strandberg, B. E., Hart, R. G., Davies, D. R., Phillips, D. C., & Shore, V. C. (1960). Structure of myoglobin: A three-dimensional Fourier synthesis at 2 Å. resolution. *Nature*, 185(4711), 422-427.
- Krizhevsky, A., Sutskever, I., & Hinton, G. E. (2012). Imagenet classification with deep convolutional neural networks. In *Advances in neural information processing systems* (pp. 1097-1105).
- Kirschner, A., and Frishman, D. (2008). Prediction of  $\beta$ -turns and  $\beta$ -turn types by a novel bidirectional Elman-type recurrent neural network with multiple output layers (MOLEBRNN). *Gene*, 422(1), 22-29.
- Kountouris, P., and Hirst, J. D. (2010). Predicting  $\beta$ -turns and their types using predicted backbone dihedral angles and secondary structures. *BMC bioinformatics*, 11(1), 407.
- Kuang, R., Leslie, C. S., & Yang, A. S. (2004). Protein backbone angle prediction with machine learning approaches. *Bioinformatics*, 20(10), 1612-1621.
- Laskowski, R. A., Watson, J. D., & Thornton, J. M. (2003). From protein structure to biochemical function?. *Journal of structural and functional genomics*, 4(2-3), 167-177.
- Lawrence, S., Giles, C. L., Tsoi, A. C., & Back, A. D. (1997). Face recognition: A convolutional neural-network approach. *IEEE transactions on neural networks*, 8(1), 98-113.
- LeCun, Y., Bottou, L., Bengio, Y., & Haffner, P. (1998). Gradient-based learning applied to document recognition. *Proceedings of the IEEE*, 86(11), 2278-2324.

- Lewis, P. N., Momany, F. A., and Scheraga, H. A. (1973). Chain reversals in proteins. *Biochimica et Biophysica Acta (BBA)-Protein Structure*, 303(2), 211-229.
- Li, Z. and Yu, Y., (2016). Protein secondary structure prediction using cascaded convolutional and recurrent neural networks. *arXiv preprint arXiv:1604.07176*.
- Li, S. Z., Lee, J. H., Lee, W., Yoon, C. J., Baik, J. H., and Lim, S. K. (1999). Type I  $\beta$ -turn conformation is important for biological activity of the melanocyte-stimulating hormone analogues. *The FEBS Journal*, 265(1), 430-440.
- Li, H., Hou, J., Adhikari, B., Lyu, Q., & Cheng, J. (2017). Deep learning methods for protein torsion angle prediction. *BMC bioinformatics*, 18(1), 417.
- Li, W., & Godzik, A. (2006). Cd-hit: a fast program for clustering and comparing large sets of protein or nucleotide sequences. *Bioinformatics*, 22(13), 1658-1659.
- Lyons, J., Dehzangi, A., Heffernan, R., Sharma, A., Paliwal, K., Sattar, A., ... & Yang, Y. (2014). Predicting backbone C $\alpha$  angles and dihedrals from protein sequences by stacked sparse auto-encoder deep neural network. *Journal of computational chemistry*, 35(28), 2040-2046.
- Maaten, L. V. D., and Hinton, G. (2008). Visualizing data using t-SNE. *Journal of machine learning research*, 9(Nov), 2579-2605.
- Magnan, C.N. and Baldi, P., (2014). SSpro/ACCpro 5: almost perfect prediction of protein secondary structure and relative solvent accessibility using profiles, machine learning and structural similarity. *Bioinformatics*, 30(18), pp.2592-2597.
- Matthews, B.W., (1975). Comparison of the predicted and observed secondary structure of T4 phage lysozyme. *Biochimica et Biophysica Acta (BBA)-Protein Structure*, 405(2), pp.442-451.

- McGuffin, L.J., Bryson, K. and Jones, D.T., (2000). The PSIPRED protein structure prediction server. *Bioinformatics*, 16(4), pp.404-405.
- McGregor, M. J., Flores, T. P., and Sternberg, M. J. (1989). Prediction of  $\beta$ -turns in proteins using neural networks. *Protein Engineering, Design and Selection*, 2(7), 521-526.
- Milner-White, E. J., and Poet, R. (1987). Loops, bulges, turns and hairpins in proteins. *Trends in Biochemical Sciences*, 12, 189-192.
- Montomerie, S., Sundararaj, S., Gallin, W. J., and Wishart, D. S. (2006). Improving the accuracy of protein secondary structure prediction using structural alignment. *BMC bioinformatics*, 7(1), 301.
- Montomerie, S., Cruz, J. A., Shrivastava, S., Arndt, D., Berjanskii, M., and Wishart, D. S. (2008). PROTEUS2: a web server for comprehensive protein structure prediction and structure-based annotation. *Nucleic acids research*, 36(suppl\_2), W202-W209.
- Mirabello, C., & Pollastri, G. (2013). Porter, PaleAle 4.0: high-accuracy prediction of protein secondary structure and relative solvent accessibility. *Bioinformatics*, 29(16), 2056-2058.
- Mikolov, T., & Zweig, G. (2012). Context dependent recurrent neural network language model. *SLT*, 12, 234-239.
- Mikolov, T., Karafiát, M., Burget, L., Cernocký, J., & Khudanpur, S. (2010, September). Recurrent neural network based language model. In *Interspeech* (Vol. 2, p. 3).
- Mooney, C., Vullo, A., & Pollastri, G. (2006). Protein structural motif prediction in multidimensional  $\phi$ - $\psi$  space leads to improved secondary structure prediction. *Journal of Computational Biology*, 13(8), 1489-1502.

- Nair, V., & Hinton, G. E. (2010). Rectified linear units improve restricted boltzmann machines. In *Proceedings of the 27th international conference on machine learning (ICML-10)* (pp. 807-814).
- Parkhi, O. M., Vedaldi, A., & Zisserman, A. (2015, September). Deep Face Recognition. In *BMVC* (Vol. 1, No. 3, p. 6).
- Pauling, L., Corey, R. B., & Branson, H. R. (1951). The structure of proteins: two hydrogen-bonded helical configurations of the polypeptide chain. *Proceedings of the National Academy of Sciences*, 37(4), 205-211.
- Pfister, T., Simonyan, K., Charles, J., & Zisserman, A. (2014, November). Deep convolutional neural networks for efficient pose estimation in gesture videos. In *Asian Conference on Computer Vision* (pp. 538-552). Springer, Cham.
- Petersen, B., Lundegaard, C., and Petersen, T. N. (2010). NetTurnP—neural network prediction of beta-turns by use of evolutionary information and predicted protein sequence features. *PLoS One*, 5(11), e15079.
- Pedregosa, F., Varoquaux, G., Gramfort, A., Michel, V., Thirion, B., Grisel, O., ... and Vanderplas, J. (2011). Scikit-learn: Machine learning in Python. *Journal of Machine Learning Research*, 12(Oct), 2825-2830.
- Pham, T. H., Satou, K., and Ho, T. B. (2005). Support vector machines for prediction and analysis of beta and gamma-turns in proteins. *Journal of bioinformatics and computational biology*, 3(02), pp.343-358.
- Ramírez-Alvarado, M., Blanco, F. J., Niemann, H., and Serrano, L. (1997). Role of  $\beta$ -turn residues in  $\beta$ -hairpin formation and stability in designed peptides. *Journal of molecular biology*, 273(4), 898-912.

- Raina, R., Battle, A., Lee, H., Packer, B., and Ng, A. Y. (2007, June). Self-taught learning: transfer learning from unlabeled data. In *Proceedings of the 24th international conference on Machine learning* (pp. 759-766). ACM.
- Radford, A., Metz, L. and Chintala, S., (2015). Unsupervised representation learning with deep convolutional generative adversarial networks. *arXiv preprint arXiv:1511.06434*.
- Remmert, M., Biegert, A., Hauser, A. and Söding, J., (2012). HHblits: lightning-fast iterative protein sequence searching by HMM-HMM alignment. *Nature methods*, 9(2), pp.173-175.
- Ren, S., He, K., Girshick, R., & Sun, J. (2015). Faster R-CNN: Towards real-time object detection with region proposal networks. In *Advances in neural information processing systems* (pp. 91-99).
- Richardson, J. S. (1981). The anatomy and taxonomy of protein structure. *Advances in protein chemistry*, 34, 167-339.
- Rost, B., & Sander, C. (1993). Prediction of protein secondary structure at better than 70% accuracy. *Journal of molecular biology*, 232(2), 584-599.
- Rost, B., & Sander, C. (1994). Conservation and prediction of solvent accessibility in protein families. *Proteins: Structure, Function, and Bioinformatics*, 20(3), 216-226.
- Rose, G.D., Gierasch, L.M. and Smith, J.A., 1985. Turns in peptides and proteins. *Advances in protein chemistry*, 37, pp.1-109.
- Sabour, S., Frosst, N., and Hinton, G. E. (2017). Dynamic routing between capsules. In *Advances in Neural Information Processing Systems* (pp. 3859-3869).



- Sanger, F., & Thompson, E. O. P. (1953). The amino-acid sequence in the glyceryl chain of insulin. 2. The investigation of peptides from enzymic hydrolysates. *Biochemical Journal*, 53(3), 366.
- Sharif Razavian, A., Azizpour, H., Sullivan, J., & Carlsson, S. (2014). CNN features off-the-shelf: an astounding baseline for recognition. In *Proceedings of the IEEE conference on computer vision and pattern recognition workshops* (pp. 806-813).
- Shen, F., Gan, R., & Zeng, G. (2016, November). Weighted residuals for very deep networks. In *Systems and Informatics (ICSAI), 2016 3rd International Conference on* (pp. 936-941). IEEE.
- Shepherd, A. J., Gorse, D., and Thornton, J. M. (1999). Prediction of the location and type of  $\beta$ -turns in proteins using neural networks. *Protein science*, 8(5), 1045-1055.
- Singh, H., Singh, S., and Raghava, G. P. (2015). In silico platform for predicting and initiating  $\beta$ -turns in a protein at desired locations. *Proteins: Structure, Function, and Bioinformatics*, 83(5), 910-921.
- Simons, K. T., Ruczinski, I., Kooperberg, C., Fox, B. A., Bystroff, C., & Baker, D. (1999). Improved recognition of native-like protein structures using a combination of sequence-dependent and sequence-independent features of proteins. *Proteins: Structure, Function, and Bioinformatics*, 34(1), 82-95.
- Srivastava, N., Hinton, G.E., Krizhevsky, A., Sutskever, I. and Salakhutdinov, R., (2014). Dropout: a simple way to prevent neural networks from overfitting. *Journal of machine learning research*, 15(1), pp.1929-1958.

- Stallkamp, J., Schlipsing, M., Salmen, J., & Igel, C. (2011, July). The German traffic sign recognition benchmark: a multi-class classification competition. In *Neural Networks (IJCNN), The 2011 International Joint Conference on* (pp. 1453-1460). IEEE.
- Sutskever, I., Vinyals, O., & Le, Q. V. (2014). Sequence to sequence learning with neural networks. In *Advances in neural information processing systems* (pp. 3104-3112).
- Szegedy, C., Ioffe, S., Vanhoucke, V., & Alemi, A. A. (2017). Inception-v4, Inception-ResNet and the Impact of Residual Connections on Learning. In *AAAI* (pp. 4278-4284).
- Tang, Z., Li, T., Liu, R., Xiong, W., Sun, J., Zhu, Y., & Chen, G. (2011). Improving the performance of  $\beta$ -turn prediction using predicted shape strings and a two-layer support vector machine model. *BMC bioinformatics*, 12(1), 283.
- Tomek, I. (1976). Two modifications of CNN. *IEEE Trans. Systems, Man and Cybernetics*, 6, 769-772.
- Targ, S., Almeida, D., & Lyman, K. (2016). Resnet in Resnet: generalizing residual architectures. *arXiv preprint arXiv:1603.08029*.
- Taherzadeh, G., Zhou, Y., Liew, A.W.C. and Yang, Y., (2016). Sequence-based prediction of protein-carbohydrate binding sites using support vector machines. *Journal of chemical information and modeling*, 56(10), pp.2115-2122.
- UniProt Consortium, (2017). UniProt: the universal protein knowledgebase. *Nucleic acids research*, 45(D1), pp.D158-D169.
- Vinyals, O., Toshev, A., Bengio, S., & Erhan, D. (2015). Show and tell: A neural image caption generator. In *Proceedings of the IEEE conference on computer vision and pattern recognition* (pp. 3156-3164).

- Xiong, W., Droppo, J., Huang, X., Seide, F., Seltzer, M., Stolcke, A., ... & Zweig, G. (2017, March). The Microsoft 2016 conversational speech recognition system. In *Acoustics, Speech and Signal Processing (ICASSP), 2017 IEEE International Conference on* (pp. 5255-5259). IEEE.
- Xu, K., Ba, J., Kiros, R., Cho, K., Courville, A., Salakhudinov, R., ... & Bengio, Y. (2015, June). Show, attend and tell: Neural image caption generation with visual attention. In *International Conference on Machine Learning* (pp. 2048-2057).
- Xue, B., Dor, O., Faraggi, E., & Zhou, Y. (2008). Real-value prediction of backbone torsion angles. *Proteins: Structure, Function, and Bioinformatics*, 72(1), 427-433.
- Wang, G. and Dunbrack Jr, R.L., (2003). PISCES: a protein sequence culling server. *Bioinformatics*, 19(12), pp.1589-1591.
- Wang, S., Peng, J., Ma, J., & Xu, J. (2016). Protein secondary structure prediction using deep convolutional neural fields. *Scientific reports*, 6.
- Wang, D., Zeng, S., Xu, C., Qiu, W., Liang, Y., Joshi, T., and Xu, D. (2017). MusiteDeep: a deep-learning framework for general and kinase-specific phosphorylation site prediction. *Bioinformatics*, 33(24), 3909-3916.
- Webb, B., and Sali, A. (2014). Protein structure modeling with MODELLER. *Protein Structure Prediction*, 1-15.
- Wood, M. J., & Hirst, J. D. (2005). Protein secondary structure prediction with dihedral angles. *PROTEINS: Structure, Function, and Bioinformatics*, 59(3), 476-481.
- Wüthrich, K. (1986). NMR with Proteins and Nucleic Acids. *Europhysics News*, 17(1), 11-13.

- Wu, S., & Zhang, Y. (2008). MUSTER: improving protein sequence profile–profile alignments by using multiple sources of structure information. *Proteins: Structure, Function, and Bioinformatics*, 72(2), 547-556.
- Wu, S., & Zhang, Y. (2008). ANGLOR: a composite machine-learning algorithm for protein backbone torsion angle prediction. *PLoS One*, 3(10), e3400.
- Xie, S., and Tu, Z. (2015). Holistically-nested edge detection. In *Proceedings of the IEEE international conference on computer vision* (pp. 1395-1403).
- Yaseen, A. and Li, Y., (2014). Context-based features enhance protein secondary structure prediction accuracy. *Journal of chemical information and modeling*, 54(3), pp.992-1002.
- Yang, Y., Faraggi, E., Zhao, H., & Zhou, Y. (2011). Improving protein fold recognition and template-based modeling by employing probabilistic-based matching between predicted one-dimensional structural properties of query and corresponding native properties of templates. *Bioinformatics*, 27(15), 2076-2082.
- Yang, Y., Heffernan, R., Paliwal, K., Lyons, J., Dehzangi, A., Sharma, A., ... & Zhou, Y. (2017). SPIDER2: A Package to Predict Secondary Structure, Accessible Surface Area, and Main-Chain Torsional Angles by Deep Neural Networks. *Prediction of Protein Secondary Structure*, 55-63.
- Zagoruyko, S., & Komodakis, N. (2016). Wide residual networks. *arXiv preprint arXiv:1605.07146*.
- Zhang, C. T., and Chou, K. C. (1997). Prediction of  $\beta$ -turns in proteins by 1-4 and 2-3 correlation model. *Biopolymers*, 41(6), 673-702.

- Zheng, C., and Kurgan, L. (2008). Prediction of beta-turns at over 80% accuracy based on an ensemble of predicted secondary structures and multiple alignments. *BMC bioinformatics*, 9(1), 430.
- Zhang, W., Liu, S., & Zhou, Y. (2008). SP5: improving protein fold recognition by using torsion angle profiles and profile-based gap penalty model. *PloS one*, 3(6), e2325.
- Zhang, Z., Miller, W., Schäffer, A.A., Madden, T.L., Lipman, D.J., Koonin, E.V. and Altschul, S.F., 1998. Protein sequence similarity searches using patterns as seeds. *Nucleic acids research*, 26(17), pp.3986-3990.
- Zhou, J. and Troyanskaya, O., 2014, January. Deep supervised and convolutional generative stochastic network for protein secondary structure prediction. In *International Conference on Machine Learning* (pp. 745-753).
- Zhou, Y., Duan, Y., Yang, Y., Faraggi, E., & Lei, H. (2011). Trends in template/fragment-free protein structure prediction. *Theoretical chemistry accounts*, 128(1), 3-16.
- Zhou, T., Shu, N., & Hovmöller, S. (2009). A novel method for accurate one-dimensional protein structure prediction based on fragment matching. *Bioinformatics*, 26(4), 470-477.
- Zhu, Y., Li, T., Li, D., Zhang, Y., Xiong, W., Sun, J., ... and Chen, G. (2012). Using predicted shape string to enhance the accuracy of  $\gamma$ -turn prediction. *Amino acids*, 42(5), 1749-1755.

## **VITA**

Chao Fang received his B.S. and M.S. degree in computer science from the University of Missouri- Columbia, Columbia, Missouri, in 2001 and 2003, respectively. He is currently a candidate for Doctor of Philosophy in Department of Electrical Engineering and Computer Science at the University of Missouri- Columbia. His research interests include deep learning and bioinformatics.